Review

An Update on Graphene Oxide: Applications and Toxicity

Sandeep Yadav,▲ Anirudh Pratap Singh Raman,▲ Harshvardhan Meena, Abhay Giri Goswami, Bhawna, Vinod Kumar, Pallavi Jain,* Gyanendra Kumar, Mansi Sagar, Devendra Kumar Rana, Indra Bahadur,* and Prashant Singh*

Read Online

ACCESS | Metrics & More | Article Recommendations

ABSTRACT: Graphene oxide (GO) has attracted much attention in the past few years because of its interesting and promising electrical, thermal, mechanical, and structural properties. These properties can be altered, as GO can be readily functionalized. Brodie synthesized the GO in 1859 by reacting graphite with $KClO_3$ in the presence of fuming HNO_3; the reaction took 3−4 days to complete at 333 K. Since then, various schemes have been developed to reduce the reaction time, increase the yield, and minimize the release of toxic byproducts (NO_2 and N_2O_4). The modified Hummers method has been widely accepted to produce GO in bulk. Due to its versatile characteristics, GO has a wide range of applications in different fields like tissue engineering, photocatalysis, catalysis, and biomedical applications. Its porous structure is considered appropriate for tissue and organ regeneration. Various branches of tissue engineering are being extensively explored, such as bone, neural, dentistry, cartilage, and skin tissue engineering. The band gap of GO can be easily tuned, and therefore it has a wide range of photocatalytic applications as well: the degradation of organic contaminants, hydrogen generation, and CO_2 reduction, etc. GO could be a potential nanocarrier in drug delivery systems, gene delivery, biological sensing, and antibacterial nanocomposites due to its large surface area and high density, as it is highly functionalized with oxygen-containing functional groups. GO or its composites are found to be toxic to various biological species and as also discussed in this review. It has been observed that superoxide dismutase (SOD) and reactive oxygen species (ROS) levels gradually increase over a period after GO is introduced in the biological systems. Hence, GO at specific concentrations is toxic for various species like earthworms, *Chironomus riparius*, Zebrafish, etc.
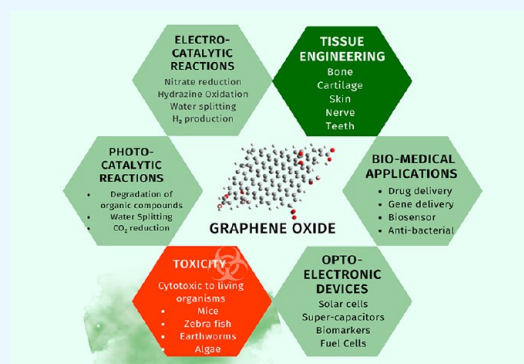
1. INTRODUCTION

Graphene is a single-layered structure with C-atoms (sp^2 hybridized) forming hexagons. Due to the presence of free electrons, the conductivity of graphene is significantly high. Good electrical and thermal conductivity, high tensile strength (stronger than steel),[1] the largest strength to mass ratio, and high surface area (1168 m^2 g^{-1})[2] are some characteristics which make graphene and graphene-based materials excellent candidates for a large number of applications. Nano-electronics,[3] drug delivery,[4] catalysis,[5] sensors,[6] energy storage (batteries),[6] and tissue engineering[7] are some areas where graphene/graphene oxide (GO) could play an important role. Lots of $\pi−\pi$ stacking between the layers causes graphene to aggregate and create a hydrophobic moiety. To overcome this problem, oxidation of graphene is done via the Hummers method followed by exfoliation.[8] GO is a single-layered oxidized form of graphene. Because of the presence of oxygen-containing groups on the surface, $\pi−\pi$ stacking is significantly reduced, which also reduces the conductivity and introduces lattice defects in GO. It can be dispersed in water and a few organic solvents due to the formation of hydrogen

bonds between hydroxyl groups present on the surface and in the solvent. It is easy to synthesize and keep stable at room temperature. Owing to this property, thin films of GO and its derivatives are easily fabricated on different substrates. GO is readily functionalized because of the presence of large oxygen-containing functional groups, making it highly receptible to complex with metal ions and different compounds. Through reduction, the electrical conductivity of GO can be enhanced. Reduced graphene oxide (rGO) is the substance formed after reduction. rGO is a near relative of graphene, but it has its own identity within the graphene family due to its unique properties. This substance has numerous applications (Table 1) and a promising future. The variety of existing and future

Table 1. Various Applications of Graphene Oxide

Catalyst in different reactions	Reactions	
	Synthesis of primary amides from aromatic aldehydes	9
	Hydrogen generation from formate	10
	Kabachnik−Fields reaction	11
	Glycosylation reactions	12
	Green synthesis of propargylamines	13
	Henry reaction	14
Tissue engineering	Different scaffolds	
Bone	GO−calcium phosphate nanocomposites	15
	GO-based tricomponent scaffolds	16
	GO−hydroxyapatite/silk fibroin	17
Neural	GO microfiber	18
	GO−PLGA hybrid nanofiber	19
	GO foam (GOF) based 3D scaffold	20
Cartilage	Chitosan/PVA/GO polymer nanofiber	21
	GO−PLGA hybrid microparticles	22
	GO-containing chitosan scaffolds	23
Skin	PEGylated GO-mediated quercetin-hybrid scaffold	24
	GO−genipin	25
	Chitosan−PV−GO nanocomposite scaffold	26
Dentistry	Sodium titanate with GO	27
	GO−titanium−silver scaffold	28
	GO-copper-coated CaP nanocomposite	29
Photocatalytic reactions	Reactions	
Degradation of organic compounds	Degradation of amoxicillin	30
	Degradation of methylene blue	31
	Degradation of gaseous benzene	32
Water splitting	S,N-codoped GO quantum dots	33
	Copper phthalocyanine@GO/TiO$_2$	34
	GO−CdS−Pt nanocomposite	35
CO$_2$ reduction	rod-like TiO$_2$−rGO composite aerogels	36
	CsPbBr$_3$ QD/GO	37
	Ag$_2$CrO$_4$/g-C$_3$N$_4$/GO	38
Electrocatalyst	Reactions	
	Electrocatalytic CO$_2$ reduction	39
	Electrochemical monitoring of mancozeb	40
	Electrocatalytic degradation ofacetaminophen	41
	Electrocatalytic oxidation of hydrazine	42
Biomedical	Area of research	
	Drug delivery	43
	Sensors	44
	Gene delivery	45
	Antibacterial nanocomposites	46

prospectives of GO and rGO applications can be observed. In recent years, GO and rGO have emerged as biocompatible C-based materials for use in a variety of systems, such as bioelectrochemical systems,[9,10] to enhance charge transfer efficiency in the redox process. In chemistry and biology, graphene has numerous more applications in conductive coatings, electronics, solar cells, photocatalysts, Li-ion batteries, supercapacitors, absorbents, pharmaceuticals, and sensors.

2. VARIOUS ROUTES FOR THE PREPARATION OF GRAPHENE OXIDE (GO)

The beginning of GO synthesis goes back to the 19th century, in 1859 B.C. Brodie was the first to oxidize graphite to GO.

Graphite and KClO$_3$ (1:3 ratio) were mixed and reacted with fuming HNO$_3$ over 3−4 days at 333 K.[47] Since then, the process has been improved by many groups and scientists such as Staudenmaier (1898), Hummers (1958), Shen (2009), Chen (2015), and many more by altering the oxidant, carbon source, and reaction temperature (Figure 1).[2−4]

The method developed by Hummers and Offeman (1958) is the most widely accepted method to synthesize GO in bulk. In the Hummers method, a mixture of graphite powder and sodium nitrate is oxidized by sulfuric acid and potassium permanganate. High-quality GO is produced in a few hours by this method. There are some flaws in the Hummers method: it produces toxic gases such as NO$_2$ and N$_2$O$_4$. Also, a large amount of acid is used in this method (2.3 L for 100 g of graphite).[49] Several modifications have been attempted to reduce the toxicity and increase the yield of the Hummers method, collectively known as the modified Hummers methods. Some of them are mentioned in Table 2.

As shown in Figure 2, the stacked layers in GO are separated out by the process of exfoliation. Exfoliation of the bulk graphite oxide is done to obtain single-layered sheets of GO. The process of exfoliation depends on many factors, such as the strength with which layers are attracted to each other, the type and amount of fictional groups present on the edge of the sheets, and the spacing between the layers. There have been numerous methods investigated up to this point. Akhavan et al. exfoliated the graphite oxide by heating the prepared material in a tube furnace at 1050 °C. An alumina boat containing graphite oxide was moved in and out of the heating zone rapidly, giving 30 s of thermal shock.[59] Zhu et al. obtained GO sheets via bath sonication of prepared crude for 1 h in propylene carbonate. Stable suspensions were prepared with different pH (3, 7, and 10), and it was observed that with the increase in pH zeta potential was increased.[60] In another example, Na ions were intercalated in between the layers of graphite. Akhavan et al. first dispersed the graphite powder in TiO$_2$ suspension: it was sonicated (40 kHz, 30 min) and then heated in air (400 °C, 15 min) so that Ti−C/Ti−O−C bonds could form, causing better movement of electrons. Later the composite was stirred for 12 h in tetrahydrofuran solution which contained sodium and naphthalene. Na-intercalated graphite−TiO$_2$ particles were obtained after centrifugation.[61]

In the recent years, tuning of the GO framework has attracted some attention. To achieve the desired d-spacing between the layers of GO, various materials have been used to intercalate between GO sheets. With different molecules, interlayer spacing, and packaging structure changes, there are some alterations in the properties as well. Several methods are used for the modification of GO sheets, such as polymer compositing, introduction of nanoparticles and 2D materials, ionic interactions, and covalent cross-linking.[62]

3. CHARACTERIZATION OF GRAPHENE OXIDE (GO)

Graphene oxide (GO) is done by various spectroscopic, microscopic, electrochemical, and other methods (Figure 3). The morphology, electronic energy levels, atomic structure, thermal stability, specific conductivity, atomic composition, and many other characteristic properties are deduced by techniques like x-ray diffraction (XRD), fourier transform infra red (FTIR), electron dispersive x ray (EDX), x-ray photo-electron spectroscopy (XPS), thermogravimetric analysis (TGA), and scanning electron microscopic (SEM) analysis, as given in Table 3.
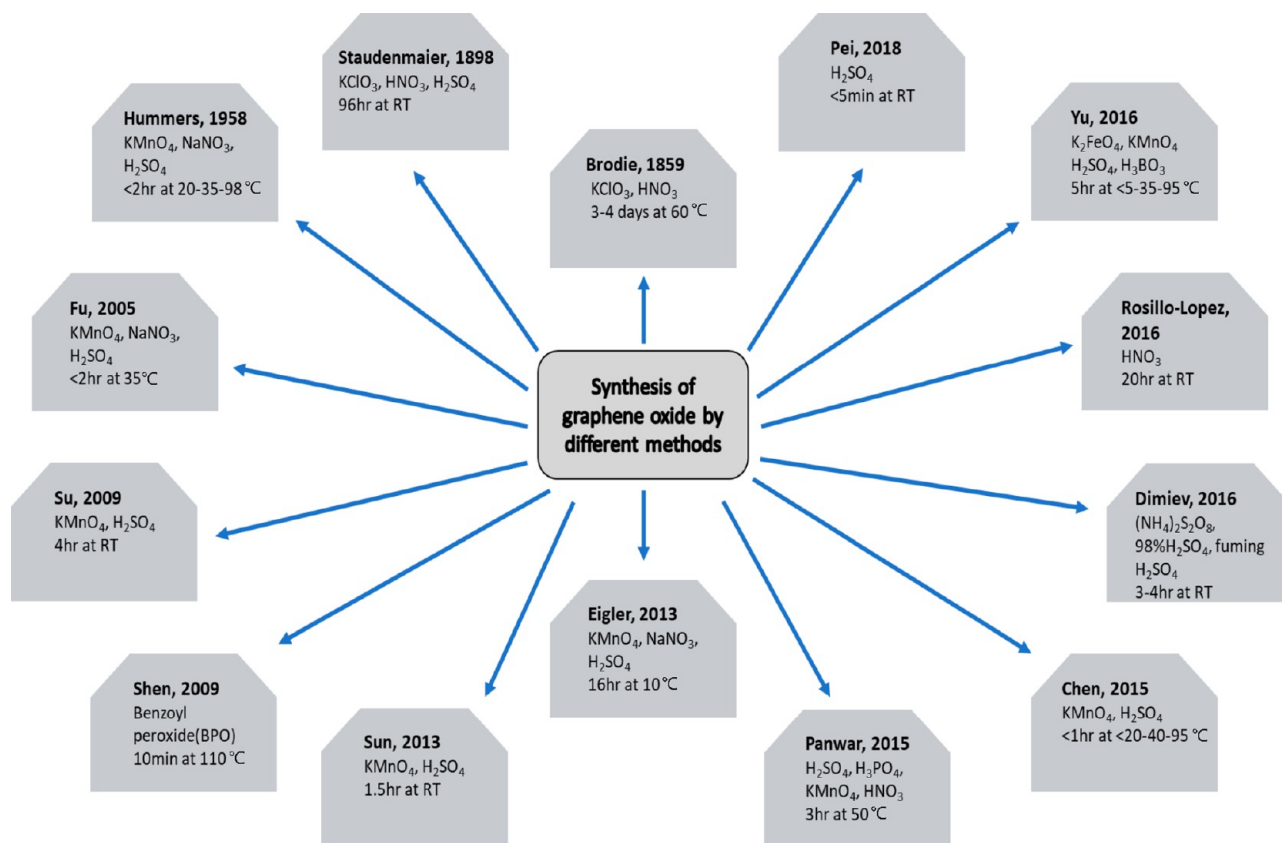
Figure 1. Various methods developed over the years for the preparation of GO.[47−58]

Table 2. Methods of Preparation of Graphene Oxide (GO)

| S. no.	Method	Oxidant	Reaction time	Temp. (°C)	Refs
1	Brodie 1859	$KClO_3$, HNO_3	3−4 days	60	47
2	Staudenmaier 1898	$KClO_3$, HNO_3, H_2SO_4	96 h	rt	48
3	Hummers 1958	$KMnO_4$, H_2SO_4, $NaNO_3$	<2 h	20−35−98	49
4	Su 2009	$KMnO_4$, H_2SO_4	<2 h	rt	50
5	Shen 2009	Benzoylperoxide	4 h	110	51
6	Sun 2013	$KMnO_4$, H_2SO_4,	10 min	RT	52
7	Eigler 2013	$KMnO_4$, H_2SO_4, $NaNO_3$	1.5 h	10	53
8	Panwar 2015	$KMnO_4$, H_2SO_4, H_3PO_3, HNO_3	16 h	50	54
9	Chen 2015	$KMnO_4$, H_2SO_4,	3 h	20−40−95	55
10	Dimiev 2016	$(NH_4)_2S_2O_8$, H_2SO_4	<1 h	rt	56
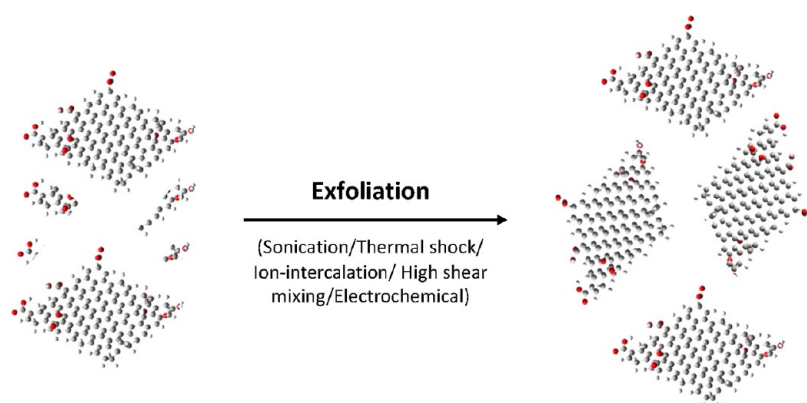
Figure 2. Exfoliation of bulk GO.

3.1. Spectroscopic Characterization.

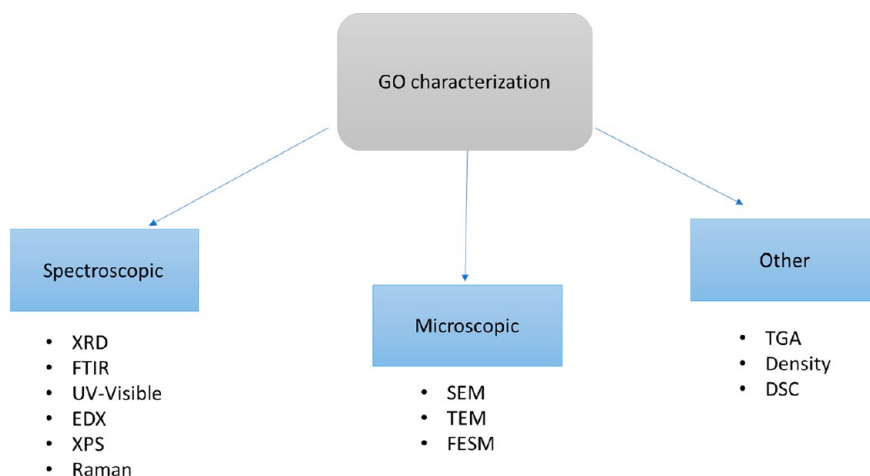X-ray photoelectron spectroscopy (XPS), UV−Visible, Raman, Fourier

Figure 3. Methods of characterization of Graphene Oxide (GO).

Table 3. Characterization Methods of GO

S. No.	Method of characterization	System	Result	Refs
1	UV−visible	GO	λ_{max1} = 230 nm; λ_{max2} = 280−300 nm	63
2	XRD	GO nanosheets	2θ = 10.44°	64
3	FTIR	GO	1720 cm^{-1} (carbonyl of −COOH)	65
			1363 cm^{-1} and 1226 cm^{-1}	
			1085 cm^{-1} (epoxy groups)	
			1630 cm^{-1} (C-atoms of arenes)	
4	Raman	Single-layered GO	1585 cm^{-1} (G-band)	71
			2679 cm^{-1} (2D band)	
5	XPS	GO	287 eV (epoxy group)	65
			289.50 eV (carbonyl of −COOH)	
			291.28 eV (ester)	
6	SEM	GO	Deformation of graphene sheet with increase in oxygen concentration	67
7	TGA	GO−M−Cu	Multiple weight decreases at different stages.	15
8	Density	Ethanol−GO	2.260 g cm^{-3}	68
		Acetone−GO	1.167 g cm^{-3}	

transformation infrared (FTIR), and X-ray diffraction (XRD) are spectroscopic techniques used for the characterization of GO as shown in Figure 4.

3.2. UV−Visible. Kigozi et al. synthesized GO from graphene by the Hummers method (HM) and modified Hummers methods (MHM1 and MHM2) and compared the GO obtained. As shown in Figure 5, the graphite flakes and GO samples were scanned between 200 and 700 nm in wavelength. The spectra's absorption peaks were noticed at two distinct wavelengths. These two distinct types are characteristic features that are utilized to distinguish GO from graphite flakes with a peak in the 320−360 nm region, as seen in Figure 5a, which emerged at a wavelength of 310 nm. In the absorbance spectra, two major peaks were observed: one at 230 nm and the other in the range 280−300 nm. The former one is because of the C−C bond's π−π* transition, and the latter one is due to the C═ bond's n−π* transition.[63]

3.3. X-ray Diffraction (XRD) Analysis. The presence of a peak at 10.44° in the XRD pattern of GO nanosheets manufactured by Muniyalakshmi and the team supports the formation of GO nanosheets and reveals that the sheets are separated by 0.846 nm after oxidation and exfoliation. As depicted in Figure 6, the diffraction pattern is captured between 5 and 50°.[64]

3.4. Fourier Transform Infrared (FTIR) Analysis. The appearance of a broad peak at about 3440 cm^{-1} (Figure 7) is due to the carboxylic group's O−H, while a sharp signal at 1720 cm^{-1} indicates the presence of carbonyl in the carboxylic group. The C−OH stretch of the carboxylic and the alcoholic groups attached to the graphene-conjugated system are related to the two signals observed at 1363 and 1226 cm^{-1}, respectively, while stretching for epoxy groups lies at 1085 cm^{-1}. Further, a signal at 1630 cm^{-1} corresponds to sp^2 carbons of arenes.[65]

3.5. Raman Spectroscopic Analysis. The typical Raman bands of single-layered GO include the G-band (1585 cm^{-1}) created by sp^2-hybridized carbons, the D-band (1350 cm^{-1}) caused by sp^3-hybridized carbons connected to hydroxyls and epoxides, and the 2D-band caused by GO sheet stacking. It has been observed that upon stacking of multiple layers (bilayer) the positions of the G- and 2D-bands shift to lower and higher values by 6 cm^{-1} and 19 cm^{-1} as shown in Figure 8(B).[71] Also, the intensity of the D-band was increased upon stacking.

3.6. X-ray Photoelectron Spectroscopic (XPS) Analysis. The presence of C and O is indicated by two strong peaks in the survey scan spectra of GO, which are designated as C 1s and O 1s peaks and correspond to binding energies of 280−290 eV and 528−536 eV, respectively. The first enlarged peak in Figure 9a corresponds to C−C bonds, whereas the
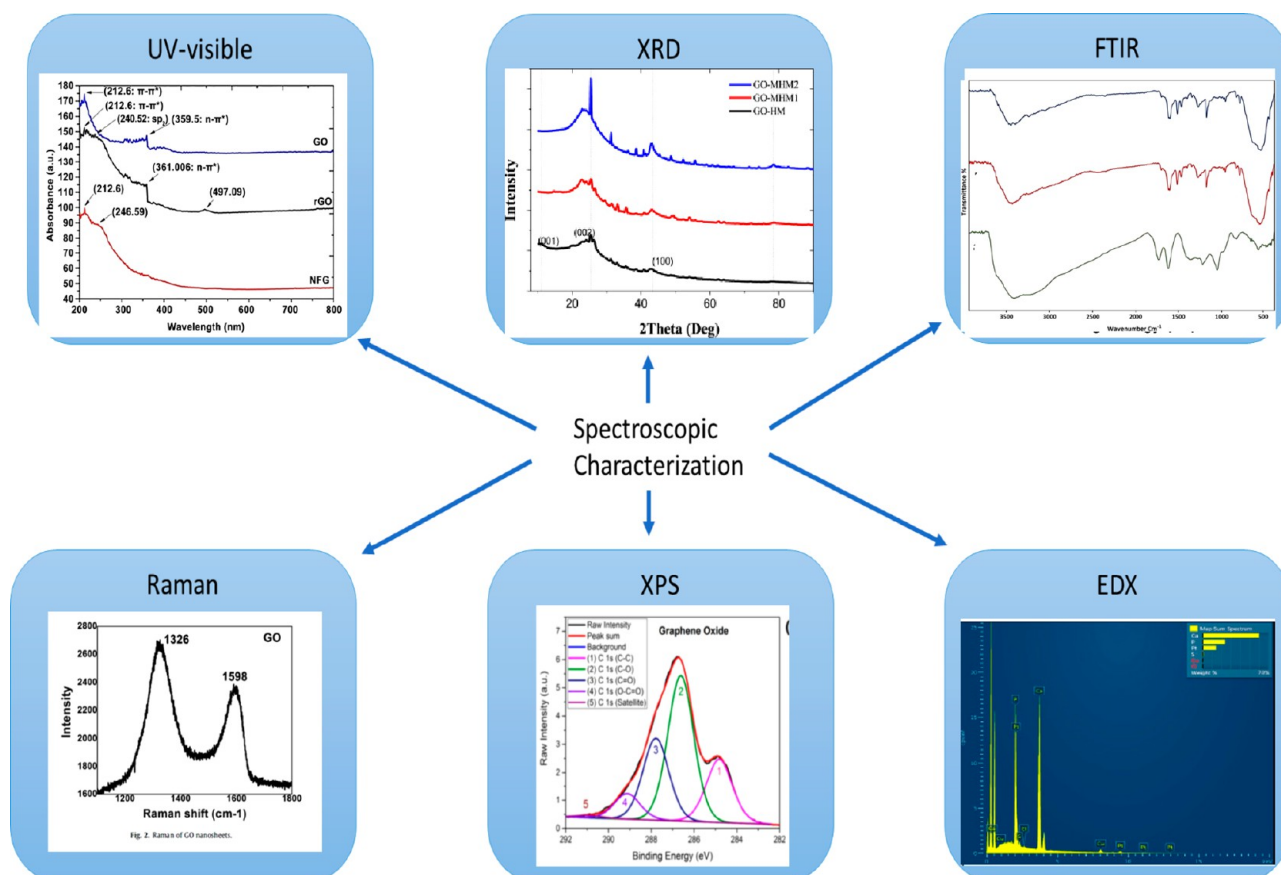
Figure 4. Different techniques for spectroscopic characterization of GO. Reproduced with permission from refs 15, 63, 64, 66, and 69.[70] Copyright@2020, Elsevier Ltd., Results in Materials (open access). Copyright@2020, Elsevier Ltd., Materials Today: Proceedings. Copyright@ 2020, Elsevier Ltd., Journal of Materials Research and Technology. Copyright@2017, Scientific Research, Graphene. Copyright@2021, Taylor and Francis Ltd., Polycyclic Aromatic Compounds.

second signal of stretching nearly at 287 eV suggests the existence of epoxy functionality. Another signal at 289.50 eV corresponds to the carbonyl of carboxylic acid, and the fourth signal at 291.28 eV indicates the presence of an ester functionality. As can be seen in Figure 9b, the C 1s peak of GO is really composed of five smaller peaks, each of which has a unique binding energy that reveals a different functional group. The first expanded peak is centered at a binding energy of approximately 284.76 eV and shows single-bond C bonds. The second peak is at around 287.00 eV and shows single-bond O bonds. The third peak is at 289.50 eV and shows double-bond O bonds. The fifth peak is at 291.28 eV and shows single-bond C═O bonds.[66]

3.7. Energy Dispersive X-ray (EDX) Analysis. The wt % of carbon is reduced to 44.59% on oxidation of graphite using the Hummers technique (HM), resulting in a 2.08% rise in the atomic percentage of oxygen. This indicates that the approach increased the amount of oxygen in the graphite, resulting in GO formation. Other atoms like sulfur, chlorine, calcium, potassium, and iron were incorporated during the process. This might be due to unfinished reactions and a GO cleaning process that is not up to par. These elements might have come from the oxidation processes' starting chemicals and reagents.[63] Figure 10 represents the EDX of (a) graphite, (b) GO–HM, (c) GO–MHM1, and (d) GO–MHM2.

3.8. Microscopic Characterization. State-of-the-art microscopy tools are used to observe graphene on substrates directly. Electron microscopy is used to identify qualitative and

quantitative details of graphene flakes. The degree of exfoliation, number of layers, lateral size, and atomic-level flaws were characterized by transmission electron microscopy (TEM), field emission scanning electron microscopy (FE-SEM), and scanning electron microscopy (SEM).[66] Figure 11 represents some techniques for microscopic characterization of GO.

3.9. Scanning Electron Micropscopic (SEM) Analysis. Figure 12 contains SEM images of the low and high oxygen concentration samples. In both cases, severely wrinkled graphene layers can be seen, indicating that the leftover oxygen has caused a deformation in the graphene layers.[67]

3.10. Thermo-gravimetric Analysis (TGA). TGA analysis was used to determine the stability of Go-M-Cu at temperatures ranging from 0 to 550 °C. From roughly 50 to 550 °C, the TGA graph exhibited three primary weight losses. The first weight loss, which begins around 50 °C and continues to 150 °C, is credited to elimination of adsorbed water, while the subsequent weight loss that begins at 200 °C and extends to 300 °C is for the decomposition of functional groups embedded on GO as well as the decomposition of organic ligands that they adsorbed physically on the surface of GO. The final and significant loss of covalently and chemically immobilized organic ligands and copper complexes on the basal plane of GO is attributed to the temperature range between 300 and 550 °C.[15]

3.11. Density. The density and specific gravity of all the samples were measured using an electronic densimeter MD-
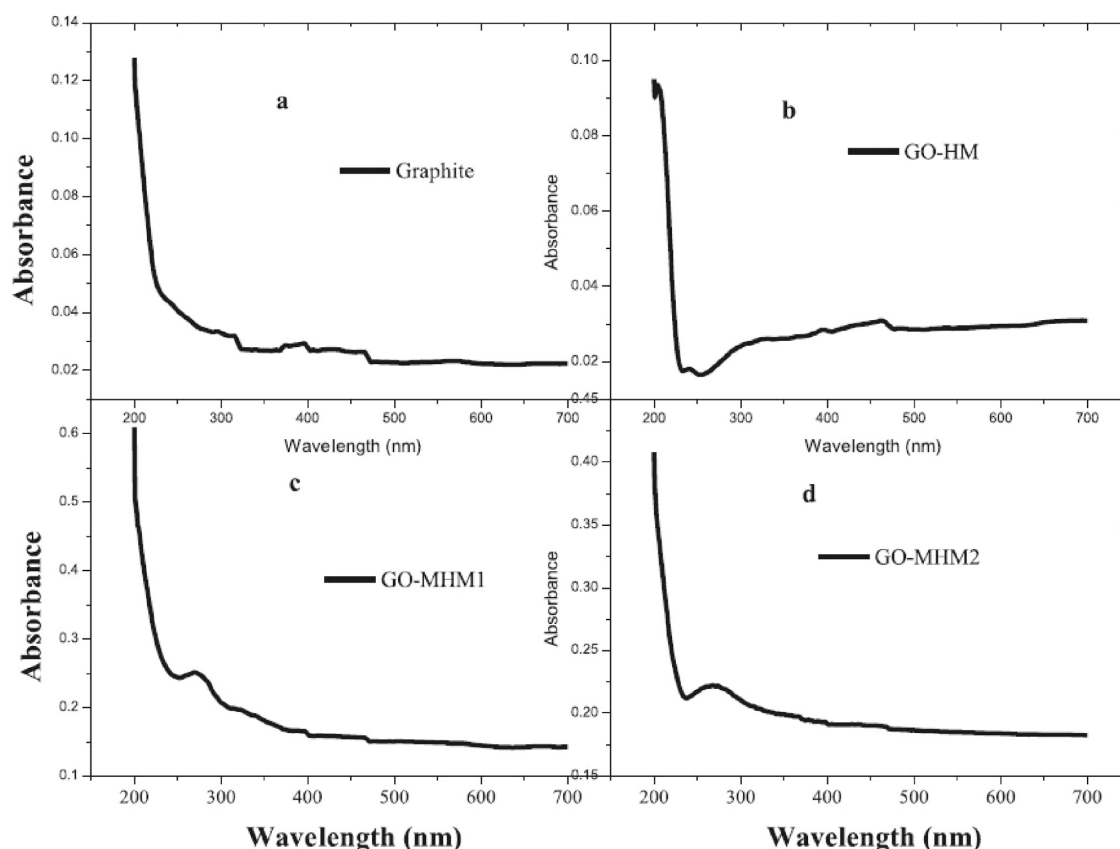
Figure 5. UV−visible spectra of (a) graphite, (b) GO synthesized by Hummers method, (c) and (d) GO synthesized by two different modified Hummers methods. Reproduced with permission from ref 63. Copyright@2020, Elsevier Ltd., Results in Materials.
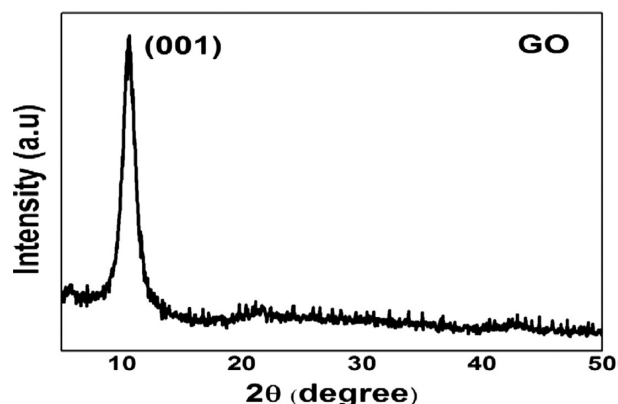

Figure 6. XRD pattern of GO nanosheets. Reproduced with permission from ref 64. Copyright@2020, Elsevier Ltd., Materials today: Proceedings.

Figure 7. FTIR spectra of GO. Reproduced with permission from ref 65. Copyright@2022, Elsevier Ltd., Nanomedicine: Nanotechnology, Biology and Medicine.

300S. In Figure 13, the density reading indicates that E-GO has the highest density (2.260 g/cm^3). This is due to agglomeration, as GO in ethanol has been reported to be slightly agglomerated. A-GO, on the other hand, had the lowest density (1.167 g/cm^3) because GO does not agglomerate in acetone. As a result, agglomeration can result in the formation of closely packed particles.[68]

4. COMPARISON OF GRAPHENE OXIDE WITH OTHER 2D MATERIALS

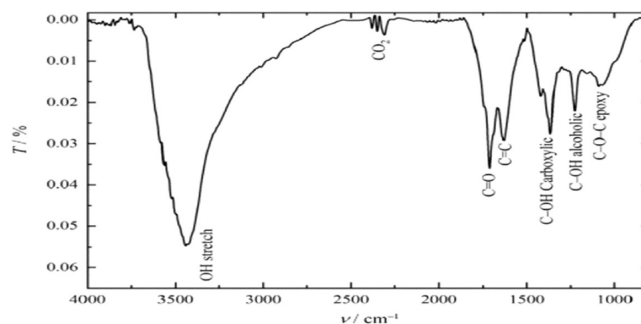Recent research has centered on the creation of semiconductor nanocomposite materials based on 2D reduced GO (rGO) to enhance its catalytic uses (Table 4). Apple juice and zinc acetate were used to produce in situ 2D rGO−ZnO (rGZn) nanocomposites, which is a commonly reported green synthesis technique. A smart cotton material coated with rGZn has been developed, and its photocatalytic self-cleaning property has been proved by the degradation of methylene blue, rhodamine B dyes, and tea stains even under sunlight irradiation, which is rare in the literature.[73] Multilayered laminates of graphite oxide (GtO) and GO are hydrophilic materials that are readily sandwiched by water and other polar solvents. The high adsorption capacity of GO materials makes them useful as sorbents for treating wastewater, elimination of numerous contaminants, humidity sensors, protective semi-permeable coatings, gas and liquid mixture separation, nanofiltration, fuel cell and battery membranes, and water
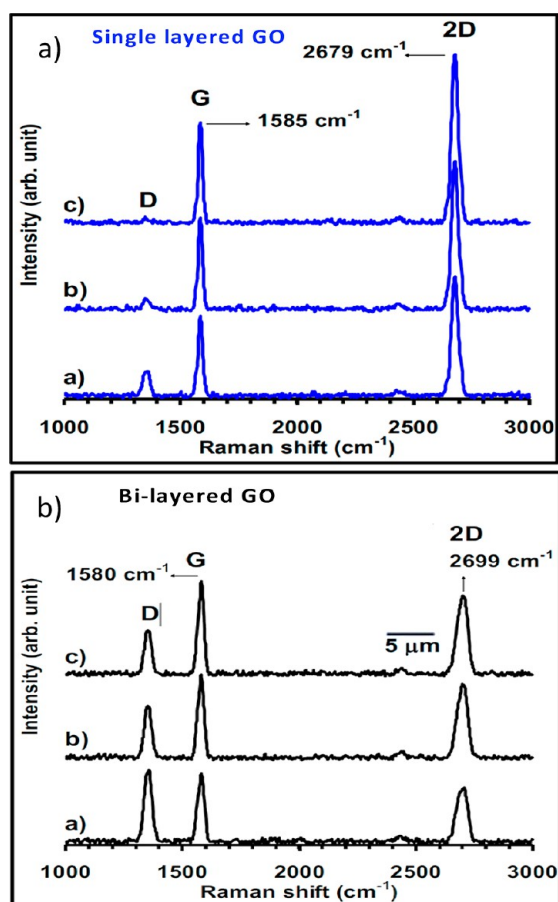
Figure 8. Raman spectra of (a) single and (b) bilayered GO. Reproduced with permission from ref 71. Copyright@2020, Elsevier Ltd., Carbon.

desalination.[74] Due to their favorable features for essential applications, ultrathin 2D MOs beyond graphene and other 2D nanomaterials (TMDs, metal carbides) have evolved into a new class of nanomaterials. Kumbhakar et al. have investigated a number of 2D MOs with varied oxidation states (MO, MO_x, and M_xO_y), spinel-type MOs, perovskite nanomaterials, and their applicability in a variety of fields. Some ultrathin 2D MOs have shown performance that has the potential to outperform existing commercial technology.[75] To develop a carbon-neutral economy, photocatalysts may gather sunlight to extract H_2 and O_2 from H_2O, fulfilling the energy demand while minimizing greenhouse gas emissions. Carbonaceous semiconductors are excellent candidates to transfer solar energy into chemical energy due to their structural and chemical modifiability.[76] In another example, it was found that the copper–graphene (Cu–Gr) nanocomposite has antiviral activity. This slows infection development by reducing viral gene expression, replication, and progeny virus particle generation, so it might reduce the spread of respiratory viruses.[77] Due to its advantageous inherent features, GO has been utilized in the construction of numerous biosensors, including electro-chemical, optical (fluorescence, colorimetric, and Raman), and mass analysis.[78]

5. APPLICATION OF GRAPHENE OXIDE AS THE CATALYSIS FOR DIFFERENT TYPES OF REACTIONS

Catalysis with higher efficiency and lower environmental impacts has emerged as a popular option for industrial processes. The oxygen-containing groups on the GO surface have a high degree of hydrophilicity and chemical activity. Furthermore, the functional groups embedded in GO operate as excellent harboring sites for numerous active catalytic species. A significant number of sp3-hybridized carbon atoms bond to a variety of oxygen-containing groups, which serves to insulate GO and leads to a resistance of 1012 sq^{-1} or larger per
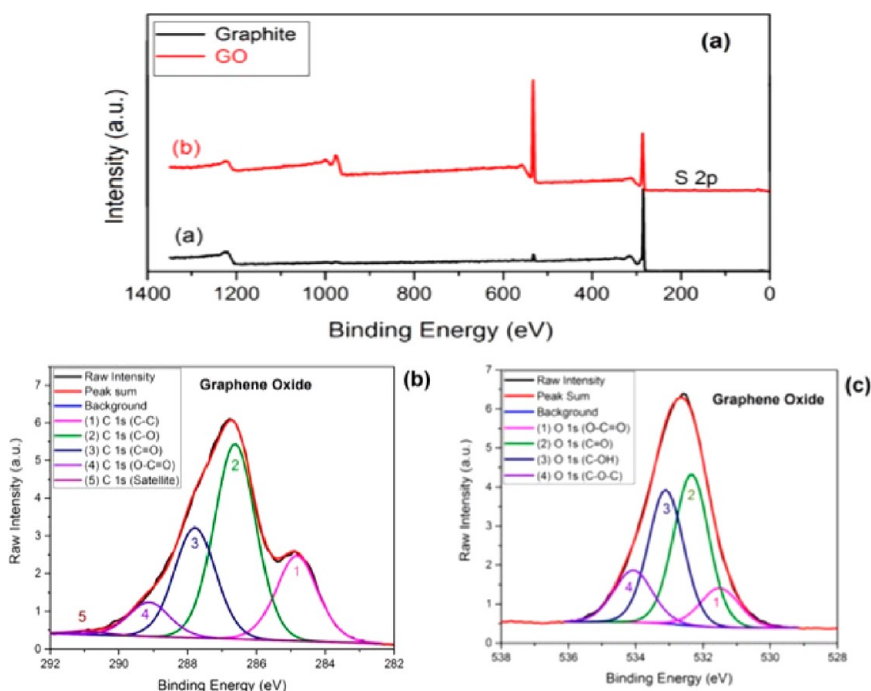

Figure 9. (a) Survey scan XPS spectra, (b) C 1s extended XPS of GO, and (c) O 1s extended spectra of GO. Reproduced with permission from ref 66. Copyright@2020, Elsevier Ltd., Journal of Materials Research and Technology.
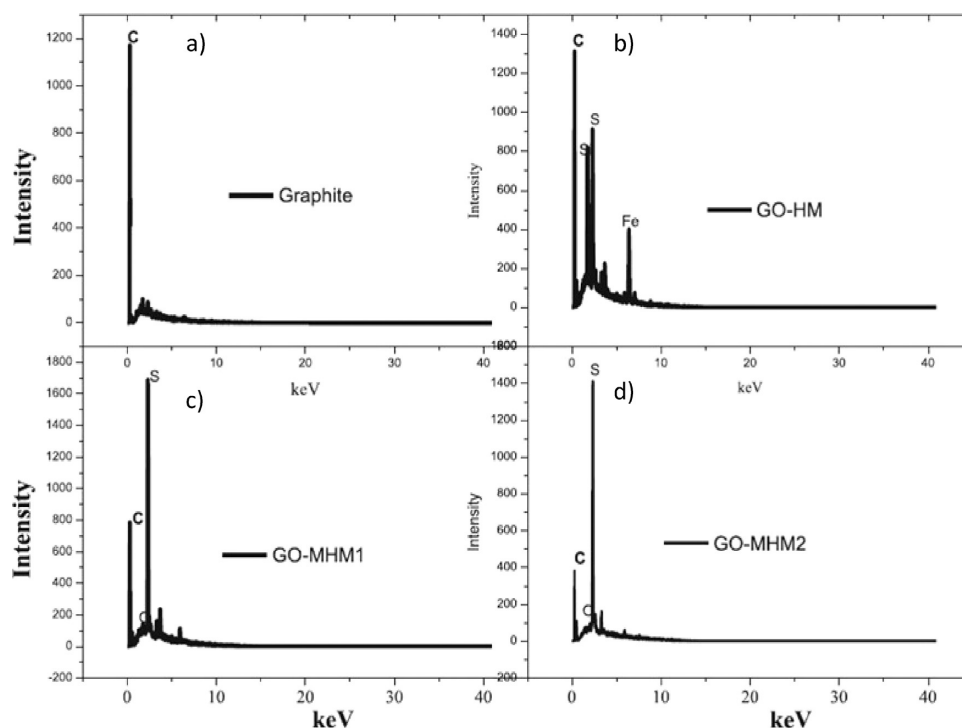
Figure 10. EDX of (a) graphite, (b) GO−HM, (c) GO−MHM1, and (d) GO−MHM2. Reproduced with permission from ref 63. Copyright@ 2020, Elsevier Ltd., Results in Materials.
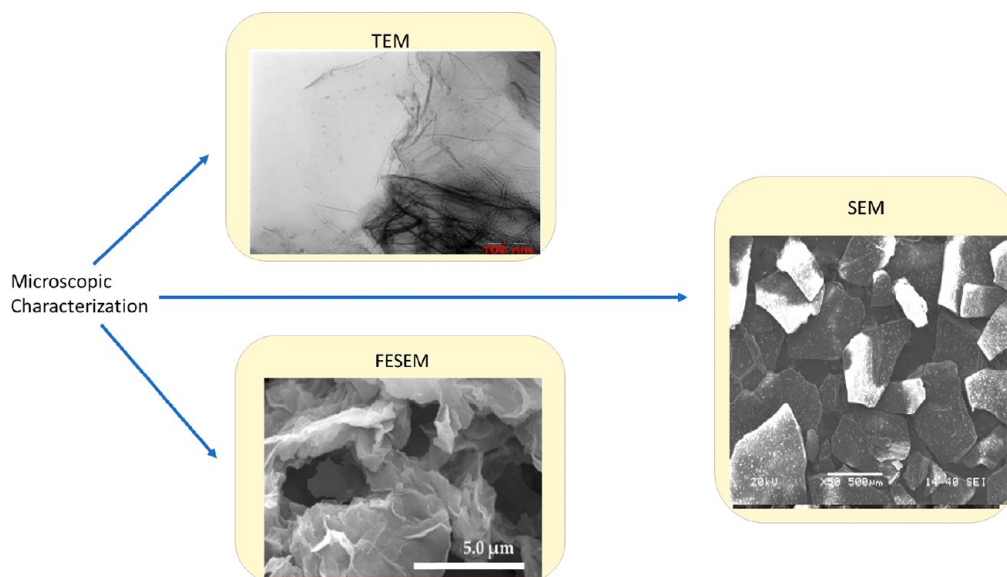

Figure 11. Some techniques for microscopic characterization of GO. Reproduced with permission from refs 65, 69, and 72. Copyright@2017, Scientific Research, Graphene. Copyright@2020, Elsevier Ltd., Nanomedicine: Nanotechnology, Biology and Medicine. Copyright@2021, Multidisciplinary Digital Publishing Institute, Nanomaterials.

sheet of GO (Table 5). The GO's sheet resistance can be reduced significantly, thereby turning it into a semiconductor. The band gap of GO can be monitored by changing the arrangement, coverage, and functional groups. GO's mechanical and conductive qualities make it an attractive material for catalysis.

Hamed et al.[9] studied the heterogeneous copper complex immobilized on GO for Beckmann rearrangement to convert aldoximes into primary amides as in Scheme 1. GO−metformin−Cu (1.6 mol %) using water as solvent gives

95% yield in 0.5 h, which is the highest among other heterogeneous catalysts.

Khatun et al.[94] reported the synthesis of carbamates via the reaction of amine (5 mmol), benzyl bromide, or n-butyl (5 mmol) in the presence of Zn(II)DETA@GO (40 mg) as a catalyst. TLC was used to monitor the reaction's development. EtOAc was added to the mixture for dilution, and after the completion of the reaction brine was used for the workup. EtOAc was recovered and dried with sodium sulfate (Scheme 2). Gas chromatography was used to examine the conversion. Column chromatography was used to purify the product, and
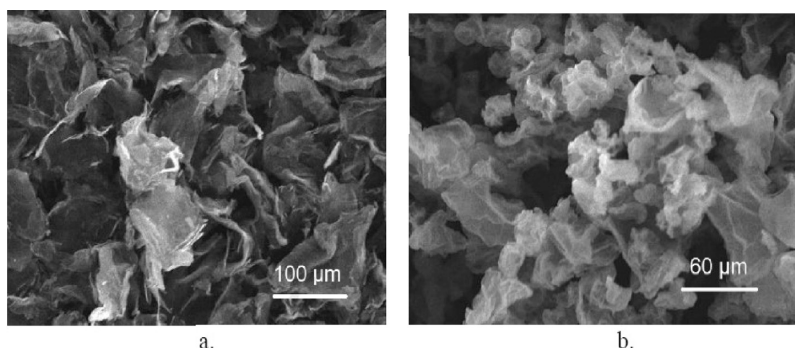
Figure 12. SEM images of (a) GO with low oxygen content and (b) GO with high oxygen content. Reproduced with permission from ref 67. Copyright@2022, Elsevier Ltd., Journal of King Saud University − Science (open access).
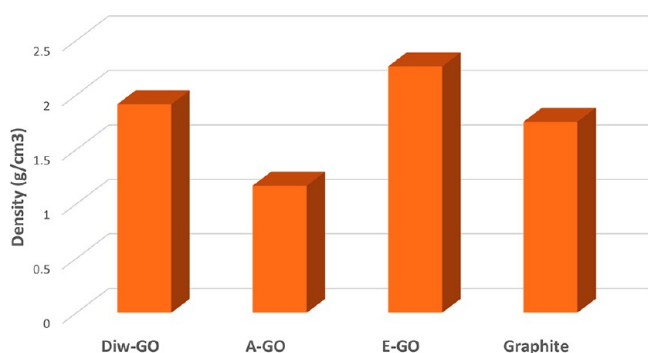

Figure 13. Density of graphite and GO dispersed in ethanol (E-GO), acetone (A-GO), and deionized water (DIW-GO). Reproduced with permission from ref 68. Copyright@2022, AIP, Ltd., AIP Conference Proceedings (open access).

^{1}H NMR was used to identify it. With this catalyst, the yield was 92% in 10 h.

Dhopte et al.[11] reported the reaction between aromatic/aliphatic amines, aromatic aldehydes, and trimethyl phosphite to get α-aminophosphonates at room temperature (Kabachnik−Fields reaction) as shown in Scheme 3. The presence of carboxylic acid and hydroxyl groups in GO may explain its higher catalytic activity in comparison to other catalysts.

Thombal et al.[12] investigated the reactions of unprotected sugars like D-glucose with allyl alcohol (glycosylation) in the presence of catalyst (sulfonated GO) in the absence of solvent. They have used 5 wt% of GO to validate the impact of GO (Scheme 4).

According to Anouar et al.,[10] liquid organic hydrogen carriers (LOHCs) can manufacture hydrogen as shown in Scheme 5. High rates (turnover frequency) must be achieved at mild circumstances and are one of the most essential requirements for being a catalyst for hydrogen production from LOHCs. The nongaseous physical nature of formic acid and its derivatives as well as its widespread availability via catalytic hydrogenation of CO_2 are the key reasons for this choice. In a 10 mL solution of 1 M NH_4HCO_2 (ammonium formate), 50 mg of the catalyst (2.5wt % of Pd) was added.

Chyana et al.[95] studied the role of GO as a catalyst for the synthesis of dihydropyrimidine (Biginelli reaction) from cinnamaldehyde. The optimal conditions for this reaction are 7.5% catalyst at 100 °C and 30 min to get a product of 83.7% (Scheme 6).

Mittal et al.[13] found that covalently grafting the Cu(II) Schiff base complex on GO resulted in a heterogeneous catalyst, which was characterized by numerous spectroscopic methods. The catalyst presented is easy to use and stable under ambient circumstances due to its ease of separation from the reaction mixture, as shown in Scheme 7. The designed catalyst could be recycled four times without losing its catalytic activity. The yield obtained was satisfactory.

Rana et al.[14] investigated the reaction between nitromethane and p-hydroxybenzaldehyde using a triamine-functionalized GO catalyst (TGO) under a N_2 environment, as shown in Scheme 8. Nitromethane (10 mL), p-hydroxybenzaldehyde (1 mmol), and TGO catalyst (0.05 g) were mixed for 2 h at 50 °C to get the product in high yield (Scheme 8).

Chattopadhyay et al.[96] found that GO contains highly mobile electrons, which might help to boost the activity of Ag−GO NPs employed as shown as in Scheme 9. The Ag−GO nanocomposite can serve better as a platform for dispersing silver NPs. As a result, the Ag−GO nanocomposite inhibits Ag NP agglomeration and has a huge surface area to get a larger number of active sites for catalysis. GO may potentially boost the catalytic activity of Ag NPs in the process, rather than only acting as a support.

Bakht et al.[97] prepared a mixture of modified isatin derivatives (1) (0.01 mol) and acid hydrazide (2) (0.01 mol) in DES (8 mL) and refluxed (Scheme 10).

Zhang et al.[98] used GO−NH₂−NEt₂ in cooperative catalysis for the conversion of benzaldehyde into β-nitro styrene, as in Scheme 11. In this reaction, tertiary amines activate the nucleophiles, while the primary amines activate the carbonyl compounds by formation of imine intermediates in the nitro-aldol reactions. The catalytic synergistic effect can be understood using GO−NH₂−NEt₂ with an NH₂:NEt₂ in different ratios. The ratio of 1:1 shows the highest catalytic activity with selectivity toward the trans-β-nitro styrene of 100%.

Epoxidation of various alkenes using H_2O_2 (oxidant) in the presence of PDA/GO was explored. High yields and low reaction times were obtained for the epoxide products. This novel catalyst was recovered and reused easily multiple times before showing a significant reduction in efficiency. The yield was 98% when $CHCl_3$ was used as solvent for 2 h (Scheme 12).[99]

Trzeciak et al.[100] studied carbonylative Suzuki−Miyaura cross-coupling, which involves the reaction of 4-iodoanisole with phenylboronic acid using Pd/GO or Pd/GO-TiO₂ as promising catalysts to get the products in a smaller span of time. At 1 atm of CO and a modest quantity of catalyst, Pd/GO showed good efficiency in the reaction, yielding the

Table 4. Comparison of GO with Other 2D Materials

| S. No.	2D material	Drug	Method	Studies	Refs
1	Phosphorene	Doxorubicin	DFT and simulation	The DOX molecule is adsorbed horizontally onto the PNS surface with the nearest contact distance being 2.5, according to both DFT calculations and MD simulations. About 49.5 kcal mol^{-1} is anticipated to be DOX's binding energy.	79
2		Thioguanine	DFT studies, electrical conductivity	Phosphorene and thioguanine's individual and combined geometries had predicted band gap values of 0.97 eV, 2.81 eV, and 0.91 eV, respectively.	80
3			Carrier mobility	It has a tunable carrier mobility of $\sim$300 cm^2 m^{-1} S^{-1} at 120 K, and at room temperature it is $\sim$1000 cm^2 m^{-1} S^{-1}.	81
4			DFT, adsorption energy, and band gap and PDOS structure	The primary component, 5−8 PNS, has a structural stability confirmed by the formation energy of 3.687 eV per P atom.	82
5		MDA-MB-231	Cytotoxicity	The great effectiveness of PTT was demonstrated when mice tumors that had been BP-treated and then exposed to radiation shrank in size in just three days, and the animals continued to live for more than a month as a result of the treatment.	83
6	BNNTs	5-Fluorouracil	DFT studies	The studies revealed that the Ni$_N$-BNNT structure can be an electronic sensor due to its increased electrical conductivity.	84
7	BC$_6$N	Hydroxyurea (HU), 5-fluorouracil (5-FU), carmustine (CMU), 6-mercaptopurine (6-MP), ifosfamide (IFO), and chloro-methane (CM)	DFT studies, QTAIM	The energy band gap (E_g) of the g-BC$_6$N nanosheet is substantially smaller following drug adsorption, according to DFT. The 6-MP/g-BC$_6$N complex was found to have the most stable structure, with adsorption energies of 18.19 and 23.53 kcal mol^{-1} for configurations M1 and M2, respectively, in the gas phase.	85
8	Silicene	Anastrozole (ANA) and melphalan (MEL)	DFT studies, MD simula-tions	Drug adsorption on the surface of SNS and FA-SNS is extremely reactive, as evidenced by adsorption energies in the range of −65.59 to −144.23 kJ/mol. Additionally, MD simulations show that van der Waals energy contributes more to drug−carrier interactions than electrostatic energy. Additionally, the outcomes show that drug molecules travel toward carriers in a natural manner.	86
9	MoS$_2$	Dox, Ce$_6$	PTT and chemotherapy	No toxicity observed even at high temperature.	87
10	WSe$_2$	Hella	MTT assay	Low cytotoxicity observed even at high concentration (i.e.,160 μg/mL).	88
11	MoS$_2$	-	Electrical conductivity	The 1.2−1.8 eV band gap is more preferable than graphene and ambipolar in nature.	89
12	MoS$_2$	INH and PZA	DFT	The variation in adsorption energies, and pH revealed that the anti-Tb drug desorbs from the 2D layer at high temperature and acidic environment.	90
13	Germanene	-	Electrical conductivity	From the equation the value of germanene gives a band gap of 0.33 V with 5 nm width of nanoribbon. The negative band gap under magnetic field has been observed.	91
14	Silicene	-	DFT studies	Unlike graphene it is demonstrated that silicene sheets are stable only if a small buckling (0.44 Å) is present.	92
15	Graphitic carbon nitride quantum dots (g-CNQDs)	Fluorescence bioimaging	DOX	The PEGylated g-CNQDs show improved physiological stability and a 9.3% quantum yield in their fluorescence emission. In contrast to neutral pH, the DOX release from the PEGylated g-CNQDs was higher in acidic circumstances.	93

Table 5. GO and GO Hybrid Catalysts

Entry no.	Catalyst	Reaction	Refs
1	GO−metformin−Cu	Synthesis of primary amides from aromatic aldehydes	9
2	Zinc composite based on modified GO: an effective catalyst	CO_2 fixation causes N-formylation and carbamate formation	94
3	GO	Kabachnik−Fields reaction	11
4	Sulfonated GO catalyst	Glycosylation reactions	12
5	Palladium supported on chitosan−GO	Hydrogen generation from formate	10
6	GO	Green synthesis of dihydropyrimidine based on cinnamaldehyde	95
7	Cu(II) Schiff base complex on GO	Green synthesis of propargylamines	13
8	Triamine-functionalized GO	Henry reaction	14
9	Ag-GO nanomaterials	Acylation of amines without solvent	96
10	GO	Synthesis of isatin−thiazolidine hybrid	97
11	GO−NH−NEt$_2$	Synthesis of β-nitro benzene	98
12	GO nanosheet supported molybdenum complex	Epoxidation of alkenes	99
13	Palladium nanoparticles embedded on GO	Synthesis of diarylketones	100
14	GO and sulfonated biochar	Lactic acid esterification	101
15	GO	Preparation of esters via the reaction between alcohols and acids	102
16	GO−N$_2$S$_2$	Suzuki−Miyaura coupling	103
17	Catalyst made of clay and GO nanocomposites	Solventless multicomponent Biginelli reaction	104
18	Mn−salen−GO	Styrene oxidation	105
19	GO	Ring opening with amine cross-linking of epoxy resins	106
20	CuO−GO nanocomposite	Formation of anilines via the hydrogenation of nitroarenes in aqueous medium	107
21	GO	Trifluoromethylation of alkynes with quinoxalinones	108
22	GO functionalized Cu(II)	Preparation of 1,2,3-triazoles	15
23	GO/rGO	Synthesis of quinoxalines	109
24	GO	Synthesis of β-amino acetones: Mannich reaction	110
25	ZnO/GO	Preparation of nitriles from alcohols in aqueous medium	111
26	GO@f-SiO$_2$@Co	Preparation of amino naphthoquinone derivatives	112
27	GO-supported MnO$_2$	Solvent-free synthesis of chalcones	113
28	GO@SO$_3$CF$_3$	Hydrolysis of the two main ulvan monosaccharides	114
29	SnO@GO	Esterification of fatty acids and trimethylolpropane	115
30	Copper phthalocyanine@GO as a cocatalyst of TiO$_2$	H$_2$ synthesis	107
31	GO	Hydration of alkynes	116
32	GO	Fridel−Craft's addition of indoles to ketones and nitro styrenes	117
33	Nanoscale GO	Oxidation of benzylic alcohols	118
34	GO	aza-Michael addition of amines and olefins	119
35	GO/TEMPO	Aerobic oxidation of 5-hydroxymethylfurfural to 2,5-diformylfuran	120

Scheme 1. Synthesis of Primary Amines from Aldoximes via Beckmann Rearrangement

$$R-Ar-CHO \longrightarrow R-Ar-CH=N-OH \longrightarrow R-Ar-\overset{O}{\underset{}{C}}-NH_2$$
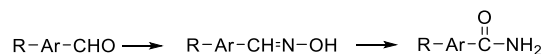
Scheme 2. Catalytic N-Formylation Reaction through CO$_2$ Fixation

$$R-NH_2 \xrightarrow[\text{CO}_2 \text{ Balloon}]{\substack{\text{Catalyst / PMHS} \\ \text{n-Bu}_2\text{O}}} R-\overset{H}{N}-CHO$$
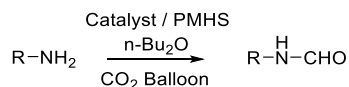
necessary diarylketones (0.2 mol %). Pd/GO-TiO$_2$ was used in four consecutive cycles and had the highest productivity, with almost 95% of the ketone production.

The catalytic efficiency was evaluated by reacting lactic acid (50%) and ethanol (esterification) by Vu et al.[101] as shown in Scheme 13. The weight ratios of the GO catalysts and sulfonated biochar to lactic acid were 1% and 5%, respectively. Because it is hard to filter GO, the weight ratio of the GO catalyst was not more than 1%.

For the esterification process, GO was discovered to be an effective and reusable acid catalyst. Many aromatic acids, aliphatic acids, and alcohols reacted well under standard conditions and produced high yields of the desired products. With strong catalytic activity, the heterogeneous catalyst may
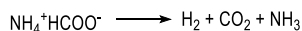
Scheme 3. A 3 mg Catalyst Loading Gives 88% Yield in 3 h Using Benzaldehyde (1 mmol), Trimethyl Phosphite (1 mmol), and Methanol (3 mL) at Room Temperature.
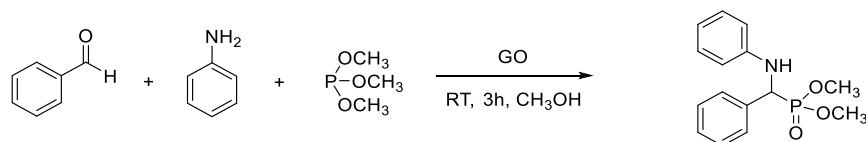
Scheme 4. Glycosylation Reaction of the Unprotected D-Glucose with Allyl Alcohol
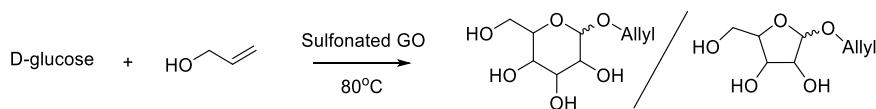
Scheme 5. Hydrogen Generation from Liquid Organic Hydrogen Carriers

$$NH_4^+HCOO^- \longrightarrow H_2 + CO_2 + NH_3$$

be readily recovered and recycled in dichloroethane solvent. To test the effectiveness of the catalysts for nucleophilic substitution processes, Yang et al.[121] explored the synthesis of iodine octane from NaI and chlorobenzene (Scheme 14). Among the GO and GO−Px catalysts, GO-P600 showed the best activity with 95% yield and nearly 100% selectivity.

Zarnegaryan et al.[103] studied cross-coupling reactions (Suzuki−Miyaura coupling) in the attendance of the GO−N_2S_2 using the reactions between phenyl boronic acid with 4-halo (Cl, I, and Br) nitrobenzene as shown in Scheme 15. The yield was 99% when GO−N_2S_2 was used with 4-iodo nitrobenzene and phenyl boronic acid.

In the synthesis of 3,4-dihydropyrimidinones, the clay−GO (10:1) nanocomposite gave good yields in a shorter period of time. Narayanan et al.[104] showed better results with GO as compared to the current reported catalysts (Scheme 16).

Styrene was oxidized according to the findings of Wu et al., who used Mn−salen−GO as a catalyst for the reaction. The yield was good (90%).[105]

Acocella et al.[106] investigated the effects of several graphite-based nanofillers in ring-opening reactions of epoxide (Scheme 17) triggered by amines for diglycidyl ether (DGEBA) or bisphenol. Their findings revealed that GO had a catalytic activity on epoxy resin cross-linking by amines as the viscosity of the reaction mixture increased with time, depicting an increase in polymerization/cross-linking (Figure 14).

In the reduction of 4-nitrobenzene with aqueous $NaBH_4$, Zhang et al.[107] studied the catalytic activity of the nano-composite to get the 4-aminobenzene in high yield (98%) as shown in Scheme 18.

Li et al.[108] established a radical addition approach in an O_2-assisted one-pot procedure to synthesize 3-trifluoroalkylated quinoxalin-2(1H)-ones under suitable conditions with 80 wt % of GO (Scheme 19). According to mechanical investigations, GO inhibited the synthesis of superoxide trifluoromethyl radicals, allowing it to execute an autotandem radical addition. In the absence of metal catalysts, this unusual multicomponent tandem process permitted access to CF_3-substituted quinox-alinones, whereas GO acted as the catalyst. These changes, in a larger sense, highlight the potential of GO as a catalyst in synthetic chemistry rather than solely as a source material to graphene-based products. GO helps CF_3SO_2Na to form the

electrophilic CF_3 radical, which allows for an addition reaction with alkynes to produce alkyl nucleophilic radicals that react with the quinoxalin-2(1H)-ones' C-3 position. With MeCN and ethyl acetate at 100 °C, 85% yield was recorded with 80 wt % of GO.

Eftekhar et al.[15] used a GO-functionalized copper complex for the synthesis of the 1,2,3-triazole derivative. This catalyst can efficiently catalyze the synthesis of 1,2,3-triazoles in H_2O. At first, the catalyst was dispersed in H_2O (10 mL) by sonication for 10 min, and then sodium azide, phenyl acetylene, and benzyl bromide were added to the mixture and refluxed to get the product of interest, that is, 1,2,3-triazole derivatives in a high yield of 95%.

Sachdeva et al.[109] reported a huge range of functional groups such as methoxy, methyl, or bromide present in either dicarbonyl compounds or nitroaniline along with aldehyde or ketone, providing promising transformations. GO/rGO can be used as a catalyst in a one-pot synthesis for good yields (83−95%) (Scheme 20). Catalysts can be recycled without losing any activity for up to four runs.

Ganesan et al.[110] exploited GO as a simple catalyst for the synthesis of β-aminoketones via a three-component Mannich reaction under moderate conditions, as shown in Scheme 21. Without any particular functionalization, native GO acts as a carbonaceous solid Bronsted acid catalyst, generating a range of β-aminoketones under metal-free conditions. The current catalytic technique eliminates the need for hazardous workup, and chromatographic purification produced a high yield of β-aminoketones. The catalyst can be used for up to six successive catalytic cycles without losing substantial activity.

Sarvi et al.[111] employed a ZnO-immobilized GO-based catalyst for the anaerobic oxidative conversion reaction of alcohols to nitriles in H_2O (Scheme 22). Under an oxygen balloon with a ZnO/GO catalyst, aliphatic/heteroaromatic/aromatic primary alcohols transformed to nitriles. Without considerable reduction in activity, ZnO/GO can be utilized for seven consecutive runs.

Mirheidari et al.[112] covalently attached an amino-function-alized SiO_2 sphere/cobalt combination to a GO surface. In the production of amino naphthoquinones in ethanol solvent, the catalyst demonstrated significant catalytic activity for one-pot synthesis to enhance the yield (96−98%) in a smaller span of time (5−8 min).

Kumar et al.[113] identified GO−MnO_2 as a possible catalyst for the production of chalcones by Claisen−Schmidt condensation (Scheme 23). When compared to pure MnO_2 and GO, the catalytic activity of GO−MnO_2 was better.
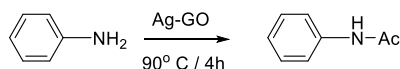
Scheme 6. Formation of Dihydropyrimidine (Biginelli Reaction) Based on Cinnamaldehyde
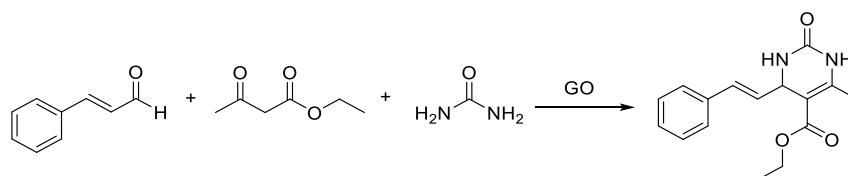
Scheme 7. Chan—Lam Coupling Reaction
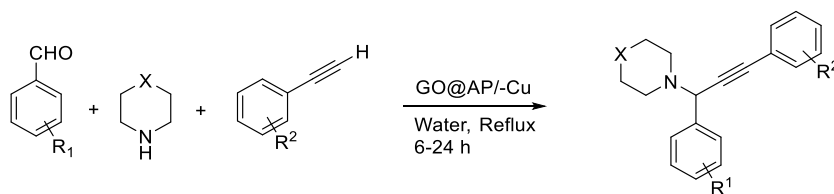
Scheme 8. Reaction between *p*-Hydroxybenzaldehyde and Nitromethane

$$HO-C_6H_4-CHO \;+\; H_3C-NO_2 \longrightarrow HO-C_6H_4-\underset{H}{\overset{H}{C}}=\underset{H}{C}-NO_2$$

**Scheme 9. Synthesis of Acetyl Aniline from Aniline with Ag—GO NPs as Catalyst**

Several reaction parameters, such as temperature, solvent polarity, and catalyst weight percent, were changed extensively to vary the reaction conditions. At 110 °C, under solventless circumstances, a high yield of chalcones was achieved in a short amount of time. The catalyst was easy to separate and may be reused several times with very slight activity changes. When compared to other catalysts described in the literature, the GO—MnO$_2$ nanocatalyst showed much higher activity in a shorter length of time.

Ulvan's chemical structure is made up of two disaccharide units, type A$_{3s}$ glucuronorhamnose and type B$_{3s}$ idurono-rhamnose, which are organized in a regular sequence inside the heteropolymer chain, as shown in Scheme 24.[114]

For esterification of fatty acid and trimethylolpropane, Su et al.[115] utilized a SnO@GO catalyst. It can facilitate the stoichiometric esterification of trimethylolpropane and fatty acids (C6—C10). The resulting lubricating oil production might be as high as 98%. Furthermore, the SnO@GO catalyst has a high reusability and minimal residual property in goods, making it an environmentally responsible and cost-effective

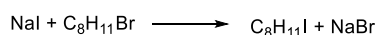**Scheme 11. Conversion of Benzaldehyde into β-Nitro Styrene**
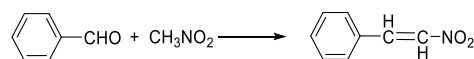
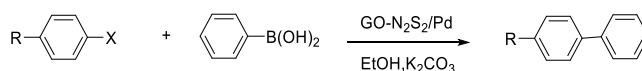
Scheme 12. Epoxidation of Cyclooctene
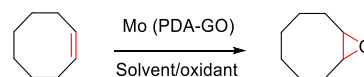
Scheme 13. Esterification Reaction between Lactic Acid and Ethanol
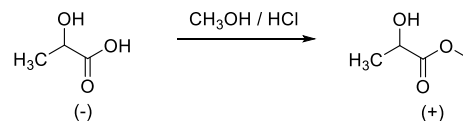
Scheme 14. Synthesis of Iodine Octane from Chlorobenzene and NaI via Nucleophilic Substitution

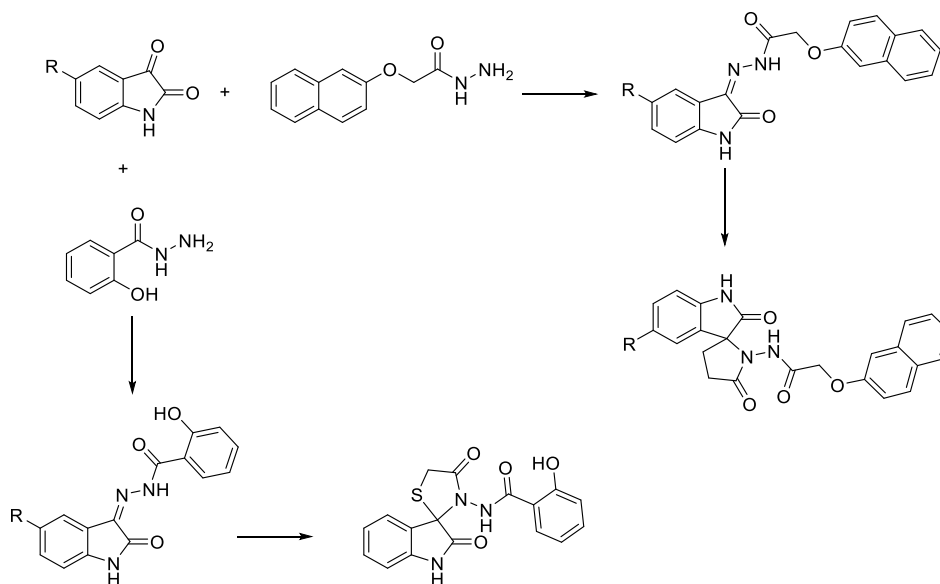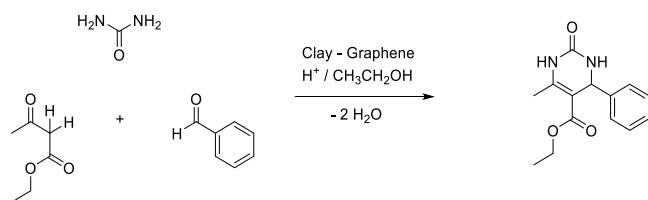$$NaI + C_8H_{11}Br \longrightarrow C_8H_{11}I + NaBr$$

Scheme 15. Suzuki—Miyaura Coupling

choice for the manufacturing of lubricating esters. The SnO@GO composition may be recycled up to six times without deactivating.

Scheme 10. Synthesis of Isatin-Linked Thiazolidine

Scheme 16[a]

[a]Reaction conditions for benzaldehyde:ethyl acetoacetate:urea are 1 mmol:1 mmol:1.3 mmol over 0.1 g of CG (clay−GO) at 130 °C.

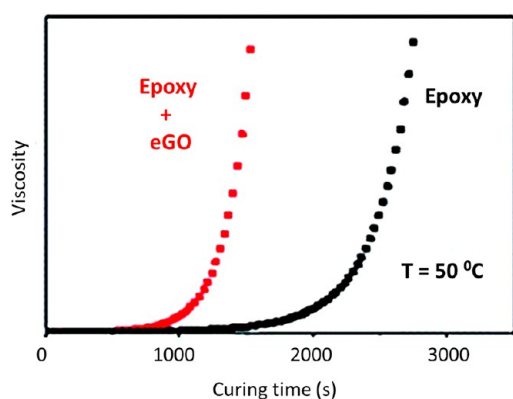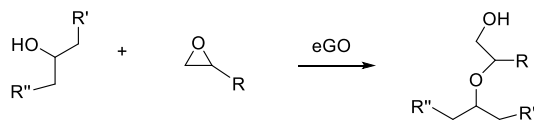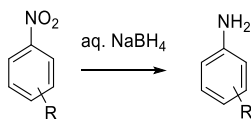**Scheme 17. Etherification Reaction in Amine Curing**

Figure 14. Viscosity vs curing time. Reproduced with permission from ref 106. Copyright@2016, Royal Society of Chemistry, Royal Society of Chemistry Advances (redrew the image from the information available).

Scheme 18. Reduction of 4-Nitrobenzene

Keshipour et al.[34] employed a two-component CuPc@GO/TiO$_2$ NP catalytic system to investigate the heterogeneous catalytic activity of phthalocyanines in the FA degradation process.

Dreyer et al.[116] reported many reactions for the hydration of alkynes, where GO was used as a catalyst (200 wt %) and the reaction mix was heated for 24 h at 373 K. A good conversion percentage was observed. Previously, it was reported that these reactions occur under acidic conditions at higher temperatures

Scheme 19. Synthesis of 3-Trifluoroalkylated Quinoxalin-2(1H)-ones

Scheme 20. GO/rGO-Catalyzed Synthesis of Quinoxalines from 2-Nitroaniline

R^1= H, Me, OMe, F
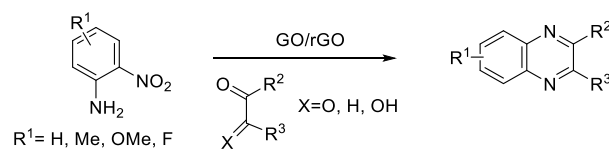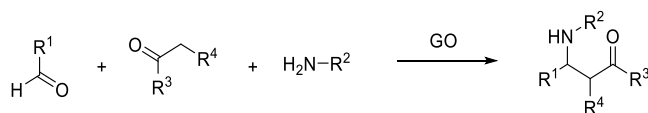
Scheme 21[a]

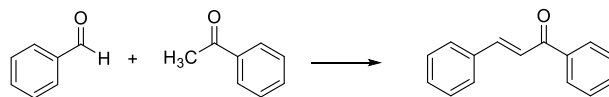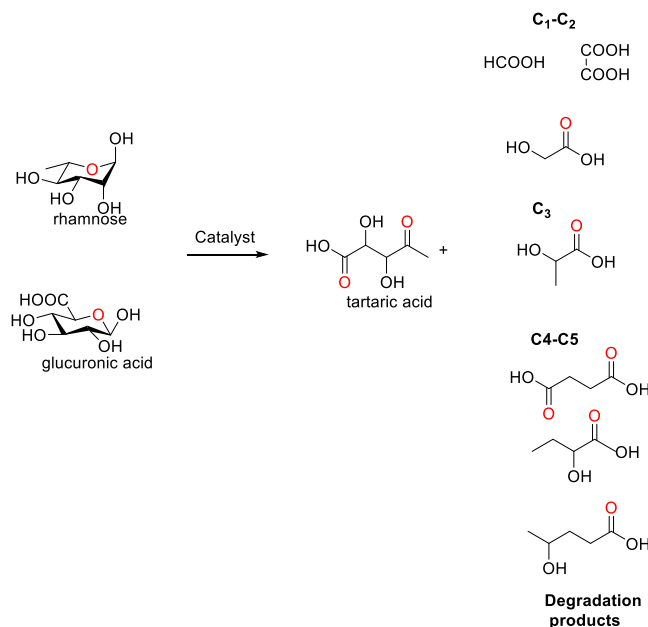[a]Reaction conditions: benzaldehyde (1 mmol), acetophenone (1 mmol), and nitrile (1 mmol). GO: 25 mg in 5 mL of solvent at room temperature for 24 h. The highest yield is 96% when ethanol is used as solvent.
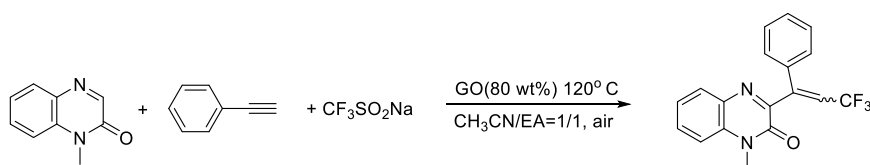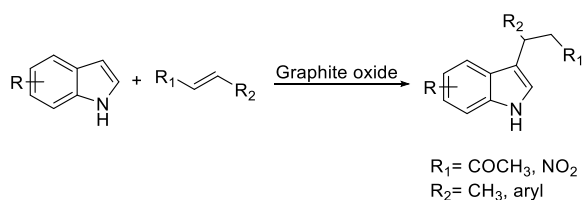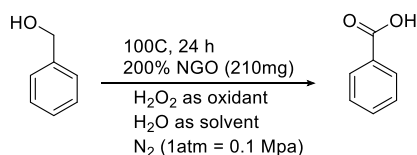
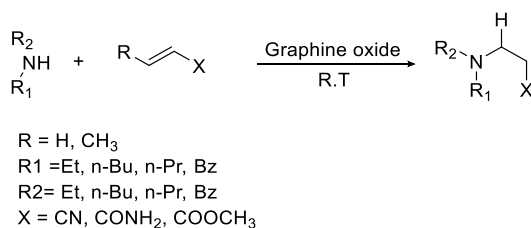**Scheme 22. Formation of Benzonitrile**
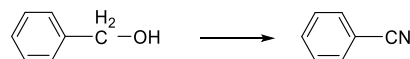
Scheme 23. Preparation of Chalcones via Claisen−Schmidt Condensation

Scheme 24. Hydrolysis of Ulvan Monosaccharides in the Presence of GO@SO$_3$CF$_3$

Scheme 25. Friedel–Crafts Addition of Indoles to α,β-Unsaturated Ketones and Nitro Styrene

R_1 = COCH$_3$, NO$_2$
R_2 = CH$_3$, aryl

Scheme 26. Oxidation of Benzyl Alcohol Using NGO as the Catalyst

100C, 24 h
200% NGO (210mg)
H$_2$O$_2$ as oxidant
H$_2$O as solvent
N$_2$ (1atm = 0.1 Mpa)

Scheme 27. aza-Michael Addition

Graphine oxide
R.T

R = H, CH$_3$
R1 = Et, n-Bu, n-Pr, Bz
R2 = Et, n-Bu, n-Pr, Bz
X = CN, CONH$_2$, COOCH$_3$

(473 K), but on inclusion of GO, the reaction temperature was lowered (373 K) along with increased conversion percentage.

Using GO as a catalyst, the Friedel–Crafts addition of indoles to α,β-unsaturated ketones and nitro styrene was investigated. As shown in Scheme 25, several indole compounds were synthesized with good yields. The manufacture of GO catalyst from easily available and simple raw ingredients makes this process more cost-effective.[117]

When the NGO catalyst was used to oxidize benzyl alcohol derivatives, the reaction continued past the aldehyde stage and yielded the corresponding carboxylic acid (Scheme 26). Based on the reaction optimization experiments, the optimal settings were 2.2 equiv of H$_2$O$_2$, 20% (mass fraction) of NGO, and 80 °C as the reaction temperature. The low yield for benzyl alcohol oxidation in the absence of NGO proved that NGO served as a good catalyst.[118]

GO is a simple and efficient catalyst for aza-Michael addition of amines and electron-deficient olefins. These reactions proceed under mild circumstances and produce high yields

in shorter durations (Scheme 27). The catalyst is easily recoverable and recyclable, with consistent catalytic activity.[119]
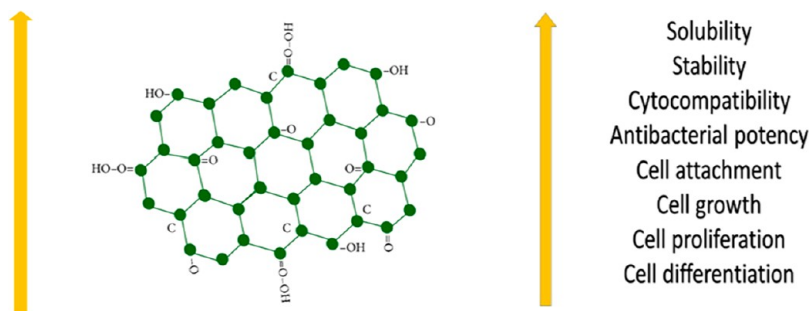
This procedure imparts GO with a high reactivity with 2,2,6,6-tetramethyl-piperidin-1-oxyl (TEMPO) as a cocatalyst for the selective oxidation of 5-hydroxymethylfurfural (HMF) to 2,5-diformylfuran (DFF) under specific conditions (100% HMF conversion with 99.6% HMF selectivity at 80 wt % GO loading and 1 atm air). According to this study, GO may act as an oxidant in the reduction of the −COOH groups in HMF during its anaerobic oxidation.[120]

6. APPLICATION OF GRAPHENE OXIDE IN TISSUE ENGINEERING

Tissue engineering, according to Vacanti et al., is the use of life science and engineering ideas for the production of biological substitutes that preserve and improve tissue function. Tissue engineering is a multidisciplinary area that includes mechanical engineering, clinical medicine, genetics, materials science, and other engineering and life science fields.[122] To create the right environment for tissue and organ regeneration, TE depends on the utilization of porous 3D scaffolds. Scaffolds are often embedded with cells and growth factors or are exposed to biophysical stimuli in bioreactors, which is a device or system that applies various forms of chemical or mechanical stimuli to cells. The scaffolds (cell-seeded) are either cultivated in vitro to produce tissues that may later be transplanted into a damaged location, or they are implanted directly into the wounded region, where tissue or organ regeneration is triggered in vivo, using the body's own mechanisms. The tissue engineering trio refers to the combination of cells, signals, and scaffolds. The 3D biomaterial before cells was inserted is referred to as the scaffold (in vitro or in vivo).

Scaffold requirements are as follows:

(i) Biocompatibility - Tissue engineering scaffolds must be biocompatible, and cells must stick to the surface, operate correctly, move freely in the scaffold, and begin to multiply before laying down a new matrix.

(ii) Biodegradability - In tissue engineering, the body's cells are expected to gradually replace the embedded scaffold over time. Scaffolds are not meant to be permanent. Thus, the scaffold should be biodegradable so that cells can create their own extracellular matrix. Degradation byproducts must be nontoxic and should escape the body without any side effects.

(iii) Mechanical properties - Scaffolds must have mechanical properties similar to the site on which they will be implanted.

Solubility
Stability
Cytocompatibility
Antibacterial potency
Cell attachment
Cell growth
Cell proliferation
Cell differentiation

Figure 15. General effect of a GO-based scaffold on biological and mechanical properties of tissues.
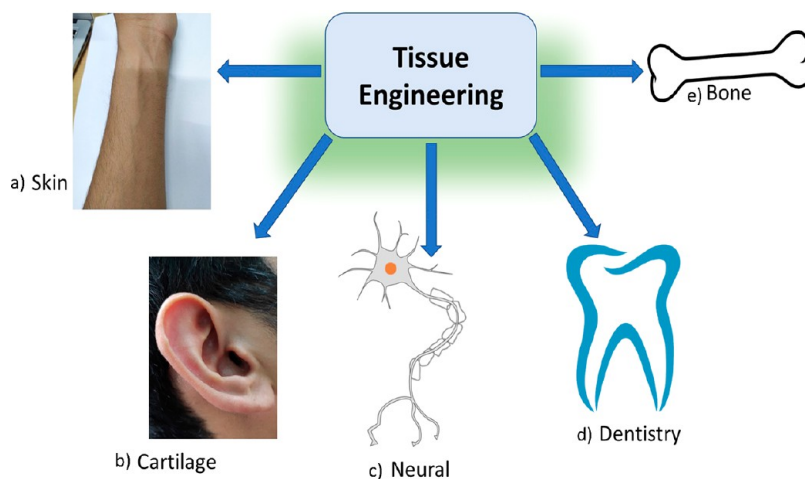
Figure 16. Tissue engineering for different body parts: (a) skin, (b) cartilage, (c) neural, (d) dentistry, and (e) bone.
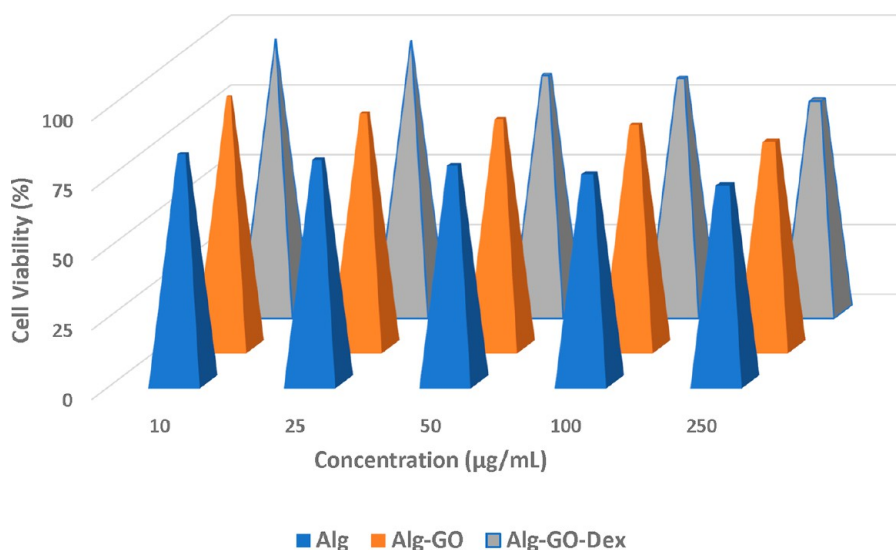

Figure 17. Effect of GO and others on cell viability with the MG-63 cell line by trypan blue dye exclusion. Reproduced with permission from ref 43. Copyright@2021, Elsevier Ltd., Journal of Drug Delivery Science and Technology (redrew the image from the information available).

Figure 18. Standard deviation of porosity values with varying concentrations of Dex microspheres. Reproduced with permission from ref 43. Copyright@2021, Elsevier Ltd., Journal of Drug Delivery Science and Technology (redrew the image from the information available).
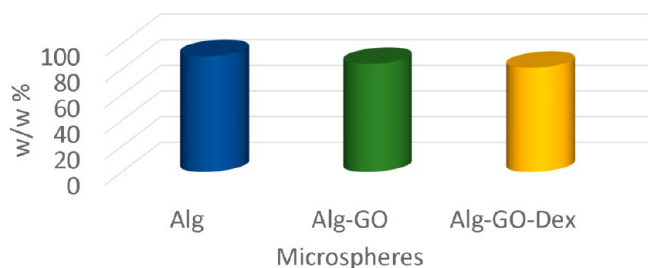
(iv) Scaffold architecture - To promote penetration into the cellular matrix and appropriate insertions of nutrients into cells within the scaffold and the extracellular matrix generated by these cells, scaffolds should have a connected pore structure with good porosity.

(v) Biomaterials - Scaffolds for tissue engineering are made from synthetic polymers, biomaterials, ceramics, and natural polymers.

The bioadaptability and preferential electroconductivity of GO as a biomaterial for tissue regeneration have piqued curiosity. GO has the potential to be used in the controlled growth of stem cells in vivo, the liberation of active biological factors from stem-cell-containing delivery systems, and the intracellular delivery of factors like growth factors, DNA, and synthetic proteins to modulate stem cell differentiation and proliferation. Growth factors (GFs), which play critical roles in migration, maturation, and proliferation, as well as the differentiation of immature precursors into functional tissues can be transported through GO because of properties like surface chemistry and size.[16] Figure 15 represents the general effect of GO-based scaffolds on biological and mechanical properties of tissues, whereas Figure 16 shows tissue engineering for different body parts.

6.1. Bone Tissue Engineering. In bone tissue engineering, GO is commonly employed. The goal of bone tissue engineering (BTE) is to successfully include bone regeneration at the defect location of the host while avoiding problems. BTE

Table 6. Different GO Scaffolds for Various Applications

| Entry	Scaffolds	Biological activity/Mechanical strength	Refs
1	GO−calcium phosphate nanocomposites	Synergistic enhancement of hMSC osteogenesis	126
2	GO-based tricomponent scaffolds	The role of GO composites was quite like that of real bone. In comparison to other composites, the GO−amylopectin−Hap composite demonstrated improved cytocompatibility, biocompatibility, and ALP activity, as well as increased cell proliferation and biocompatibility. This can be due to the larger pore size and porosity of the GO−amylopectin−Hap composite (studied in human osteosarcoma cells).	125
3	GO−hydroxyapatite/silk fibroin	The scaffold boosts mouse mesenchymal stem cell attachment, growth, and the production of osteogenic gene and osteogenic differentiation.	17
4	GO−poly-(ε-caprolactone)	GO−PCL possesses appropriate porosity and mechanical strength. GO's introduction improved the protein adsorption of fibers by up to 1%.	127
5	GO−chitosan−hyaluronic acid scaffold	Simvastatin-loaded composite scaffolds have shown to be biocompatible and may be employed as an osteoinductive scaffold in place of natural and synthetic polymer-based scaffolds (studied in Mouse osteoblast cells).	128
6	Aligned porous chitosan/GO scaffold	Advantages in mechanical strength, directing cell alignment, shape-memory, and protein adsorption.	129
7	Bidoped bioglass/GO nanocomposites	The biocompatibility of bioglass and its composite with GO was improved by bidoping.	130
8	Scaffold of gelatin−alginate−GO	Cell attachment and proliferation are improved.	131
9	Bioinspired polydopamine-coating-assisted electrospun polyurethane− GO nanofiber	Mineralization cell attachment and proliferation increases in coated constructs.	19
10	Nano GO	Hippo/Yes-associated protein (YAP) activates LPAR6 and stimulates the production of migratory tip cells via nano GO-coupled LPA (lysophosphatidic acid) without the need for reactive oxygen species (ROS) activation or further complex modifications.	132
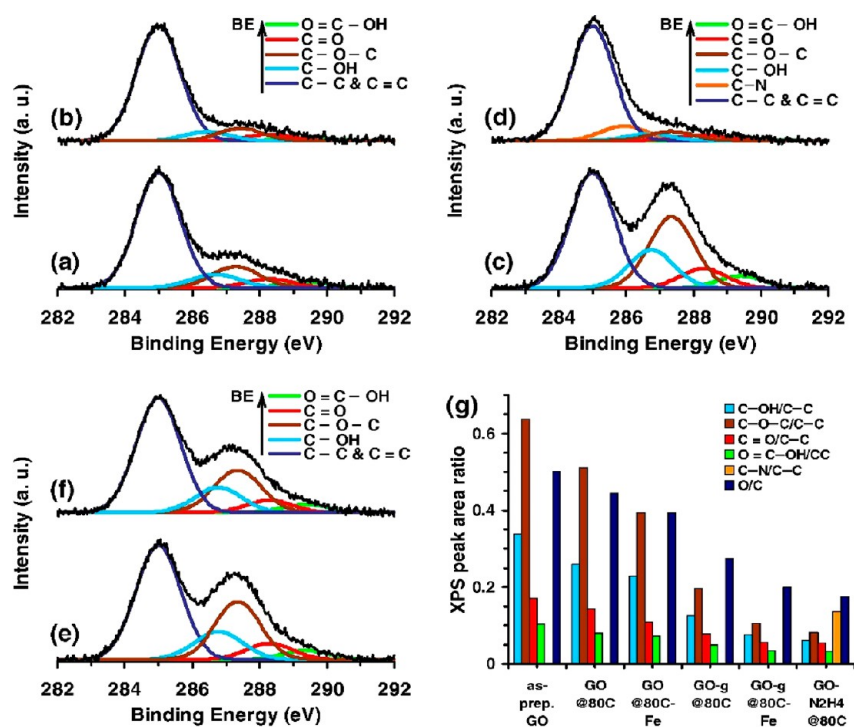
Figure 19. XPS peak deconvolution of the C(1s) core level of GO reduced by ginseng (a) in the absence and (b) in the presence of Fe catalyst, as compared to the spectra of (c) as-prepared GO and (d) the GO reduced by hydrazine (as benchmarks) as well as the GO heat treated (e) in the absence and (f) in the presence of Fe catalyst at 80 °C for 10 min. (g) The peak area ratios of the oxygen-containing bonds to the C−C bond for each sample. Reproduced with permission from ref 139. Copyright@2014 Elsevier Ltd., Carbon.

is made up of four main elements: osteogenic cells, a biocompatible framework or scaffold, vascularization, and morphogenetic signals. Bone tissue regeneration requires these following characteristics: (a) osteoinduction, which permits the biomaterial to encourage progenitor cells to differentiate into osteoblasts; (b) osteoconduction, which allows the biomaterial to assist bone tissue growth; and (c) osteointegration, which helps the biomaterial integrate with the surrounding bone tissue by supporting it. In the host environment, biomaterials should be stable mechanically and

chemically. For adequate bone tissue regeneration, the scaffold should be biocompatible, osteoconductive, and compatible with cell adhesion as well as proliferation on the surface and inside its pores; should have good mechanical characteristics and compressive strength for better cancellous and cortical bone; and should have pore interconnectivity (the sizes of the pore are essential for BTE so transportation of nutrients and oxygen is fluent) and good biodegradability. Important considerations in developing a scaffold for use in tissue engineering include biocompatibility and cytotoxicity. The
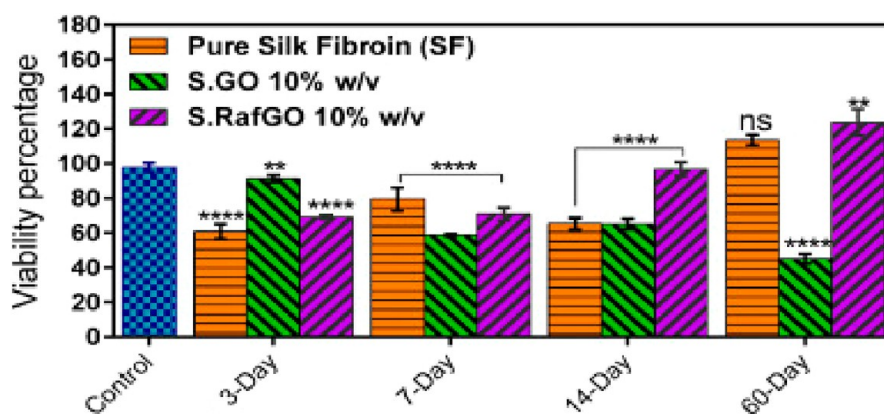
Figure 20. MTT assay plotted for viability of the scaffolds toward PC12 cells at time points of 3, 7, 14, and 60 days. Reproduced with permission from ref 140. Copyright@2021, Elsevier Ltd., Materials Science and Engineering: C.

Table 7. Various GO-Based Scaffolds for Neural Tissue

| Entry	Scaffolds	Biological activity/Mechanical strength	Refs
1	GO sheets	G-NFs (stable electrical conductivity, soft physical feature, and good biocompatibility).	141
2	Rolled GO foams	hNSCs (human neural stem cells) proliferate and differentiate effectively throughout the pores and interfaces of the scaffold.	142
3	GO acrylate sheets−CNT−poly(ethyleneglycol) acrylate−oligo(polyethyleneglycol fumarate) hydrogel	Cytotoxicity testing on PC12 cells demonstrated no significant cytotoxicity, and the hydrogel gives an ideal surrounding for neural outgrowth and cellular propagation. These findings imply that the hydrogel might be used in neural tissue engineering.	143
4	GO-coated PLLA-aligned nanofibers	The surface roughness and hydrophilicity of aligned PLLA nanofibers were enhanced by GO coating. It improved cell orientation and SC growth and stimulated PC12 neurite development and cell differentiation.	144
5	GO-based GPS having hierarchical structures	Neuroprosthetics and biosensors.	145
6	GO microfiber	Effective neural development substrate for the CNS after injury.	18
7	GO−PLGA hybrid nanofiber	Improves functional locomotor recovery, decreased the formation of cavity, and increased the number of neurons at the injury site.	22
8	GO aerogel	The development of fibro glandular tissues and structures is inhibited by GO in the neural canal. The multiplication and expansion of neural stem cells.	146
9	GO and electroactive rGO-based composite	Enhances electrical conductivity of the scaffold and enhances metabolic activity and proliferation.	147
10	GO foam (GOF)-based 3D scaffold	The hNSCs were effectively proliferated and differentiated throughout the scaffold because of the cross-section of the rolled GOF. Increased cell proliferation and faster neuron development were observed after electrical stimulation of hNSCs.	20
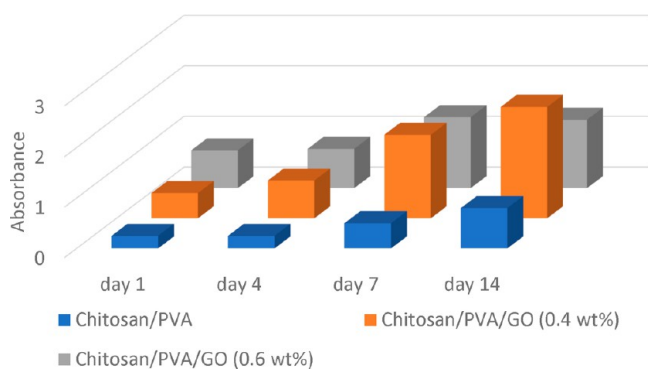
Figure 21. Growth of ATDC5 cells on chitosan/PVA/GO (6 wt %), chitosan/PVA/GO (4 wt %), and chitosan/PVA after 1, 4, 7, and 14 days of culture. Reproduced with permission from ref 21. Copyright@ 2017, Elsevier Ltd., Materials Science and Engineering C (redrew the image from the information available).

effect of GO and other compounds on MG-63 cell viability is depicted in Figure 17.[43]

Alginate microspheres have a porosity of roughly 92%, while alginate−GO microspheres have a porosity of around 87%. The porosity of alginate−GO−dexamethasone was 84%, which was lower than the porosity of alginate and alginate−GO microspheres, indicating that dexamethasone is likely cross-

linked with alginate and GO. The unique composite microsphere (alginate−GO−dexamethasone), which stimulates cell migration and enhances bone regeneration, has a porosity of more than 80% (Figure 18). The observed porosity difference is observed due the hydrophilic functional group.[43]

The recent research in BTE has concentrated on the design of porous biomaterials with a superior biocompatible and mechanical reinforcement matrix that replicates the behavior, form, and microstructure of bone (Table 6). GO has the potential to be lighter than air, have good electrical and mechanical conductivity qualities, and have a high capacity for heat isolation and absorption that makes it effective in tissue engineering applications. Lee et al. explained the significant noncovalent binding properties of GO, which make it possible for it to serve as a preconcentration base for osteogenic inducers, causing quicker MSC growth in the direction of the osteogenic lineage. To study the binding properties of GO and rGO toward various growth factors allows researchers to better understand the molecular causes of rapid differentiation.[123] Omid Akhwan synthesized graphene nanogrids and studied the differentiation and proliferation of hMSCs, which were facilitated by the use of GO as selective 2D templates. Especially in comparison to those that flourished on graphene sheets and PDMS, the size of the cytoskeleton fibers on nanogrids was much lower. The rGONR grids demonstrated
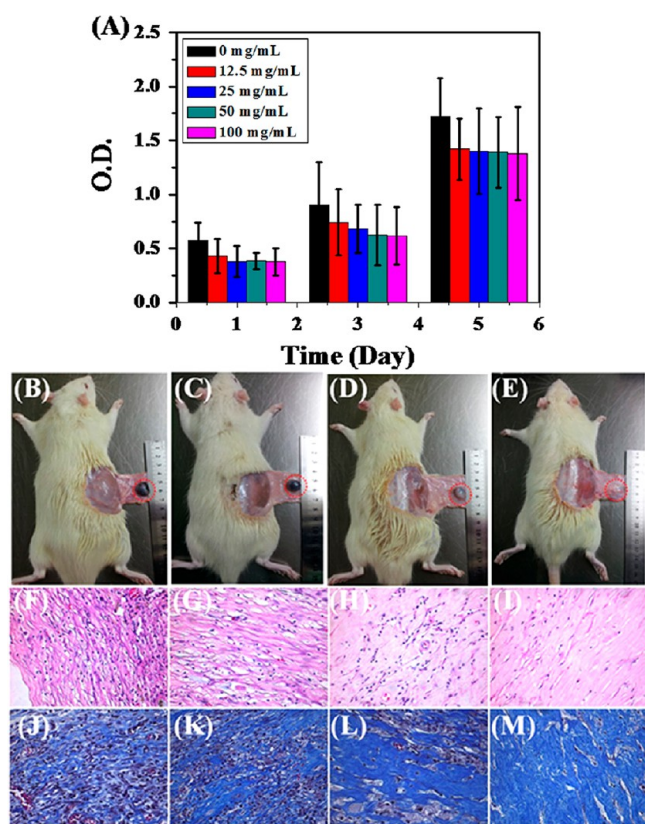
Figure 22. (A) Cell viability of 3T3 cells in the leachates of the scaffold. The photographs of subcutaneous implanted CSMA/PECA/GO scaffold on the back of mice for (B) 1, (C) 2, (D) 4, and (E) 8 weeks. Histological section of the subcutaneous implanted CSMA/PECA/GO scaffold for different periods. Images F, G, H, and I were of H&E staining at 1, 2, 4, and 8 weeks. (J), (K), (L), and (M) were of Masson staining at the same time as H&E staining (original magnification × 400). Reproduced with permission from ref 148. Copyright@2015, Nature, Scientific reports (open access).

the hMSCs' quickest osteogenic development when the chemical inducers were present.[124] The composite scaffolds showed different decomposition behavior with time. Rapid and high decomposition could be deduced with the glycosidic bond cleavage of β-G and bacterial cellulose.[125]

6.2. Neural Tissue Engineering. GO may help nerve regeneration by increasing the rate of neural differentiation in embryonic and neural stem cells. Seeding of GO with a bioactive component to increase the biological activity is facilitated by its various functional groups. NSC survival, proliferation, and neuronal differentiation can all be enhanced by a PLGA/GO-TH composite (L-theanine).[133] In an in vivo investigation, GO release and PCL (polycaprolactone) biodegradation are investigated. A 15 mm sciatic nerve deficit might be effectively repaired using the GO/PCL nerve conduit.[134]

The shapes of graphene-based nanomaterials might change their firmness and flexibility in addition to affecting how they interact with cells and tissues.[135] Akhavan et al. synthsised self-organized hNSCs with the pulser laser simulation. The prepared sample was tested and found to be more biocompatible, thermally, and electrical conductive.[136] Heo et al. developed a noncontact electric field stimulation procedure and a graphene/PET stimulator that can improve brain cell-to-cell communication in vitro. A modest electric field encourages the formation of new cell-to-cell coupling and strengthens already-existing connection. Using a graphene/PET stimulator provides good flexibility and transmittance, as well as a weak field operation with a high electric field optical amplifier. These alterations in cell-to-cell interaction were caused by these abnormalities in the regulation of protein synthesis involved in cell mobility in conjunction with the cytoskeleton.[137]

The research revealed that rGO/TiO_2 works as a biocompatible stimulator for efficient development of hNSCs into neurons. On rGO/TiO_2, the differentiation of cell nuclei grew 1.5 times in response to the stimulation, but on TiO_2 and GO/TiO_2, it was enhanced by just 24% and 48%, respectively.[138]

The amount of deoxygenation and electrical conductivity for GO sheets was the same with ginseng and hydrazine. In an aqueous solution, the ginseng—rGO showed better stability against agglomeration as compared to hydrazine—rGO, as observed from XPS and shown in Figure 19. Despite that the aquaphobic film of hydrazine—rGO has little toxicity against hNSCs, no substantial cell proliferation was seen in these films.[139]

6.3. Scaffolds in PC12 Cells. From 3 to 60 days, the biocompatibility of the silk fibroin—raffinose trisaccharide—GO toward PC12 (rat pheochromocytoma) cells improves gradually (Figure 20).[140]

6.4. Cartilage Tissue Engineering. Cartilage damage can occur as a result of an accident or as a result of illnesses like osteoarthritis. Tissue engineering utilizing mesenchymal stem cells (MSCs) is a regenerative therapeutic technique that includes three fundamental components: (1) stem cells, (2)

Table 8. Different GO-Based Scaffolds for Cartilage Tissue Engineering

| Entry	Scaffolds	Biological activity/mechanical properties	refs
1	CSMA/PECA/GO	CSMA/PECA/GO was not toxic and was biocompatible with favorable breakdown time for cartilage tissue regeneration.	148
2	Chitosan/PVA/GO polymer	Addition of GO increased the nanofiber's mechanical qualities without compromising its biocompatibility.	21
3	GO	TGF-β3 (growth factor) was adsorbed with no significant conformational change and better stability.	149
4	GO—PLGA hybrid microparticles	Promotes the development of human embryonic cartilage rudiment cells into osteogenic cells.	22
5	GO-containing chitosan scaffolds	Human articular chondrocytes cultured for prolonged periods of time after being deposited on nanocomposite scaffolds showed increased proliferation with increasing GO percent (14 days).	23
6	GO-incorporated hydrogels	Better mechanical strength and compressive modulus as well as continued release of TGF-β3.	150
7	GO-modified 3D acellular cartilage extracellular matrix scaffold	The internal structure and mechanical characteristics of the scaffold are improved by GO modification. In vitro, the GO-modified composite scaffold (2 mg/mL) increases cell adhesion, proliferation, and chondrogenic differentiation. The composite scaffold displayed high biocompatibility and a minimal inflammatory reaction in rats after being implanted subcutaneously.	151
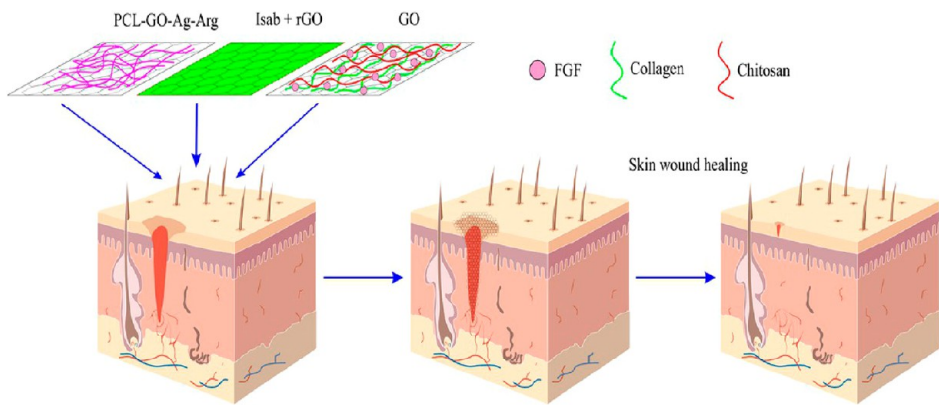
Figure 23. Different concentrations of PCL-GO-Ag-Arg against L929 mouse fibroblast cells. Reproduced with permission from ref 152. Copyright@ 2020, De Gruyter, Biomolecular Concept.
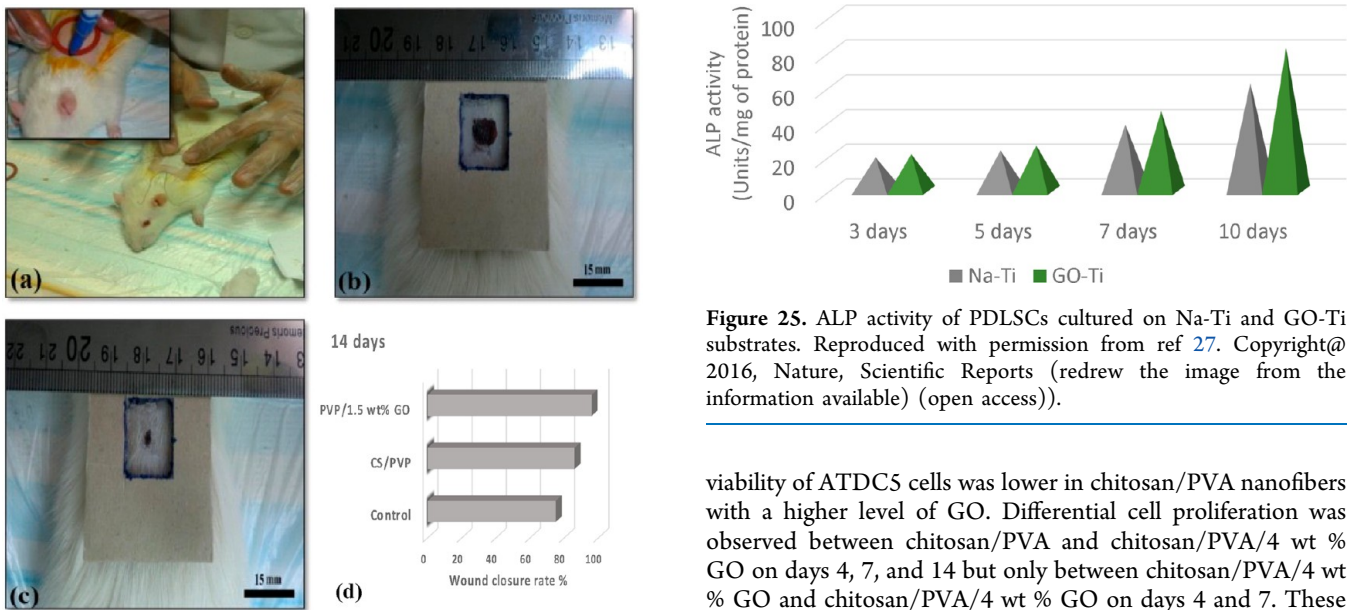

Figure 24. (a) Surgery process of a rat for implanting nanofibrous membranes on an open wound and wound healing 14 days postsurgery for (b) a pristine CS-based mat and (c) 1.5% GO-containing membrane. (d) Wound closure rate for the examined materials compared with the control. Reproduced with permission from ref 153. Copyright@ 2017, Elsevier Ltd., Materials Science and Engineering: C.
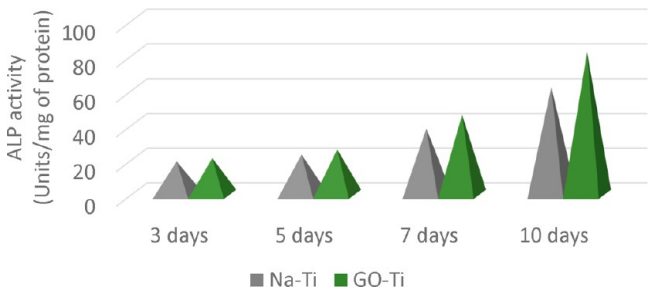

Figure 25. ALP activity of PDLSCs cultured on Na-Ti and GO-Ti substrates. Reproduced with permission from ref 27. Copyright@ 2016, Nature, Scientific Reports (redrew the image from the information available) (open access)).

viability of ATDC5 cells was lower in chitosan/PVA nanofibers with a higher level of GO. Differential cell proliferation was observed between chitosan/PVA and chitosan/PVA/4 wt % GO on days 4, 7, and 14 but only between chitosan/PVA/4 wt % GO and chitosan/PVA/4 wt % GO on days 4 and 7. These results show that cell division is increased over time (Figure 21).[21]

Internal implantation of the CSMA/PECA/GO scaffold was done by varying the concentrations and period of exposure (1, 2, 4, and 8 weeks). It has been observed that there is a significant increase in cell viability as the period of exposure increases. The implanted composite on the mice slowly degraded over a period of time, as shown in Figure 22.

Liao et al. studied the subcutaneous implantation of CSMA/PECA/GO scaffolds in a rat animal model. The scaffold's morphology varied over time after it was implanted (Table 8). The deterioration of the hybrid scaffold progressed in tandem

three-dimensional scaffolds, and (3) growth factors (GFs) (Table 7).[21] After 14 days, ATDC5 cell viability was greater in the chitosan/PVA/GO than in the chitosan/PVA, but the

Table 9. Different GO-Based Scaffolds for Skin Tissue Engineering

Entry	Scaffolds	Biological activity and mechanical strength	Refs
1	GO and graphene sheets	GSs are more cytotoxic as compared to GO when aggregated on fibroblast. GSs are more closely connected and release more reactive oxygen species when attached to skin cells.	154
2	PEGylated GO-mediated quercetin hybrid scaffold	The hybrid scaffold had a biocompatible, cell-adhesive surface for promoting MSC attachment and proliferation.	24
3	GO—genipin	The degradation rate of pure ECM sponges was found to be substantially greater than that of genipin-cross-linked ECM sponges.	25
4	Scaffolds of polycaprolactone/polyurethane composite with GO	Adding GO to a PU/PCL composite can improve scaffold hydrophilicity and biocompatibility.	155
5	Chitosan—PV—GO nanocomposite scaffold	L929 cells could adhere on the 50CS—50PVA/3 wt % GO scaffold.	26

Table 10. Different GO-Based Scaffolds for Dental Tissue Engineering Applications

Entry	Scaffolds	Biological activity/mechanical strength	Refs
1	GO—silk fibroin	PDLSCs (periodontol ligament stem cells) in GO—fibroin showed a discrete proliferation.	157
2	Sodium titanate with GO	PDLSC's higher proliferation and higher alkaline phosphatase activity.	27
3	GO—titanium—silver scaffold	Improvement in cell osteogenic differentiation, biocompatibility, cell proliferation, and antibacterial qualities.	29
4	GO-copper-coated CaP nanocomposite	Enhance the attachment and osteogenic growth of rat BMSCs.	158

with the implantation. It took two months for the scaffold to totally decay.[148]

6.5. Skin Tissue Engineering. New skin tissue engineering methodologies have been created that have the ability to imitate the biological features of natural tissue with a high degree of intricacy, flexibility, and repeatability. Biocompatibility, morphology, pore size, porosity, mechanical strength, and water absorption capability of hybrid scaffolds are all improved by GO concentration (Figure 23).

The biological performance of a GO-modified chitosan/PVP nanocomposite was examined by Mahmoudi et al. In the rat, electronic pictures demonstrate that nanofibrous membranes and GO have a significant influence on wound closure, as shown in Figure 24 and Table 9. The inclusion of GO nanosheets provides additional benefits in terms of strength, permeability, and cell attachment. There were no signs of scarring or inflammation in the region that was evaluated.[153]

6.6. Tissue Engineering in Dentistry. Antimicrobial activity, regenerative dentistry, oral cancer therapy, drug delivery, improvement of dental biomaterials, and BTE are all possible using GO in dentistry. Because of its biocompatibility, GO scaffolds can be used in bone tissue regeneration, osteointegration, and cell growth. Researchers have also developed GO for biofilm, which takes preventions and changes on the surface for better antibiofilm and antiadhesion capabilities.[156] The bioactivity of periodontal stem cells on Na_2TiO_3 coated with GO was investigated by Zhou et al. ALP activity has long been employed as a marker for osteoblast-like cells. On days 7 and 10, PDLSCs on GO—Ti substrates displayed higher ALP activity than those on Na—Ti substrates (Figure 25 and Table 10), showing that the presence of GO promoted an early stage of bone formation.[27]

7. PHOTOCATALYTIC BEHAVIOR OF GRAPHENE OXIDE

The basic mechanism behind the photocatalytic reactions involves irradiation of the photocatalyst surface with light energy equal to more than the band gap of photocatalysts. After absorption of energy containing light photons, the electrons get excited. The transfer of electrons from the valence band (VB) to the conduction band (CB) of holes is generated in the VB. These electrons and holes in the CB and VB eventually migrate to the photocatalyst's surface for photocatalytic reactions.

GO attracts researchers' attention toward photocatalytic reactions because its band gap is easily tunable. Moreover, it paved its way for being an electron-trapping layer. In the mechanism of photocatalysis, there are possibilities that the photogenerated charge carriers might recombine and stop the photocatalytic activity. GO serves as a support to prevent this charge recombination by forming heterojunctions or composites with other materials. The formation of the heterojunction enables transfer of electrons from one material to another; i.e., the photogenerated charge carriers lie on the surface of different materials, and hence their probability to recombine is
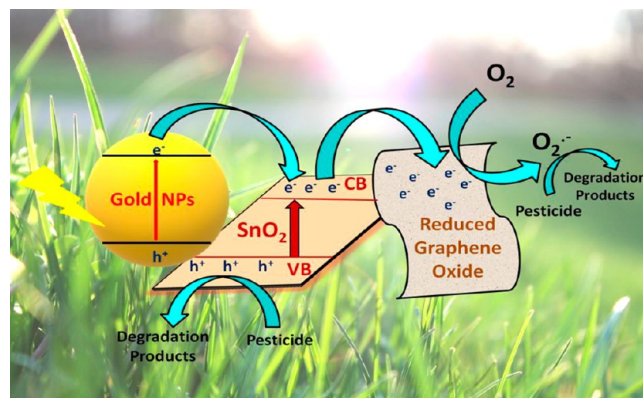

Figure 26. Schematic representation for electron transfer in the Au—SnO_2—rGO heterojunction. Reproduced with permission from ref 161. Copyright@2020, Elsevier Ltd., Journal of Hazardous Materials.

prohibited. Three major photocatalytic applications of GO are, i.e., photocatalytic hydrogen generation, photocatalytic CO_2 reduction, and photocatalytic degradation of organic contaminants.

7.1. Photocatalytic Degradation of Organic Contaminants. Industrialization has been increasing on a very fast pace which ultimately leads to a scarcity of energy resources and a release of toxic organic contaminants into the environment. An increasing population results in increasing energy demands. These contaminants have dangerous effects on the environment as well as on human health. Looking at freshwater scarcity, it has become an essential need to provide fresh water. Photocatalysis has been an easy and useful technique to deal with these environmental concerns. The primary source being sunlight, present abundantly in this method, makes it superior over other alternative methods present to deal with environmental concerns.

GO-based semiconductor composites have been most appropriately utilized in the photocatalysis process for environmental pollutants. The chemically active surface of GO causes different organic entities to get attached to its surface, which ultimately modify its electronic properties. The binding of different pollutants to the GO surface is due to π—π interaction between aromatic pollutants and sp^2-hybridized graphene.[159] This property of GO is of utmost use in photocatalysis, as GO can improve the photocatalytic behavior of various semiconducting materials by forming composites or heterojunctions with them. GO has been known to enhance the photoactive response of metal oxides such as ZnO. A combination of ZnO with GO exhibited remarkable photocatalytic performance due to the ability of GO to decrease the aggregation of ZnO particles, acting as an electron acceptor and inhibiting charge recombination. ZnO—GO hybrid material has been reported to degrade methylene blue (MB) dye with a photocatalytic efficiency of 80%. The oxygen functional groups of GO interact with those of ZnO, facilitating electron transfer from ZnO to GO upon light
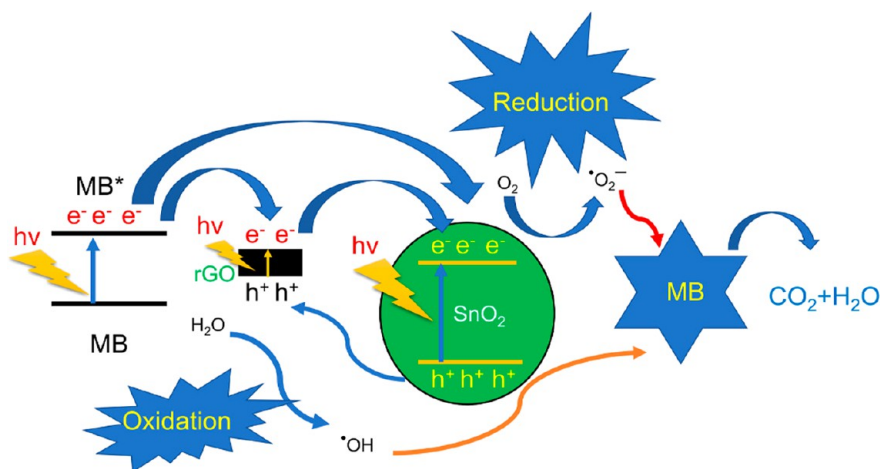
Figure 27. Schematic of the generation of electron−hole pairs, charge transfer, and the degradation of MB pollutant dye through oxidation and reduction reactions. Reproduced with permission from ref 166. Copyright@2022, Elsevier Ltd., Optical Materials.

irradiation. In this way, GO contributes to an enhancement of photoactivity of ZnO by reducing charge recombination.[160] Mohanta et al. fabricated a ternary heterojunction, i.e., Au−SnO$_2$−rGO, for photocatalytic degradation of clothianidin. rGO by serving as an electron sink prohibits an electron−hole recombination process.[161] The mechanism of the electron transfer in Au−SnO$_2$−rGO has been shown in Figure 26.

Akhavan et al. synthesized GO platelets and deposited them on anatase TiO$_2$ thin films. These GO platelets were reduced at different irradiation times, and the reduced platelets were utilized for *E. coli*'s degradation photocatalytically. Under solar light irradiation, the photoactivity for bacterial degradation was enhanced by a factor of 7.5.[162] Also, Akhavan et al. explored graphene-tungsten oxide-based composite film for photoinactivation and photodegradation of viruses.[163] Another graphene-based nanocomposite, i.e., the sulfur-doped GO/Ag$_3$VO$_4$ nanocomposite, was found to exhibit excellent photocatalytic degradation of cationic and anionic dyes. Also, the nanocomposite photocatalytically degraded dithiocarbamate fungicide thiram within 1 h to yield thiourea as a product. The nanocomposite was reported to show complete mineralization with more than 90% organic content removal.[164] Graphene/TiO$_2$ composite films with sheet-like surface morphology exhibited excellent photocatalytic performance by inducing cytotoxicity on the *C. elegans* nematode. This photoinactivation of the nematodes was attributed to the high-level reactive oxygen species (ROS) generation under solar light irradiation.[165]

Tuan et al. synthesized SnO$_2$−rGO nanocomposites via a one-step simple hydrothermal method for photoassisted degradation of MB. The 90% photocatalytic degradation of MB using SnO$_2$−rGO nanocomposites over 30% photocatalytic degradation by SnO$_2$ signifies the importance of GO. Band gap narrowing was observed in SnO$_2$ on doping with rGO. The band gap changes from 3.93 to 3.13 eV for SnO$_2$ to 2% SnO$_2$−rGO. rGO has been playing the following major roles in the photodegradation of MB using this composite: increasing the adsorption capacity of MB over the composite's surface, reducing the band gap along with the formation of a large no. of electrons and holes, and reducing the recombination of carriers, etc. The basic mechanism of the work is displayed in Figure 27.[166]

A metal−organic framework (MOF) composite with graphene, i.e., MIL-68(In)-NH$_2$/GO has been reported to exhibit increased photocatalytic activity for amoxicillin (AMX) degradation. The enhanced activity (93% degradation) for the composite has been attributed to GO which acts as an efficient electron transporter.[30] Concerning the photocatalytic behavior of GO, one of the key points is band gap opening as well as engineering of GO-based materials. One of the methods for band gap engineering of GO is fabrication of a graphene nanomesh. The GO sheets were vertically immobilized at the surface of ZnO NRs having a diameter of 140 nm and less than 1 μm of average length to achieve graphene nanomeshes via local photodegradation of GO sheets. The graphene nanomeshes have shorter oxygen-containing carbon bonds and higher carbon defects. Moreover, the valence band of GO sheets was found to be at different energies than Fermi energy levels. For graphene nanomeshes, binding energies of 1.6 were discovered to be the closest to the Fermi energy level. These materials can be utilized to stimulate hNSC using NIR photocatalysis. The hNSC's proliferation on the GO nanomeshes was correlated to the presence of excess oxygen functional groups formed on the edge of the GO nanomeshes that leads to superhydrophilicity of the surface. The graphene layers revealed cell differentiations, higher differentiation of neurons than glia, and more elongations of the cells under NIR laser stimulation.[167] These semiconductor nanomeshes have been used to laser-stimulate human brain stem cells. With a band gap energy of 1 eV, GO nanomeshes were created by Akhavan et al. and successfully used in NIR laser stimulation of hNSC differentiation into nerve cells. A few other GO-based composites for removal of certain organic pollutants, such as gaseous benzene, oxytetracycline, heavy metals, etc., in the environment have been reported in Table 11.

7.2. Photocatalytic Approach to Generate Hydrogen via Splitting of Water. Coupling GO with semiconductors has been a fascinating approach for photocatalytic H$_2$ generation during water-splitting reactions. This coupling should be appropriate, keeping in mind the band position of both GO and the semiconductor. GO-supported semiconductors have been reported to show higher yields of hydrogen in photocatalytic water-splitting reactions. This has been attributed to properties of GO, such as expanding light absorption tendency and acting as a supporting material to

Table 11. List of Some Important Examples of Photocatalytic Degradation of Organic Contaminants Using GO-Based Photocatalysts

| Graphene-oxide-based entity	Method of preparation	Photocatalytic activity	Degradation efficiency	Role of GO	Refs
MIL-68(In)-NH$_2$/GO composite	Hummers method	Degradation of amoxicillin	93% in 120 min	GO acts as an electron transporter by inhibiting recombination of photogenerated charge carriers	30
Nb-doped TiO$_2$ nanotube/rGO	Hydrothermal method	Degradation of methylene blue	95% in 30 min	Formation of electron transport channel by GO contributing toward photoinduced charge separation	31
ZnO–GO hybrid	Ultrasonication	Degradation of methylene blue	80% in 70 min	Photoinduced charge transfer interactions contributing to reduced charge recombination	160
Anatase TiO$_2$–GO nanocomposite	Solvothermal method	Degradation of gaseous benzene	-	Synergistic effect of graphene and TiO$_2$ results in efficient charge separation	32
Honeycomb-like TiO$_2$@GO nanocomposites	Solvothermal method	Degradation of oxytetracycline		Graphene-promoted red shift of absorption band and improved absorption efficiency of TiO$_2$@GO	168
ZnO/CdS/RGO composites	Hydrothermal process	Removal of Cr(VI) ions	93.2%	RGO-reduced agglomeration of NPs and increased specific surface area	169
Photoreduced GO/TiO	UV-assisted photoreduction method	Removal of VOC (methanol)	100% in 40 min	Suppression of charge recombination	170
SnO$_2$/rGO nanocomposite	Hydrothermal method	Degradation of methylene blue	90%	rGO reduced the band gap of SnO$_2$, making it photocatalytically efficient	166
Au–SnO$_2$–rGO	Microwave irradiation	Degradation of clothianidin	97%	rGO decreased the charge recombination rate by acting as an electron sink	161
GO/TiO$_2$	Sol–gel, Hummers method	Degradation of E. coli	7.5 times better degradation	Reduction of GO platelets to graphene, thereby improving antibacterial activity	162
S-doped GO (sGO)/Ag$_3$VO$_4$	Modified Hummers method	Degradation of methylene blue, rhodamine B, and acid red 18	3.67, 49, 50, and 3.19 times better degradation for Ag$_3$VO$_4$, sGO, and sGO/Ag$_3$VO$_4$, respectively	sGO is an excellent carrier separator boosted by electrons and surface defects	164
Graphene–TiO$_2$	Drop casting method	Degradation of Caenorhabditis elegans	19 times better degradation	The rate of recombination of photoexcited electron–hole pairs is slowed down by graphene	165
GO–tungsten (W)	Modified Hummers method	Degradation of bacteriophage MS2 virus (having RNA genome enveloped in protein capsid)	<10% reduction in the RNA efflux	Trapping cells within aggregated graphene nanosheets	163
	Drop casting method			Generation of ROS by graphene	
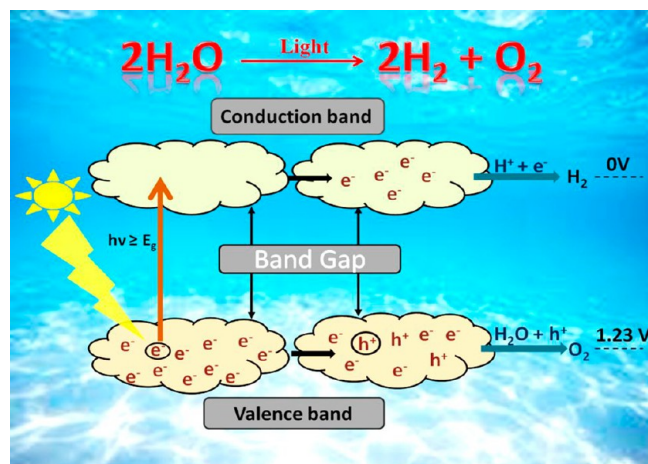
Figure 28. Schematic representation for the mechanism of photocatalytic water splitting. Reproduced with permission from ref 171. Copyright@2022, Royal Society of Chemistry, New Journal of Chemistry.
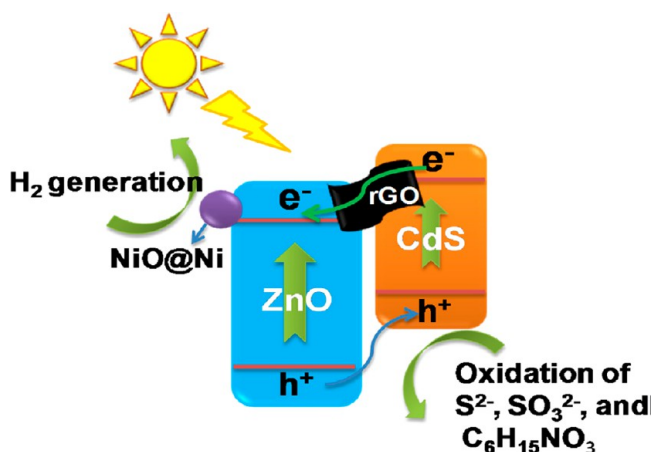

Figure 29. Scheme of the photocatalytic reaction process in the NiO@Ni-ZnO/rGO/CdS heterostructure. Reproduced with permission from ref 172. Copyright@2017, Elsevier Ltd., Applied Surface Science.

prevent charge recombination. Figure 28 provides a basic mechanism of water splitting by a photocatalytic approach.[171]

Wang et al. prepared a CuS-ZnO/rGO/CdS composite for visible-light-induced H_2 production (Figure 29). The heterostructure showed a good photocatalytic hydrogen generation rate of 1073 μmol/h/g. The role of rGO in this heterostructure has been justified, as it prevents the agglomeration of Zn particles during synthesis, serves as a migration channel to provide efficient separation of photogenerated charge carriers, and hence helps in improvement of the migration rate. The role of rGO as a carrier transport channel has also been depicted by Chen et al. in photocatalytic H_2 generation using the NiO@Ni-ZnO/rGO/CdS heterostructure. The higher hydrogen rate using this heterostructure has been attributed to the synergistic effect between ZnO and CdS supported by rGO which behaves as a transport channel for the flow of photoexcited carriers.[172] Wang et al. synthesized the rGO/Pt-TiO_2 nanocomposite and found that the composite exhibited a photocatalytic hydrogen generation efficiency of 1075.68 μmol/h/g. rGO in the composite developed synergetic interactions with TiO_2 to improve the absorption of light tendency and efficient charge separation, which results in excellent hydrogen generation rate, found to be 5-fold and 81-fold greater than Pt/TiO_2 and pure TiO_2, respectively.[173] There are various studies on the hydrogen generation through water-splitting reactions using GO-based photocatalysts tabulated in Table 12.

7.3. Photocatalytic CO_2 Reduction. The significant rise in global temperature due to an increase in greenhouse gases is the most challenging concern of this century. Graphene, being a narrow band gap photocatalyst, has shown immense results with respect to photocatalytic CO_2 reduction in Table 13. The rational design of graphene with wide band gap materials to develop graphene-based photocatalysts has been currently drawing researchers' attention. The Cu_2O/rGO composite has been reported for photoreduction of CO_2. In the microwave-assisted fabrication of this composite, rGO not only prevents the charge recombination by electron trapping but also improves the stability of Cu_2O by acting as a stabilizer. The stability of Cu_2O after fabrication of rGO was analyzed through inductively coupled plasma optical emission spectrometry (ICP-OES). The results showed that Cu_2O under-

Table 12. List of Some Important Examples of Hydrogen Generation through Water-Splitting Reaction Using GO-Based Photocatalysts

Photocatalyst	Preparation methods	Photocatalytic efficiency	Refs
Dye-sensitized GO	Hummers method	-	174
S,N-codoped GO quantum dots	Hydrothermal method	6.138 mol/h/g	33
Copper phthalocyanine@GO/TiO_2	Microwave+sonication	1.65 mmol	34
Ni_xCo_{1-x}P/rGO/g-C_3N_4	Calcination	576.7 μmol/h/g	175
GO−CdS−Pt nanocomposite	Reduction of formic acid and two-phase mixing method	123 mL/h/g	35
rGO/Pt−TiO_2 nanocomposite	Hummers method	1075.68 μmol/h/g	173
Cu_2ZnSnS_4/MoS_2-rGO heterostructure	Hummers method	52 μmol/h/g	176
NiO@Ni-ZnO/rGO/CdS heterostructure	Hummers method	824 μmol/h/100 mg	172
CuS-modified ZnO rod/rGO/CdS heterostructure	Hummers method	1073 μmol/h/g	177
Au@Pt-N-doped $La_2Ti_2O_7$/rGO		-	178
ZnS−CdS/GO heterostructure	Hummers method	1.68 mmol/h	179
TiO_2/Pt/rGO composite	Hydrothermal method	-	180
AgBr/polyoxometalate/GO	Ionic liquid assisted hydrothermal method	256 μmol/h/g	181
rGO-supported g-C_3N_4-TiO_2	Ultrasound-assisted simple wet impregnation method	23 143 μmol/h/g	182
CdS nanorods decorated by thin MoS_2 layer rGO nanohybrids	Ultrasonication followed by distillation	234 mmol/h/g	183

Table 13. List of Some Important Examples of Photocatalytic CO_2 Reduction Using GO-Based Photocatalysts

GO-based entity	Preparation method	Photocatalytic efficiency	Refs
Ag/TiO$_2$/rGO	Hummers method	Graphene increased the reaction efficiency to 9.4- and 3.3-fold as compared to TiO$_2$ and Ag/TiO$_2$.	185
Cu$_2$O/rGO	Microwave-assisted chemical method	rGO coating increased the activity to nearly 6 times that of Cu$_2$O and to 50 times that of Cu$_2$O/RuO$_x$.	184
rod-like TiO$_2$−rGO composites	Freeze-drying and hydrothermal method	TiO$_2$−rGO showed CO$_2$ conversion efficiency of 21.38 μmol/g which is 15.7-fold that of pure P25.	36
CsPbBr$_3$ QD/GO	Precipitation method	GO enhanced the electron consumption rate.	37
Ag$_2$CrO$_4$/g-C$_3$N$_4$/GO	Precipitation method	To facilitate charge separation, GO functions as an electron acceptor and has a CO$_2$ conversion efficiency of 1.03 μmol/g.	38
N-doped GO reduced titania	-	N-doped GO-reduced titania exhibited an efficiency of 252.0 mmol/g toward conversion of CO$_2$ to CH$_4$.	186
ZnO/N-doped rGO	Hydrothermal method	The composite exhibited a methanol production rate of 1.51 μmol/g/h.	187
rGO@CuZnO@Fe$_3$O$_4$	Hydrothermal method	Photoreduction efficiency for CO$_2$ reduction is 2656 μmol/g.	188
Cs$_4$PbBr$_6$/rGO	Precipitation method	The production efficiency of CO from CO$_2$ was found to be 11.4 μmol/g/h.	189
Ag−rGO−CdS	Solvothermal followed by thermal reduction and photodeposition	The photocatalyst exhibited successful conversion of CO$_2$ to CO.	190
rGO−TiO$_2$	Solvothermal method	The intimate contact between TiO$_2$ and rGO accelerated transfer of electrons to inhibit charge recombination and exhibited a photocatalytic efficiency of 0.135 μmol/g/h toward reduction of CO$_2$.	191
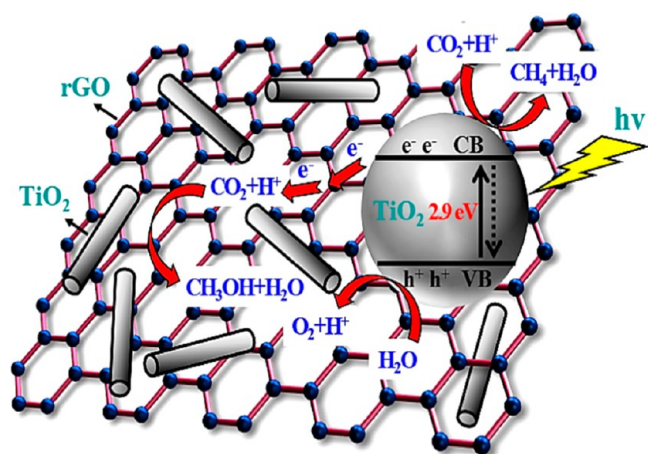
Figure 30. Schematic representation of the mechanism of charge separation in the TiO$_2$−rGO composite. Reproduced with permission from ref 36. Copyright@2021, Elsevier Ltd., Journal of Alloys and Compounds.

goes a photocorrosion of 2670 ppm after 3 h of reaction, while after compositing with rGO, Cu leaching due to photo-corrosion was reduced to 96 ppm.[184] Liu et al. introduced the rGO aerogel to rod-like TiO$_2$ through freeze-drying and hydrothermal reactions. The complex thus formed exhibits a large surface area of 287.3 m^2/g with 0.72 cm^3/g pore volume. This higher surface area facilitates enhanced light absorption tendency, and graphene sheets accelerate electron transfer. Moreover, the composite formed has a 2.9 eV band gap which is found to be lower compared to pure TiO$_2$ (3.2 eV), resulting in a red shift and hence contributing to higher photocatalytic visible-light-driven CO$_2$ reduction with an efficiency of 21.38 μmol/g.[36] The mechanism of charge transfer in TiO$_2$-rGO for photocatalytic CO$_2$ conversion has been shown in Figure 30.

8. ELECTROCHEMICAL NATURE OF GRAPHENE OXIDE

GO consists of numerous oxygen groups like carboxyl, epoxide, hydroxyl, and carbonyl, which are covalently bonded to sp^3-hybridized C networks.[192] However, the exact structure of GO is a much-debated topic and requires further in-depth studies.

Due to its unique structure, a variety of intriguing properties emerge, including electrical, optical, thermal, mechanical, and electrochemical. Recent investigations in the realm of GO's electrochemical characteristics are the most popular. This is evident due to the advantageous electron mobility and the unique surface characteristics of GO.[193] Some of these surface features include a thickness of one atom and a large surface area, which aid in tolerating active species and enable electron transport at the electrode surface.[193,194] In addition to this, GO also exhibits a surmountable amount of electrocatalytic activity and high electrochemical capacitance with good cycle performance.[195]

Different methods can be used for the preparation of GO-based electrodes, such as simple dispersion of GO-based materials, on an electrode or by confining GO on a functionalized electrode substrate. Alternatively, the method of spin-coating is also used for the preparation of GO electrodes. Self-assembling is also deemed an important technique which boosts the potential applications of GO electrodes in sensor fabrications because it can adjust the electrode dimensions efficiently to form a nanoelectrode assembly.[192]

The fundamental process which is directly linked to electrochemical reactions is termed as heterogeneous electron transfer (HET). It denotes the process of electron transfer into or out of the graphene sheets from its surrounding environment. The edge plane and the basal plane are the most common sites for HET studies. However, studies have shown that the basal plane is electrochemically inert, while the edge plane shows efficient HET kinetics and is supposed to contain defects.[196] Further reduction of GOs through a chemical or electrochemical process can increase their efficiency. For instance, the cyclic voltammetry of GO sheets has been determined to be reduction waves ranging from −0.60 V (vs Ag/AgCl reference electrodes) to a maximum of −0.87 V. This process is pH dependent, wherein the reduced GOs were observed to have higher conductivity, and the mechanism for this reduction through electrochemical means is suggested to be as follows:
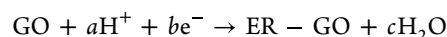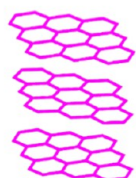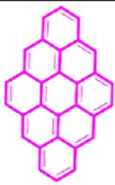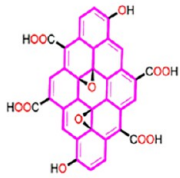
$$GO + aH^+ + be^- \rightarrow ER - GO + cH_2O$$

Table 14. GO-Based Materials for Their Electrocatalytic Activity

heterojunction	electrocatalytic activity	refs
$CoSe_2$-$MoSe_2$/rGO	Electrocatalytic hydrogen production	200
N-$CoMe_2Pc$/NRGO	Electrocatalytic CO_2 reduction	39
WO_3/rGO nanocomposite	Electrochemical monitoring of mancozeb	40
$NiCo_2S_4$/N,S-codoped rGO	Electrocatalytic water splitting	202
F-doped GO	Electrocatalytic degradation of acetaminophen	41
In_2O_3-rGO	Electrocatalytic reduction of CO_2	203
rGO@$CoNiO_x$ nanocomposite	Electrocatalytic degradation of acetaminophen	204
rGO-$NiFe_2O_4$	Electrocatalytic oxidation of hydrazine	42
Ni@GO	Electrocatalytic urea oxidation	202
Cu/rGO/graphite plate	Electrocatalytic reduction of nitrate	205
Coupled Mo_2C@rGO	Elecctrocatalytic hydrogen evolution	201
Graphene nanowalls	Electrochemical biosensing	197
Mg^{2+}-charged spongy graphene electrodes	Electrochemical detection of Leukemia	198

Table 15. Various Systems of Graphite/Graphene/GO

Graphite	Graphene	GO
Graphite term was coined by Abraham Gottlob Werner in 1789. Greek word graphene means to draw/write for its use in pencils. It's one of the allotropes of carbon, most stable and does not readily burn at elevated temperature for this reason it is used in nuclear reactor. It is hydrophobic in nature.	It is single layer of graphite. Its thickness is about one atom. Due to planer sheet of sp^2-hybridized carbon atoms. It arranges in a hexagonal or honeycomb like lattice [219]. It is hydrophobic in nature.	GO is oxide form of graphene with different chemical and physical properties than graphite and graphene. Oxygen is introduced by chemical oxidation like epoxy, hydroxy, carbonyl etc. C:O ratio 2:1 to 2:9 It is hydrophilic in nature.

Because of the large surface-to-volume ratio, its dispersibility in water and organic solvents, and the large reactive functionalized surface, GOs are widely studied for electrochemical applications. In addition to moderate conductivity and good chemical stability, GO is known to demonstrate direct electron transfer to proteins and enzymes as well. Therefore, GOs have applications in the field of electroanalysis, electrochemical luminescence, electrochemical sensors, etc.[196] Akhavan et al. have explored rGO nanowalls (rGONWs) synthesized using the modified Hummers method. The electrochemical activity of free nucleotides, ssDNA, and dsDNA was studied using the synthesized rGO nanowalls. Based on the observed results, they concluded that single nucleotide polymorphism (SNP) can be detected for up to 10 DNA/mL for a specific sequence, which was effective as label-free detection. Therefore, the electrochemical biosensor developed exhibits potential for the detection of nucleotides up to resolution of single DNA.[197]

Later, the same researchers fabricated spongy graphene electrodes (SGEs) that are charged with Mg^{2+} ions via electrochemical deposition. They used the synthesized SGE for electrochemical oxidation of guanine for ultrasensitive detection of leukemia. Based on their results, they exhibited an improved detection limit of up to 0.02 cells/mL.[198] They further investigated the point of care diagnosis of leukemia using functionalized GO nanoplatelets (GONPs). The GONPs were synthesized using the modified Hummers method. They exhibited guanine oxidation in leukemic cells. Also, they compared the GONPs with rGONWs and observed that guanine oxidation is five times higher in GONPs over rGONWs. However, it is based on the polymerase chain reaction and, therefore, is expensive, and the results are obtained in a couple of days. Yet, it is an effective technology for leukemia diagnosis.[199]
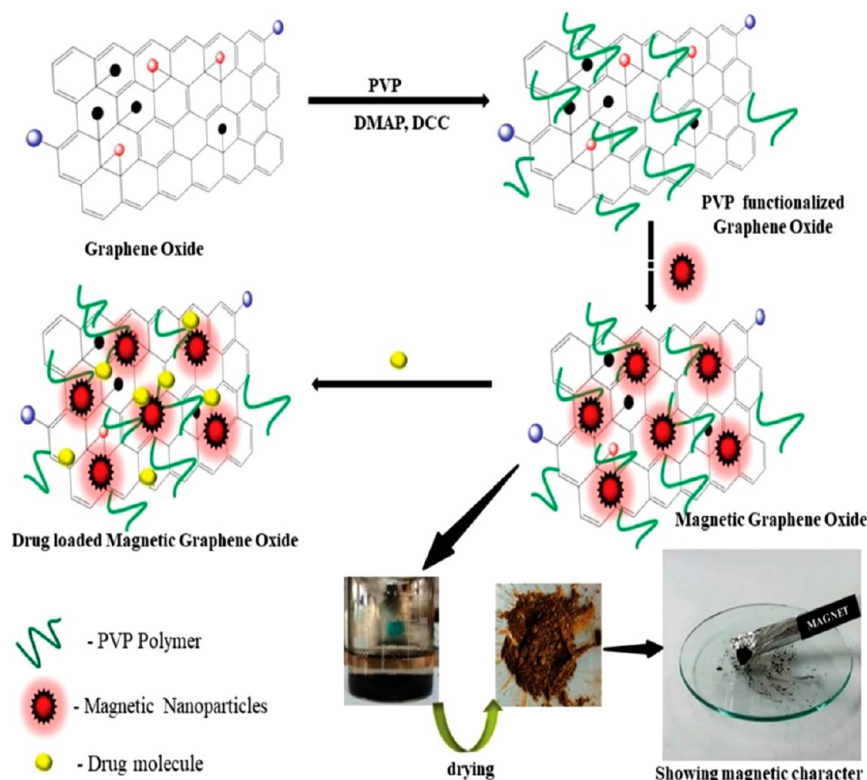
Figure 31. Schematic representation of the synthesis of magnetic GO and drug loading on magnetic GO. Reproduced with permission from ref 231. Copyright @2022, Royal Society of Chemistry, Royal Society of Chemistry Advances.

9. GRAPHENE OXIDE AS AN ELECTROCATALYST

GO possesses excellent electrocatalytic behavior as seen in many reactions (Table 14). This behavior of GO can be attributed to its superistic properties such as high surface-to-volume ratio, active functional groups bounded to its surface, high chemical stability, good conductivity, good electron transfer capability, and desirability in water and organic solvents. Zhu et al. constructed rGO-based heterostructures for enhanced electrocatalytic hydrogen production. The heterostructure $CoSe_2-MoSe_2(1-1)/rGO$ containing a 1:1 proportion of Co/Mo exhibits a good hydrogen evolution reaction (HER) in both acidic and alkali media. The appreciating performance in both media is due to the excellent electron transfer facilitated by rGO. Also, the $CoSe_2-MoSe_2$ interface provides several active sites for the adsorption of hydrogen.[200] The heterostructure exhibits an overpotential of 107 mV and 182 mV at 10 mA/cm^2 with a slope of 56 mV/dec and 89 mV/dec in acidic and alkaline conditions, respectively. This study elaborates the role of GO in constructing energy storage conversion electrodes. Li et al. integrated polyoxometalates (POMs) and pyrrole (Py) on graphene sheets with uniform distribution to obtain ternary nanohybrids, i.e., POMs—polypyrrole/rGO. The GO-synthesized ternary nanohybrid exhibited excellent electrocatalytic HER activity with 0 mV overpotential and a small slope of 33.6 mV/dec The nanohybrid exhibited good stability in an acidic medium.[201]

10. BIOMEDICAL APPLICATIONS

GO has gained considerable interest as a potential nanocarrier platform including biomedical applications.[206] GO has a large surface area, low toxicity, biodegradability, high drug holding capacity, and targeted drug delivery system.[207] Graphite/
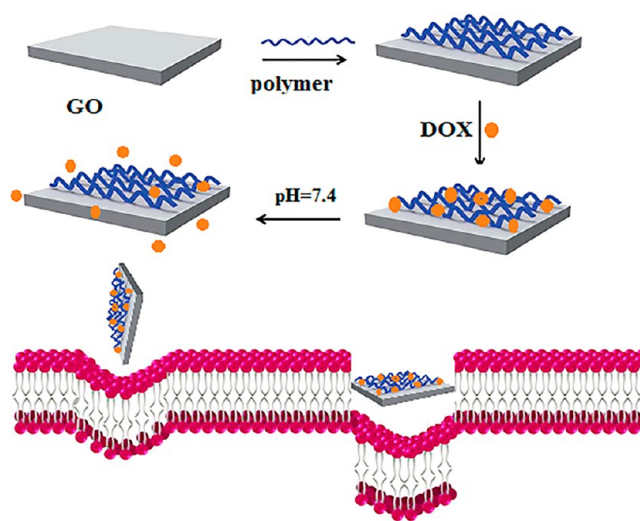

Figure 32. Preparation of doxorubicin (DOX)-loaded graphene (GO) nanocomposites. Reproduced with permission from ref 232. Copyright@2021, Elsevier Ltd., International Journal of Biological Macromolecules.

graphene/GO (Table 15) is an allotrope of carbon nanomaterials and a relatively new field of major implications for biomedical use. In 2011, Feng et al. published a paper on graphene for biomedical applications.[208] In 2012, Shen et al. were given the great idea of interesting studies to investigate the uses of graphene and its composites in diverse areas like drug delivery, sensors, gene delivery, and GO-based antibacterial nanocomposites. The first stage used GO as a drug carrier, and it was remarkably useful in anticancer drugs with doxorubicin. Notably, the GO could interact with the
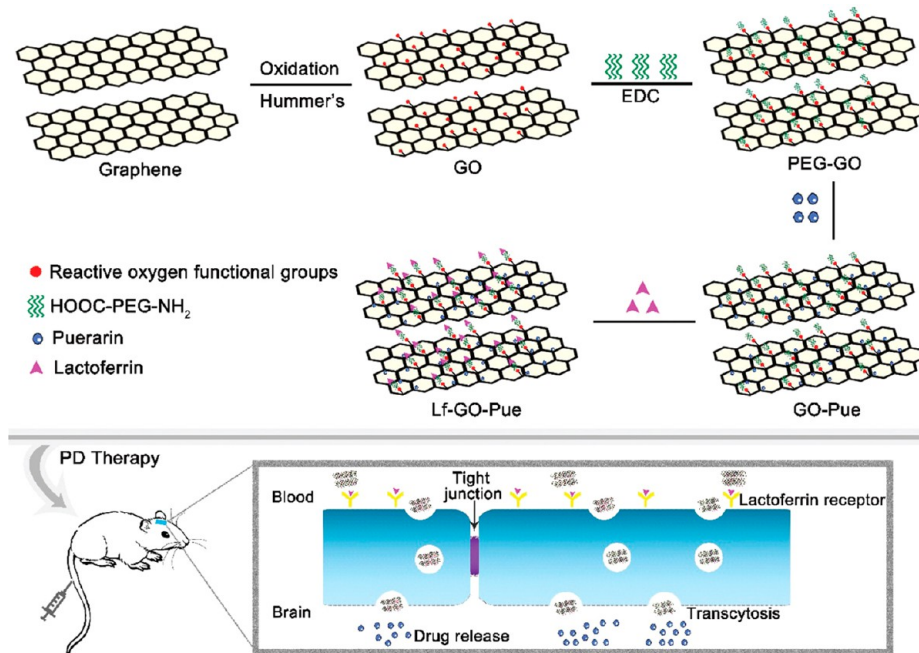
Figure 33. Lf-GO-Pue for the multifunctional brain-targeted drug delivery system for the treatment of PD. Reproduced with permission from ref 233. Copyright @2022, Royal Society of Chemistry, Biomaterials Science.
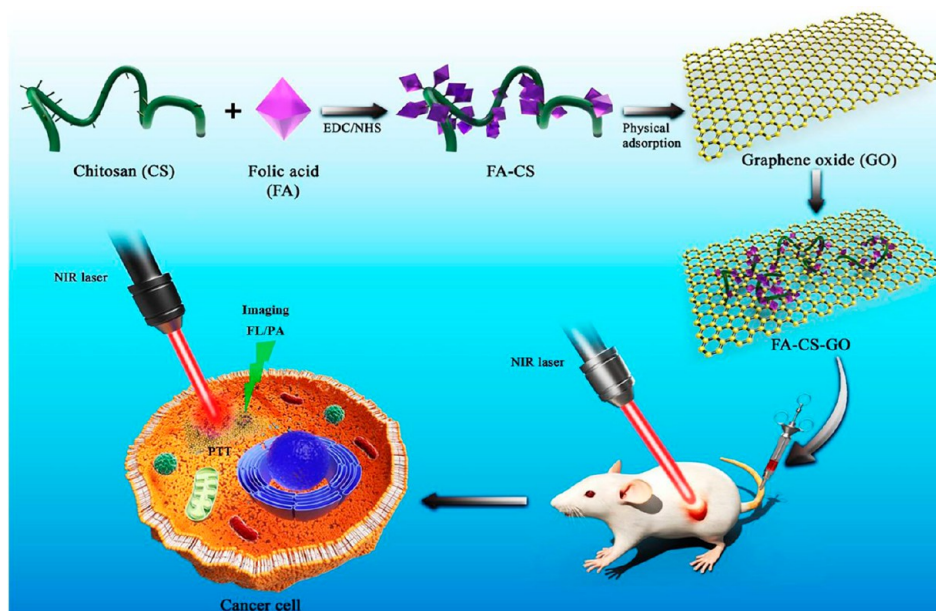

Figure 34. Chitosan (CS)-functionalized GO nanosheets were conjugated with folic acid for targeted photothermal tumor therapy. Reproduced with permission from ref 234. Copyright @ 2020, Elsevier Ltd., International Journal of Biological Macromolecules.

doxorubicin by overlapping π-orbitals, and the β-cyclodextrin unit may identify receptors of folic acid in cancer cells.[209] Electrostatic interactions between GO and ionized pharmaceuticals (H-bonding) are the main mechanisms for drug loading, and the aromatic structures may be essential (such as DOX). The in situ drug-loaded nanocomposites are desirable candidates for upcoming nanomedicine therapeutic techniques in malignancies and acidic organs like the stomach.[210]

In 2021, aptamers that are smaller, more chemically stable, and less toxic may be able to attach to their targets with more specificity and affinity. However, GO may still connect with single-stranded DNA/RNA (aptamers) efficiently through

hydrophobic or π−π stacking interactions. GO-derived novel 2D materials with aptamer functionality can be used to build extremely sensitive biosensors for cancer detection. Materials that are GO−aptamer-conjugated are superior to cancer screening and diagnosis methods based on antibodies. They are quite effective at assisting with the identification and diagnosis of several types of cancer.[211]

It was suggested that the nanostructure Au@AF−GO could be a useful medication. It was successfully applied to SPECT imaging and in vivo targeted therapy. An intriguing nanomaterial for upcoming diagnostic techniques is the Au@AF−GO nanostructure due to its exceptional qualities, which include
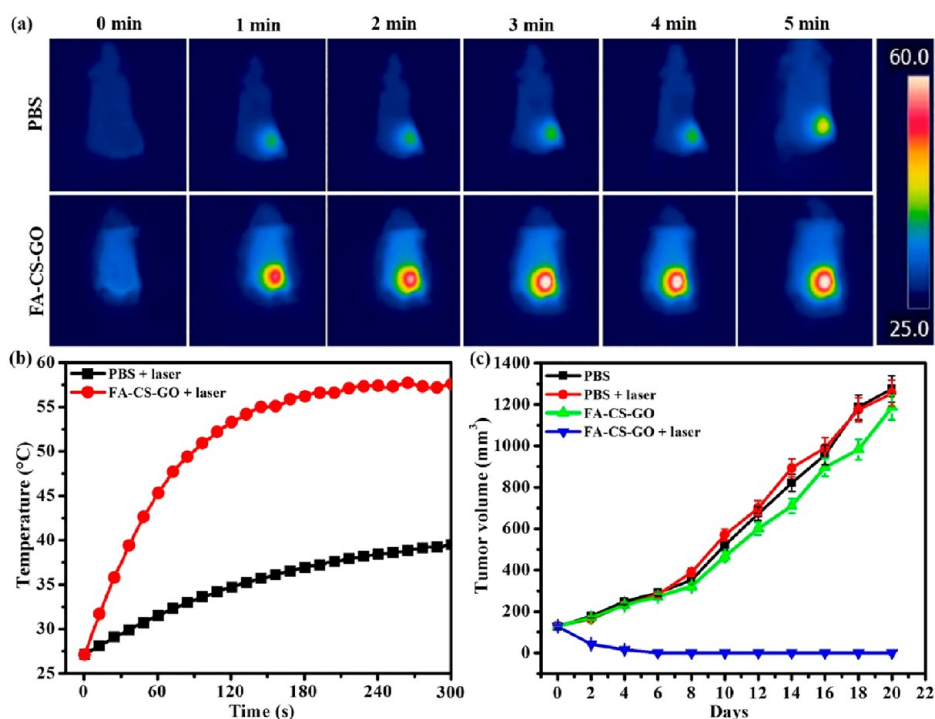
Figure 35. (a) IR thermal images of tumor-bearing mice with or without injection of FA-CS-GO exposed for 5 min to a laser ($2.0 \, W/cm^2$). (b) Temperature variations of the tumor region of the mice treated with PBS and FA-CS-GO exposed for 5 min to a laser ($2.0 \, W/cm^2$). (c) The tumor growth curves of different groups of tumors after various treatments. Reproduced with permission from ref 234. Copyright@ 020, Elsevier Ltd., International Journal of Biological Macromolecules.
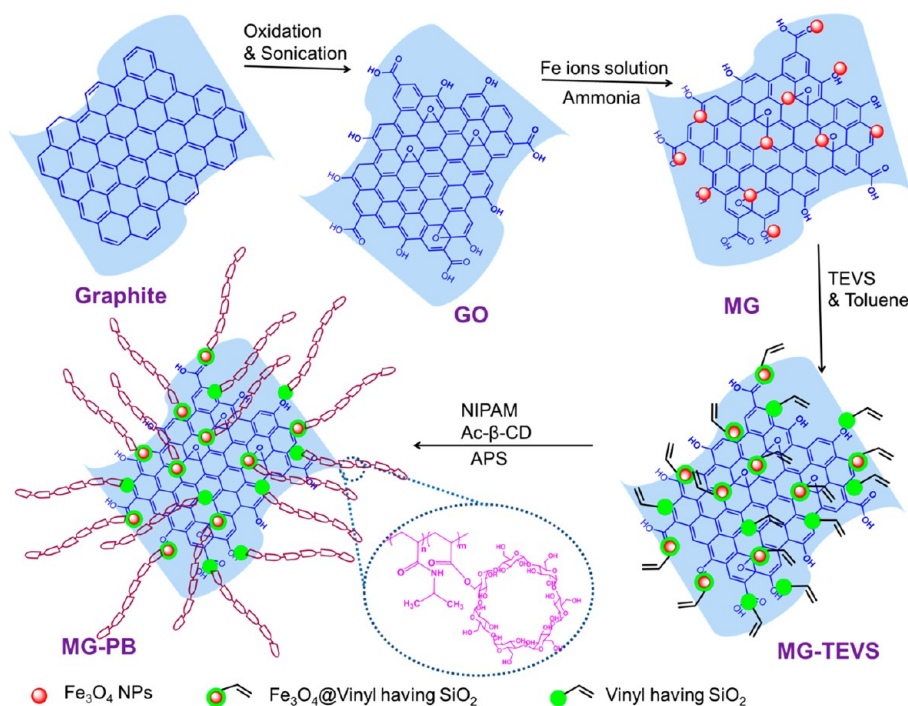

Figure 36. Schematic illustration of the preparation of MG−PB. Reproduced with permission from ref 235. Copyright@2021, Elsevier Ltd., European Polymer Journal.

quick body clearance, effective tumor targeting/imaging, and short Au radioisotope half-lives.[212] For instance, employing the rGO nanomess, one of the most recent graphene constructions with very high near-infrared absorption, allows for extremely successful photothermal treatment.[213]

GO has also been studied in the biomedical field due to its surface area.[214] Due to its large surface area, it may also be considered a good adsorbent material such as in drug encapsulation. Additionally, the presence of unsaturation bonds could conjugate with several drug molecules through covalent cross-linking $\pi-\pi$ stacking interactions.[215] Through
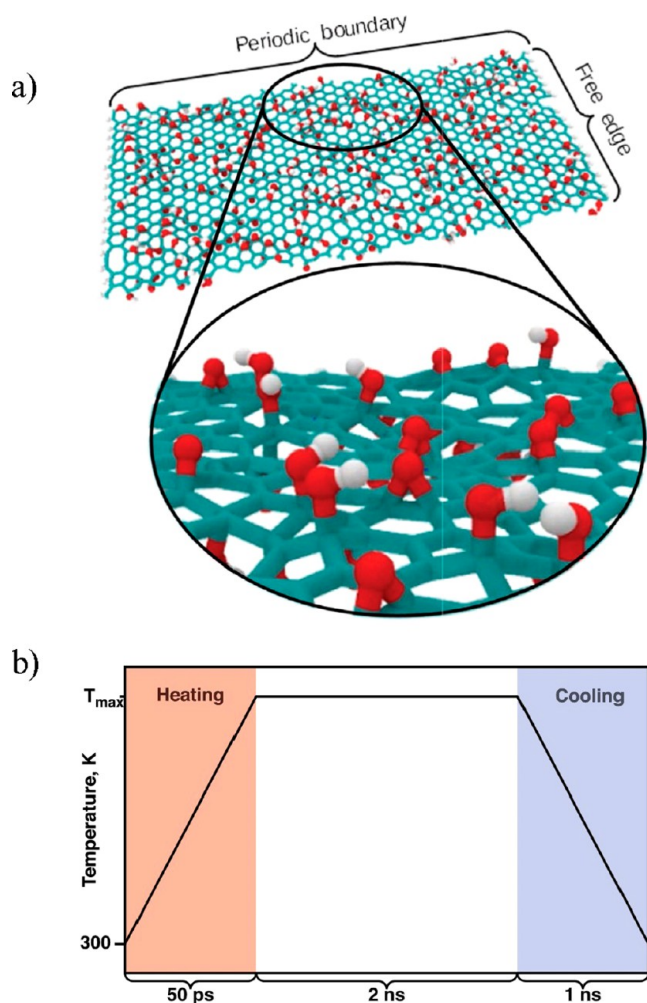
Figure 37. (a) Atomistic structure of GO and (b) the scheme of the thermal regime. Reproduced with permission from ref 244. Copyright@ 2022, Elsevier Ltd., Carbon.

Figure 38. (a) Time evolution of the total number of atoms, (b) number of carbon atoms, and (c) number of oxygen atoms along the simulation at different temperatures. Atoms of carbon, oxygen, and hydrogen are shown in blue, red, and gray, respectively. Reproduced with permission from ref 244. Copyright@2022, Elsevier Ltd., Carbon.

hydrophobic interactions and $\pi-\pi$ stacking, graphene's 2D structure with large surface area may be exploited for efficient drug loading. Furthermore, because of its large surface area, GO may be biofunctionalized at a high density using both covalent and noncovalent surface modification techniques. However, pure GO loses a bioactive site to support cell growth, which is limited to use in biomedicine. The application of graphene in gene delivery is a nonviral graphene-based gene vehicle for transfecting pDNA in mammalian cells. An innovative mixture of ethidium bromide (EtBr) and carboxylated graphene (G-COOH) is used for efficient gene delivery into AGS cells.[216] For simultaneous gene and photothermal cancer treatment, the conjugated histone methyltransferase enzyme SET1 (hSET1) on decreased polydopamine-loaded GO nanosheets was employed (rGO-PDA). Higher near-infrared absorption is provided by the rGO-PDA nanocarriers, which also better integrate with hSET1 antisense. hSET1 antisense is delivered to breast cancer cells by nanocarriers.[217] Polyethylene glycol is used to stabilize and target gold nanorods or nanospheres coated with GO (P-L-Arg). P-L-Arg raised cellular uptake and gene-retarding effects of coated substances.

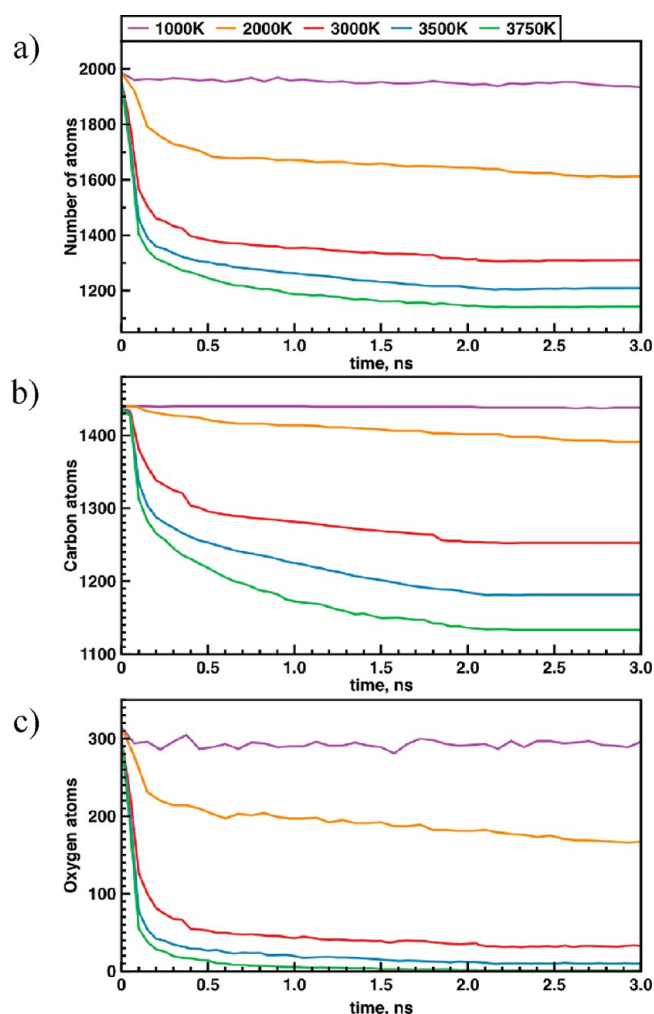Currently, researchers developed the modified GO with carboxymethyl cellulose (GO−CMC) composites as a drug carrier, which bonded small molecules of the doxorubicin hydrochloride (DOX) drug through $\pi-\pi$ interaction or hydrogen bonding.[218]

A lot of research has been done in recent years to include nanotechnology for drug delivery, and as a result, several drug delivery systems (DDS) have been designed.[218−221] In initially designed DDS, anticancer drugs could not differentiate between cancerous and healthy cells, which caused several side effects and adverse implications for the human body.[218] The DDS should deliver the accurate dose of medicine only at accurate sites. Thus, finding a carrier for the drug is one of the major problems. A good amount of potential drug carriers like nanoparticles, micelles,[222] dendrimers,[223] biopolymers,[224] as well as synthetic polymers have been designed for targeted drug delivery. Nanocarriers have the potential to greatly improve the efficiency and accuracy of drug delivery while also reducing adverse effects, particularly when the drug is insoluble in water.[225] In DDS, GO and GO functionalized with nanoparticles and polymers were frequently employed[226,227] because of their suitable properties, low cost, simple synthesis,
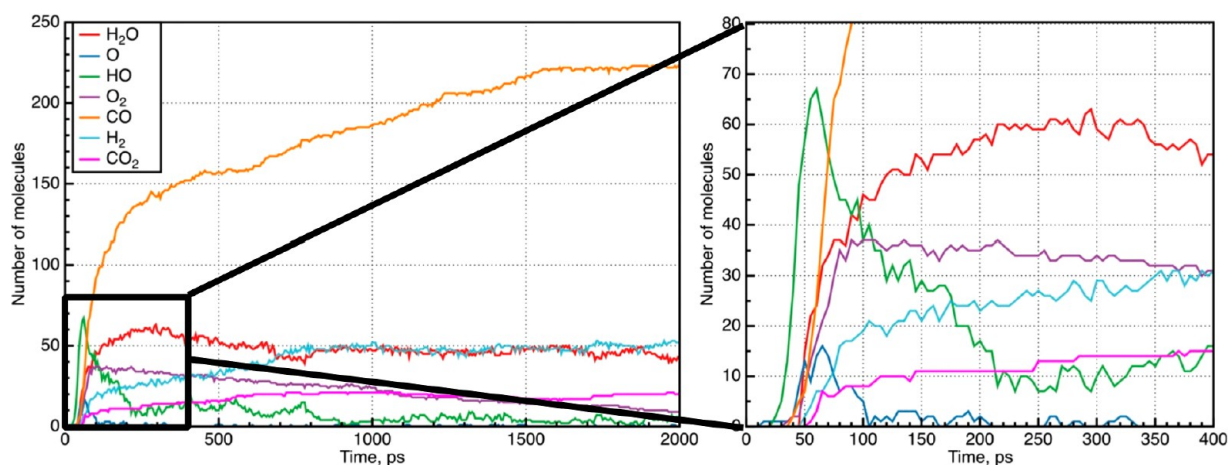
Figure 39. Time-dependent evolution of the concentrations of gas-phase products during the simulation of GO oxidation at T_{max} at 3500 K. Reproduced with permission from ref 244. Copyright@2022, Elsevier Ltd., Carbon.
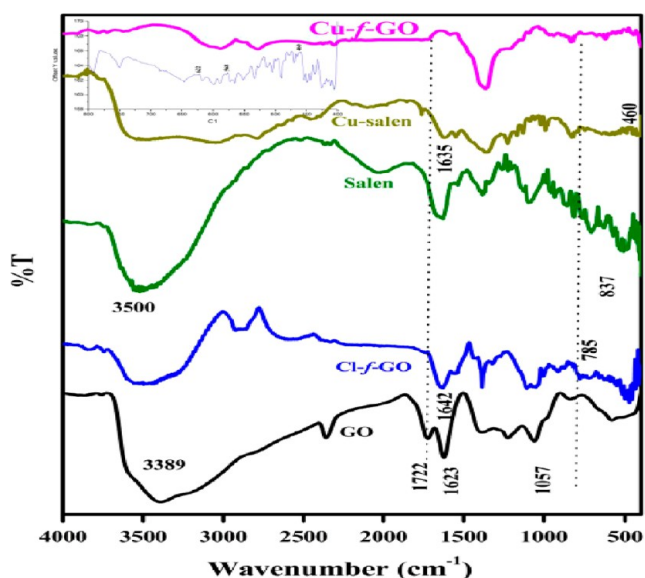

Figure 40. FTIR spectra of GO, Cl-f-GO, Cu-salen, and Cu-f-GO. Reproduced with permission from ref 247. Copyright@2022, Elsevier Ltd., Journal of Molecular Structure.
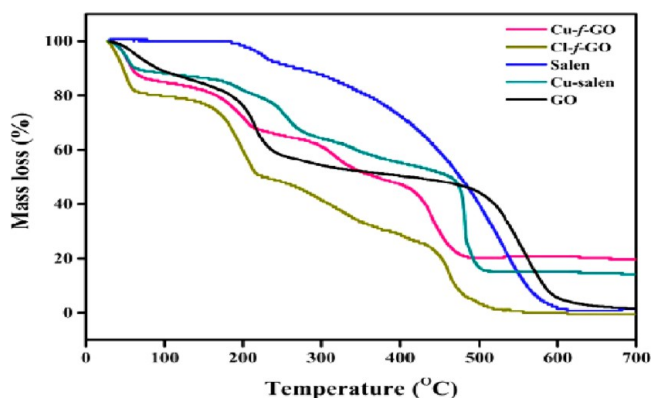

Figure 41. TG analysis of GO, Cl-f-GO, Cu-salen, and Cu-f-GO. Reproduced with permission from ref 247. Copyright@2022, Elsevier Ltd., Journal of Molecular Structure.

and π-conjugated structure.[228] As a result, a significant amount of research is done on GO and its derivatives for DDS.[229,230]

In 2022, polymer-grafted magnetic GO (GO-PVP-Fe_3O_4) was successfully developed and employed in anticancer drug delivery.[231] GO was first functionalized with polyvinylpyrrolidone (PVP) before being implanted with magnetic nanoparticles (Fe_3O_4) using a simple and efficient chemical process. Noncovalent interactions were used to load an anticancer drug quercetin (QSR) on GO-PVP-Fe_3O_4, as shown in Figure 31. The drug-carrying capacity was found to be 1.69 mg g^{-1}. Comparison of the cytotoxicity of the nanocarrier in human breast cancer cells and nontumorigenic epithelial cells was done with and without drugs. The results demonstrate that the drug-embedded GO-PVP-Fe_3O_4 nanohybrid is more harmful than the free drug to cancerous cells while being biocompatible to epithelial cells. A smart DDS that includes polymer-grafted magnetic GO (potential nanocarrier) which is pH-responsive for cancer treatment should be useful for drug delivery influenced by an externally applied magnetic field.

In 2021, the new nanoscale GO polymer composite DDS was developed and studied as a potential drug (doxorubicin) for oral drug delivery.[232] A novel doxorubicin-loaded nanocomposite composed of GO/copolymer was formed by reversible addition−fragmentation chain transfer (RAFT) and ring-opening polymerization (ROP), which is given in Figure 32. Doxorubicin was incorporated into the nanocomposite and had a size of 51 nm with a satisfactory encapsulation of 82% ± 1.12%. DOX was bonded to the surface of graphene by $\pi-\pi$ stacking and aquaphobic interactions. The anticancer effect of the DOX@GO nanocomposite was revealed in cytotoxicity studies on breast cancer cells named 4T1 murine and could be useful in breast cancer therapy.

In 2021, the global aging population will exponentially increase the rate of Parkinson's disease (PD) incidence.[233] PD is a neurodegenerative disorder and is caused by defaced dopamine neurons in the substantia nigra pars compacta (SNpc), abnormal synuclein (-Syn) deposition, and progressive neurodegeneration in striatal regions. Even after a lot of research into the pathophysiology of PD and the development of therapies to control its progression, no substantial cure has been found to date. Puerarin (Pue) is a naturally occurring substance that possesses outstanding anti-PD capabilities. Due to its poor pharmacological properties, including low water solubility, weak bioavailability, and insufficient blood−brain barrier (BBB) penetration, its use
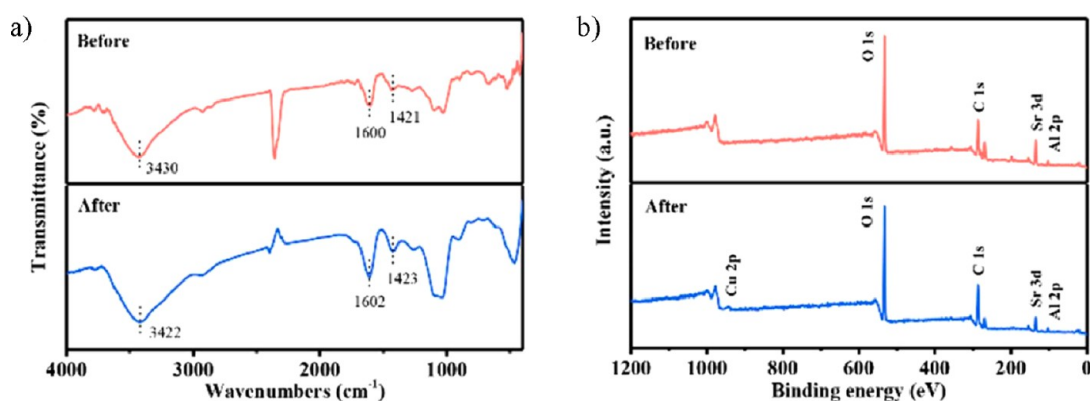
Figure 42. (a) FTIR spectra of Sr-G/M before and after adsorption. (b) Full XPS spectra of Sr-G/M before and after adsorption.[251] Copyright@ 2022, Elsevier Ltd., Journal of Hazardous Materials.
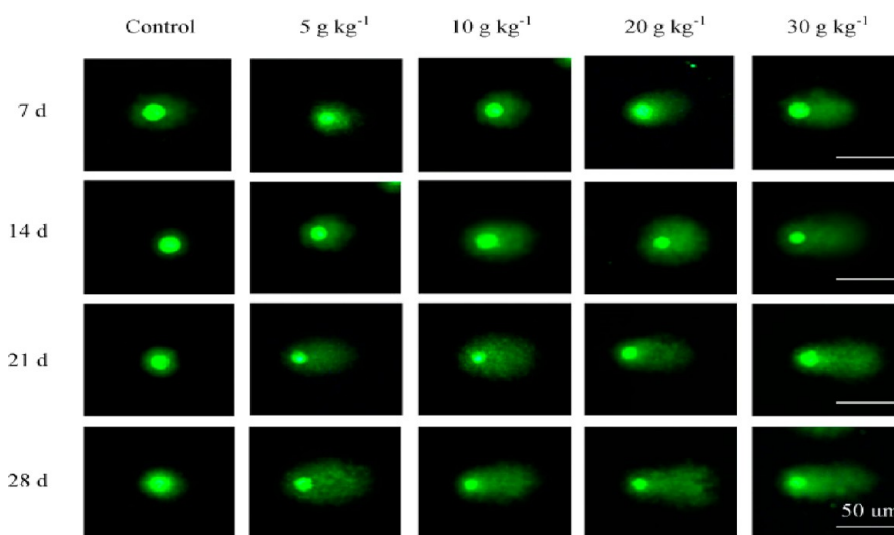

Figure 43. Comet image of DNA damage to coelomocytes in *E. fetida*. Reproduced with permission from ref 255. Copyright@2021, Elsevier, Environmental Pollution.

Table 16. Number of Organisms Affected and Percentage of Effect on *C. dubia* after 48 h of Exposure to GO Nanoparticles

Concentration (mg/L)	Immobility/ mortality	Total no. of organisms	Effect
control	1	20	5
0.1	1	20	5
0.2	1	20	5
0.4	2	20	10
0.8	2	20	10
1.6	10	20	50
3.2	20	20	100

Figure 44. Crawling assay analysis (Chem ZnO vs Green ZnO vs GO NPs). The average no. of squares crossed by larvae treated with Green ZnO is greater than that of squares crossed by larvae treated with both chemical ZnO and GO. Reproduced with permission from ref 257. Copyright@2019, Elsevier, Ltd., Toxicology Reports.

for the treatment of Parkinson's disease (PD) has been restricted. However, nanotechnology advancements have revealed potential advantages of targeted drug delivery into the brain for PD treatment. Xiong et al. developed for the first time the Pue-loaded GO nanosheets with better drug-carrying capacity, changeable functional groups on the surface, and high biocompatibility. Pue was then moved across the BBB into the brain with the help of lactoferrin (Lf) (targeting ligand) which is capable of binding to the BBB's vascular endothelial receptor. Studies demonstrated that Lf-GO-Pue could be a

safe as well as effective treatment for Parkinson's disease (PD),[233] which is represented in Figure 33.

In 2020, Jun et al. synthesized chitosan-functionalized GO nanosheets coupled with folic acid for photothermal cancer therapy guided by near-infrared fluorescence: cancerous cells
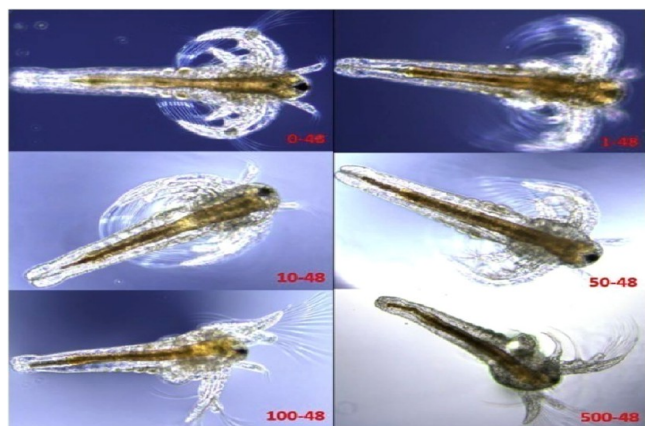
Figure 45. Microscopy images of GO uptake by *Artemia salina* in 0, 1, 10, 50, 100, and 500 mg/L of GO suspension at 48 h. Reproduced with permission from ref 258. Copyright@2018, Elsevier, Ltd., Chemosphere. Copyright@2018, Elsevier Ltd., Chemosphere.

were fully killed in vitro following laser irradiation.[234] Additionally, in vivo experiments demonstrated that tumors were entirely destroyed within 20 days after the deployment of this targeted nanosystem under laser irradiation, which is given in Figure 34. After 24 h of injection of FA-CS-GO, a photoacoustic signal was observed around the tumor area in a mouse. FA-CS-GO showed a high tumor-targeting efficiency, outstanding PAI, and powerful photothermal effect. This is the first work to demonstrate the use of nanomaterials with multifunctionalities for highly efficient FL/PAI-guided PTT, which represents an amazing new direction for nanomedicine (Figure 35).

In 2020, this work promised to enhance doxorubicin's (DOX) therapeutic efficacy as an anticancer agent by embedding it into a nanostructure.[235] A nanocomposite was prepared by loading a stimuli-responsive copolymer in magnetically active GO, and its evaluation as a stimuli-responsive DDS was done. Initially, the magnetic GO nanohybrid (MG) was successfully created in this regard. Polymerization of acrylic monomers occurred on addition of vinylic groups to the MG surface to produce N-isopropylacrylamide (NIPAM) and acrylate cyclodextrin (Ac-CD) copolymer brushes, as shown in Figure 36. The MG−PB hybrid nanosystem could be presented as a potential candidate for

drug delivery in breast cancer treatment, as it is nontoxic and effective.

11. COMPUTATIONAL STUDIES

The computational work revealed the conformational information of the nonbonding interaction of GO. Fark et al studied the effects of the interaction of GO with NO_2, CO_2, SO_3, and SO_2 using DFT-based Raman spectroscopy and VCD. They also confirmed stable conformers by MD simulation. Their work notes that VCD spectroscopy can be an alternative for analyzing the interaction between GO and molecules.[236] The physiochemical features of GO are intimately connected to its biological/toxicological activities.[237] It is tough to precisely control the physical and chemical characteristics of GO as they change as soon as it interacts with the environment. Adsorption−desorption interactions between colloids and GO have been observed in a variety of environments (water, soil, and sediment). The agglomeration of GO with organic colloids or other nanoparticles is known as heteroaggregation.[238] Sharifi et al. worked on the interaction of polydiallyl methyl ammonium chloride nanocomposites with nano GO (NGO/PDADMAC). Thermodynamic studies based on B3LYP/6-31+G** revealed that the configuration of the complex produced in the carboxy (−COOH) and hydroxy (−OH) positions has better structural integrity than the epoxy group and that when comparing the groups in experimental and analytical IR spectra the hydroxy agent has a higher probability of overlap.[239] GO showing electronic absorption spectra in solvents potentially gives a different characterization of the GO−solvent interaction, which is significant in GO-based photocatalyst and optoelectronic applications. Meng et al. in their work explained the effect of the polarity of the solvent and H-bonding using DFT by comparing two solvents (NMP and water). The transfer of electrons over GO surfaces dominates the hole−electron pair transition according to the natural transition orbital (NTO) study.[240] A DFT computational study was used to investigate alkali and alkali earth metal interactions with graphene sheets, and the B3LYP theory with a LanL2DZ basis set was used to investigate transition metal interactions. The measured results were compared to the calculated complexation energies ($E_{Adsorption}$). These experiments revealed a substantial relationship between the binding energies and charge density of metal ions, implying that there is some charge transfer occurring between the metal ion and
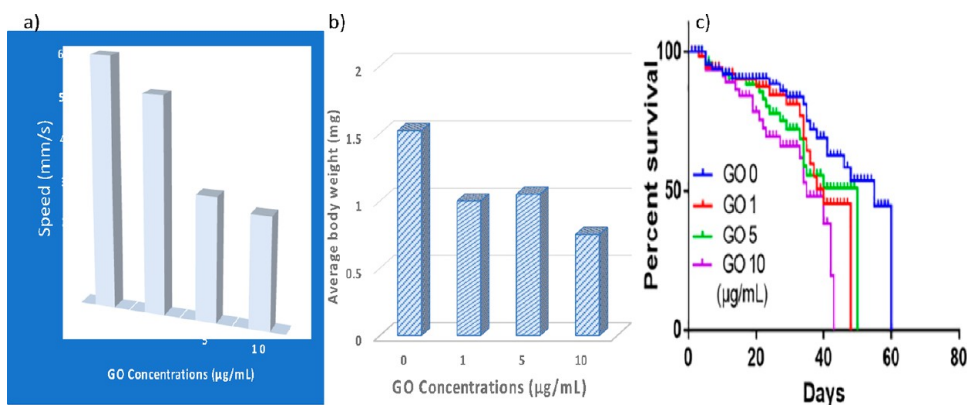

Figure 46. (a) Crawling speed, (b) body weight, and (c) life span of 43 flies. Reproduced with permission from ref 259. Copyright 2022, Elsevier, Ltd., Science of The Total Environment.
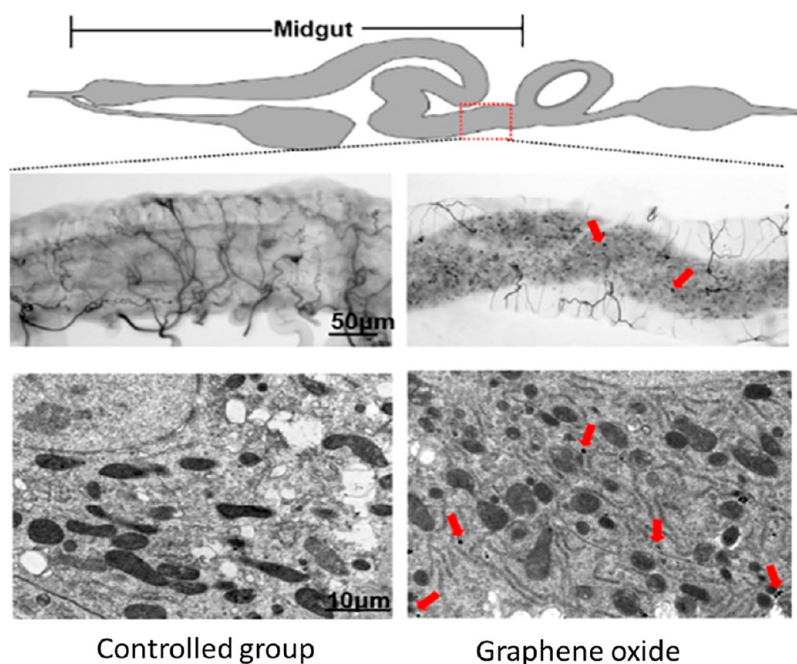
Figure 47. Treatment with 10 μg/mL led to significant accumulation in the posterior midgut. Reproduced with permission from ref 259. Copyright 2022, Elsevier, Ltd., Science of The Total Environment.
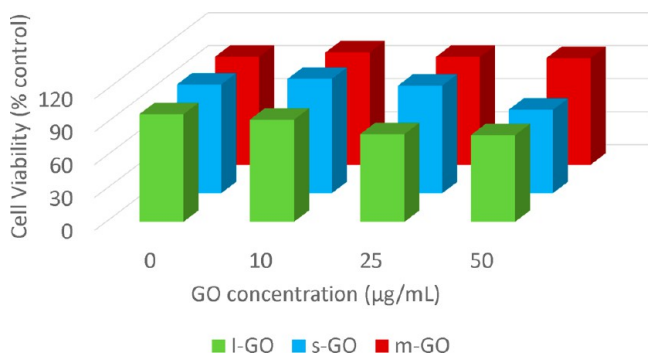

Figure 48. Viability of A459 cells after being exposed to GO for 24 h. Reproduced with permission from ref 260. Copyright@2011, Elsevier, Ltd., Toxicology Letters (redrew the image from the information available).

graphene.[241] With the use of MD simulation, the influence of varying size and shape of GO and SiO_2 nanoparticles on the high viscosity of fluids was investigated. Tersoff and Lenard-Jones (LJ) interatomic force fields were used to evaluate the viscosity of fluids containing C, O, Si, and H. MD simulations revealed that on addition of GO and SiO_2 nanoparticles to the virgin fluid the viscosity increased. The viscosity of the pure fluid and GO-incorporated fluid was statistically resolved to 88 Pa s and 94 Pa s, respectively.[242] Hasem et al. created biocompatible, antibacterial, and antiviral nanocomposites in their research. To make dialdehyde cellulose, the initial step was to oxidize cellulose with periodate (DAC). In the second phase, DAC was combined with S-containing amino acids in the vicinity of GO. FTIR, SEM, TEM, and TGA were used to characterize the produced nanocomposites. Furthermore, computational techniques and molecular docking revealed the reactivity and stability of compounds with biological action against gram-positive, -negative, and HSV-1 bacteria. From the experimental and computational data, the interaction of DAC with amino acids improved their reactivity and interaction.[243]

MD simulations were used to look at how the presence of an electric field helped separate H_2O/O_2 gas molecules over a double-layered nanoporous GO membrane. In an external electric field of 10^{-4} V, the rate of gas permeation through the membrane for H_2O molecules was found to be 3.26×10^{-3} mol m^{-2} s^{-1}. Examining the change in interaction energy with electric field intensity has also shed light on the process of improved H_2O/O_2 separation. Hydrogen bond interactions between H_2O molecules and H_2O membranes are inhibited by the electric field. Accelerating desorption in the presence of electric fields would allow for an additional adsorbent surface on the membrane, enabling the passage of H_2O molecules.[241]

Orekhav et al. reported a computational and experimental evaluation for the reduction of GO using nanosecond infrared laser irradiation (Figures 37, 38, and 39). Researchers reported that rapid aerobic heating to 3800 K results in a unique regime of high-quality GO reduction. This surprising outcome is the consequence of two different processes: (i) combustion on extremely defective regions of GO and (ii) defective reduction in the rest of the material. Under certain pulse regimes, GO transforms into rGO.[244]

The application of B- and N-codoped rGO (BN-GN) as an electrolyte electrochemical degradation of paracetamol was described in this study. DFT calculations, characterization, quenching tests, and electron paramagnetic resonance analyses were utilized to investigate the reaction process, which focused on the catalyst surface at the atomic level and dominating radical species created by the reaction. The inclusion of N and B functionalities into GN increased the catalytic activity by generating new surface defects, active sites, and improving conductivity, according to the characterization data. Experimental and theoretical results revealed that codoped BN-GN boosted the catalytic activity significantly, and the B elements in C−N−B groupings were considered as the major reactive sites.[245] Computational and experimental methodologies were used to investigate tetracycline adsorption on magnetic GOFe$_3$O$_4$ in the work. The structural and electrical character-
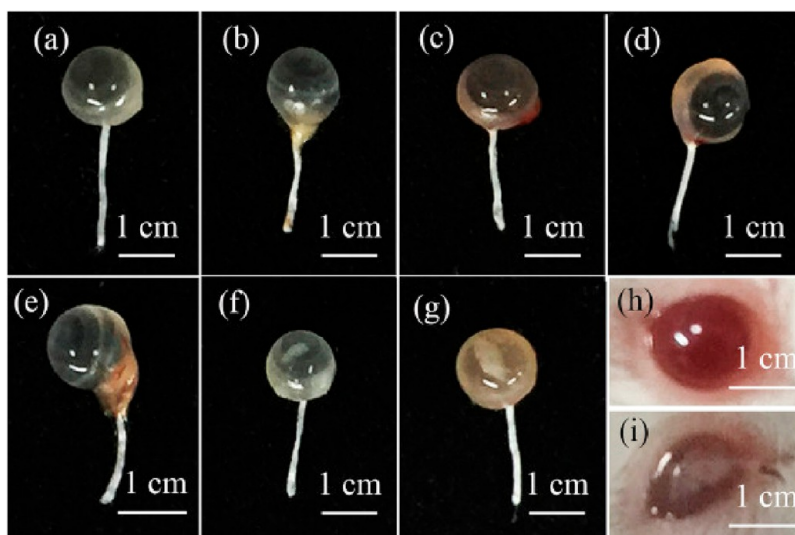
Figure 49. (a) Eyeball exposed to double-distilled water for 7 days (control group). (b) Eyeball exposed to 25 μg/mL of RGO for 7 days. (c) Eyeball exposed to 50 μg/mL of RGO for 7 days. (d) Eyeball exposed to 100 μg/mL of RGO for 7 days. (e) Eyeball exposed to 25 μg/mL of GO for 7 days. (f) Eyeball exposed to 50 μg/mL of GO for 7 days. (g) Eyeball exposed to 100 μg/mL of GO for 7 days. (h) Eyeball exposed to 25 μg/mL of GO for 10 days. (i) Eye exposed to 100 μg/mL of GO for 7 days in vivo.[261] Copyright@2018, Elsevier, Ltd., Experimental Eye Research.
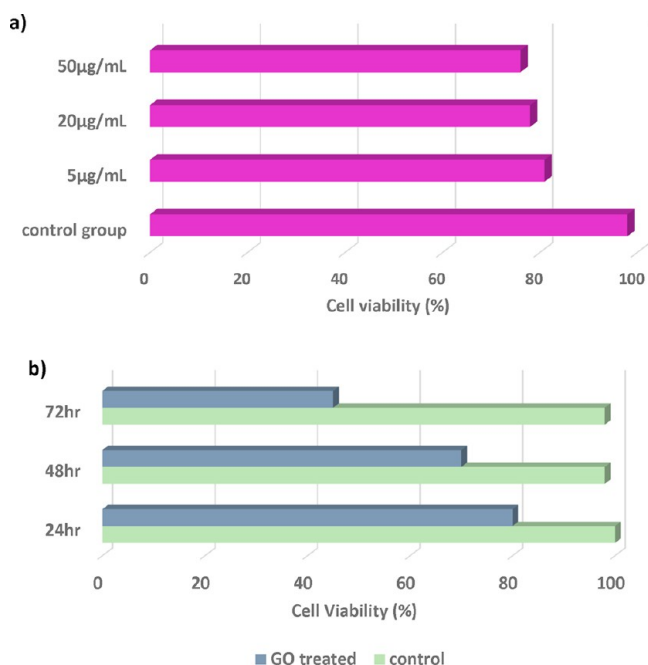

Figure 50. Effects of GO exposure on corneal epidermal cell viability. (a) Cell viability after exposure to GO at 5 μg/mL, 20 μg/mL, and 50 μg/mL for 24 h. (b) Cell viability after exposure to GO at 5 μg/mL for 24 h, 48 h, and 72 h. Reproduced with permission from ref 261. Copyright@2018, Elsevier, Ltd., Experimental Eye Research.

Figure 51. Effect of GO on total cell growth of *E. coli* and *S. aureus*.[262] Copyright@2017, Elsevier Ltd., Science of The Total Environment.

istics of magnetic nanoadsorbent and tetracycline are revealed by combining ab initio and DFT, demonstrating chemical adsorption between tetracycline and GOFe$_3$O$_4$. The reaction was spontaneous, exothermic, and chemical, according to the thermodynamic characteristics. Theoretical and experimental analyses were in agreement, demonstrating that tetracycline adsorption on GOFe$_3$O$_4$ is mediated by a chemisorption process.[246]

A complex of Cu with *N,N′*-bis(4-hydroxysalicylaldehyde)-ethylenediamine (Salen) was incorporated on Cl-modified

GO, resulting in a heterogeneous catalyst (Cu-f-GO). The structural and electrical characteristics as well as the system that determines SOCl$_2$ with each accessible functional group of GO were investigated using first-principles-based DFT. Other thermodynamic parameters were calculated like HOMO, LUMO, chemical potential, electronegativity, energy band gap, adsorption energy, and global electrophilicity, as shown in Figures 40 and 41. According to the data observed, the prepared catalyst performed poorly.[247]

The reduction of U(VI), Se(VI), Se(VI), Re(VII), and Se(IV) in a homogeneous Fe(II) solution is not thermodynamically viable. Surface-mediated Fe(II) reduction, on the other hand, has long been thought to represent a primary avenue for the immobilization of these radionuclides. In this article, a study using DFT calculation and spectroscopic

Figure 52. Biofilm formation after incubation with GO and rGO for 48 h of *E. coli* and *S. aureus*. Reproduced with per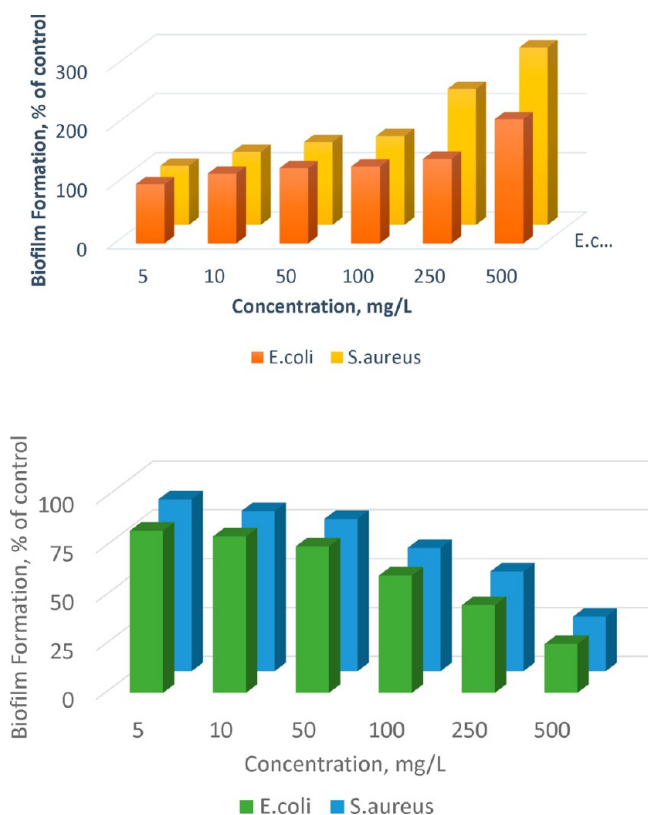mission from ref 262. Copyright@2022, Elsevier, Ltd., Science of The Total Environment (redrew the image from the information available).
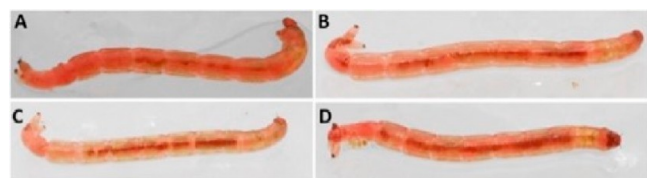

Figure 53. Presence of GO in the digestive tract of *C. riparius* larvae exposed to 3000 μg/L for 24 h. Control (A), sGO (B), lGO (C), and mlGO (D). Reproduced with permission from ref 264. Copyright@ 2022, Elsevier, Ltd., Science of The Total Environment.
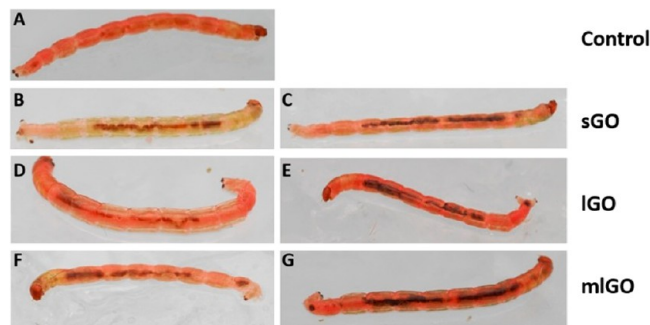

Figure 54. Presence of GO in the digestive tract of *C. riparius*. Control (A); 50 μg/L of sGO (B); 3000 μg/L of sGO (C); 50 μg/L of lGO (D); 3000 μg/L of lGO (E); 50 μg/L of mlGO (F); and 3000 μg/L of mlGO (G) for 96 h. Reproduced with permission from ref 264. Copyright@2022, Elsevier, Ltd., Science of The Total Environment.

examination demonstrated that GO mediates the reduction of U(VI), Se(VI), Se(VI), Re(VII), and Se(IV) by aqueous Fe(II). The pseudo-second-order model was very well explained by the dynamics of all adsorption systems, indicating a chemical interaction. The Freundlich model might better represent the isotherms for all reaction systems than the Langmuir model. Spectrophotometry analyses revealed that the implementation of GO was due to the graphitic surface's easier transfer of electrons and, in particular, the lowered redox potential caused by Fe^{2+} surface adsorption on GO. Furthermore, the inclusion of fulvic acid (FA) may increase the rate by boosting the electron transport capacity.[248]

Researchers developed a design that uses the aluminum atom to boost the optoelectronics, optical properties, and absorption capacity of the GO. In this paper, they provide results from DFT approaches that enabled us to comprehend the consequences of aluminum atom doping on GO nanosheets in the gas phase.[249]

The interface architectures and interaction mechanisms between cellulose derivatives and GO were determined using first-principles calculations. It has been reported that H-bonds and weak surface forces play a significant role in the synthesis of composite systems. The amount of hydrogen bonds is also influenced by steric hindrance: the lower the steric hindrance, the more hydrogen bonds are formed.[250]

Alkaline earth metal functionalized GO and montmorillonite (MMT) aerogels were produced by Xin Hao and colleagues for effective Cu(II) removal of wastewater. As revealed by systematic adsorption studies, Sr-G/M possesses denser slit-shaped pores, causing an effective 97.1% Cu(II) removal efficiency. In Figure 42(a), the peaks of 1421 and 1600 cm^{-1} shift to 1423 and 1602 cm^{-1}, suggesting that the −COOH group is coordinated with Cu^{2+}, while the characteristic peak of −OH moves from 3430 to 3422 cm^{-1}, indicating that the −OH group is involved in adsorbing Cu^{2+}.[251]

Ionic liquids (ILs) and GO membranes have been proposed for the CO_2/CH_4 gas separation method. CO_2/CH_4 dynamical properties and interactions in 1-butyl-3-methylimidazolium tetrafluoroborate ([Bmim][BF$_4$]), 1-butyl-3-methylimidazolium bis(trifluoromethylsulfonyl)imide ([Bmim][TF$_2$N]), and 1-butyl-3-methylimidazolium hexafluorophosphate ([Bmim]-[PF$_6$]) have been reported. Because of the strong bond between GO cations, the interaction between cations and anions is reduced, making CO_2 adsorption simpler. CO_2/CH_4 is mostly distributed in the IL part of the IL/GO membrane, allowing for gas selectivity. The CO_2/CH_4 IL RDFs reveal that the limited IL/GO system performs better than bulk ILs at collecting gases.[252]

Energy that can be harvested from commonplace moisture is gaining popularity as a means of directly powering electrical equipment. Fabricating high-performing moisture-electric generators (MEGs) with high and steady electrical output remains a challenge. Relying on the instrument fabrication of GO/PVA MEGs, we present a straightforward technique for modifying the oxygen-based groups of GO using HCl treatment, which enhances the electric output. The MEG that results has a constant voltage of 0.85 V and a current of 9.28 A (92.8 A cm^{-2}), which are some of the highest values ever documented. Much better, by simply connecting four MEG units in series or parallel, electric output may be increased even further.[253]
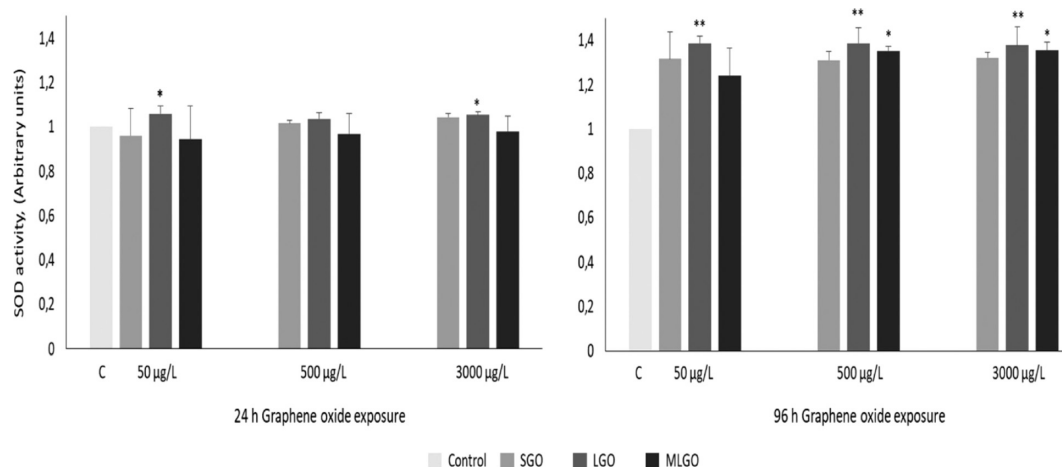
Figure 55. SOD activities on *Chironomus riparius* after 50, 500, and 3000 μg/L of sGO, lGO, and mlGO (*$p < 0.05$, **$p < 0.01$). Reproduced with permission from ref 264. Copyright@2022, Elsevier, Ltd., Science of The Total Environment.
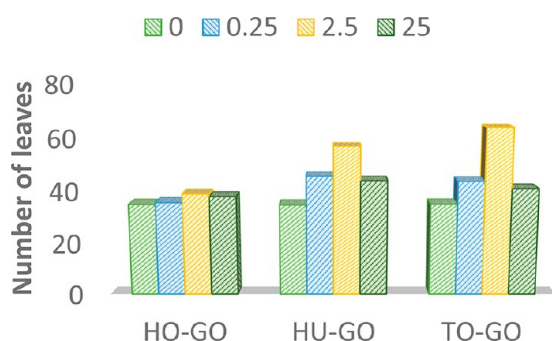

Figure 56. Leaf number of *Lemna minor* treated for 7 days with HO-GO, HU-GO, and TO-GO samples. Reproduced with permission from ref 267. Copyright@2022, Elsevier, Ltd., Chemosphere (redrew the image from the information available).
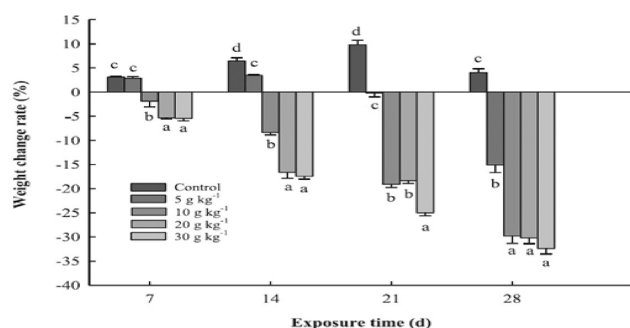

Figure 58. Mortality of embryos at 24, 48, 72, and 96 h postfertilization (hpf). Reproduced with permission from ref 269. Copyright@2019, Elsevier, Ltd., Science of The Total Environment.

Figure 57. Weight change rate of *E. fetida* after 28 days exposure to GO. Reproduced with permission from ref 268. Copyright@2022, Elsevier, Ltd., Ecotoxicology and Environmental Safety.
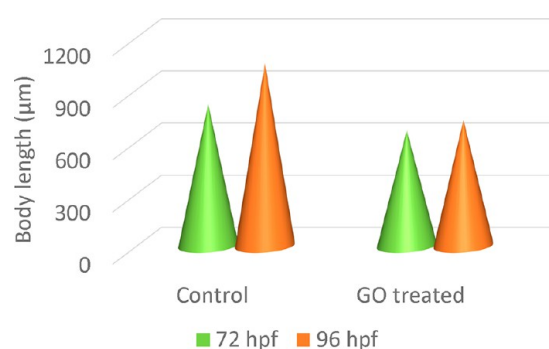
Figure 59. Variation of body length distance in zebrafish embryos and larvae exposed to GO at 72 and 96 h postfertilization (hpf). Reproduced with permission from ref 269. Copyright@2019, Elsevier, Ltd., Science of The Total Environment.

12. TOXICITY OF GRAPHENE OXIDE ON DIFFERENT SPECIES

12.1. *Daphnia magna*. *Daphnia magna* is a planktonic crustacean that belongs to the subclass Phyllopod. GO having a size of 200−300 nm was prepared, and the toxicity evaluation of GO on *Daphnia magna* was done. EC_{50} and LC_{50} values of GO after an exposure of 72 h were found to be 43.3 and 45.4 mg/L, respectively.[254]

12.2. Earthworms. To figure out the toxic effect of GO, many doses of GO (0, 5, 10, 20, and 30g/kg) were introduced

to earthworms and terrestrial invertebrates. DNA migration was found under 5 g/kg of GO in the early days of exposure (7−14 days). Higher the doses of GO caused the migration of most of the DNA under 20 and 30 k/kg on days 21 and 28. SOD activity increases in the first two weeks but decreases on the 21st and 28th day (Figure 43).[255]

12.3. *Ceriodaphnia dubia*. *Ceriodaphnia dubia* is a type of water flea in the class Branchiopoda. GO showed toxicity toward *Ceriodaphnia dubia*, and after 48 h, the EC_{50} value was found to be 1.25 mg/L. After 24 h exposure to a sublethal
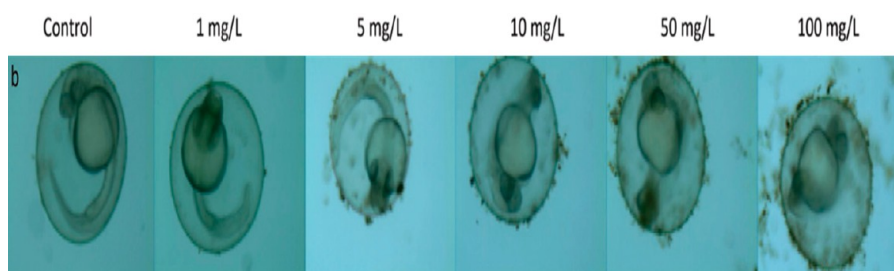
Figure 60. Effect of exposure to different concentrations (control, 1, 5, 10, 50, and 100 mg/L) of GO for 24 h of exposure. Reproduced with permission from ref 271. Copyright@2014, Elsevier, Ltd., Biomedical and Environmental Sciences.
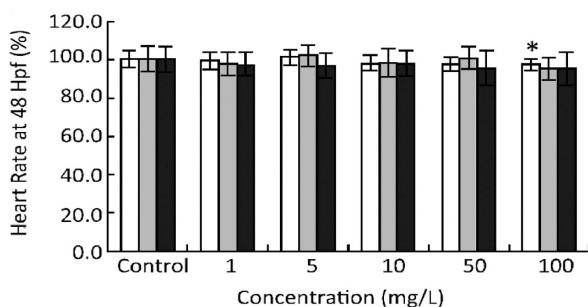
Figure 61. Heart rate of zebrafish embryos at 48 hpf exposed to MWCNTs (white), GO (gray), and RGO (black) at 1 to 100 mg/L concentrations. Reproduced with permission from ref 271. Copyright@2014, Elsevier, Ltd., Biomedical and Environmental Sciences.
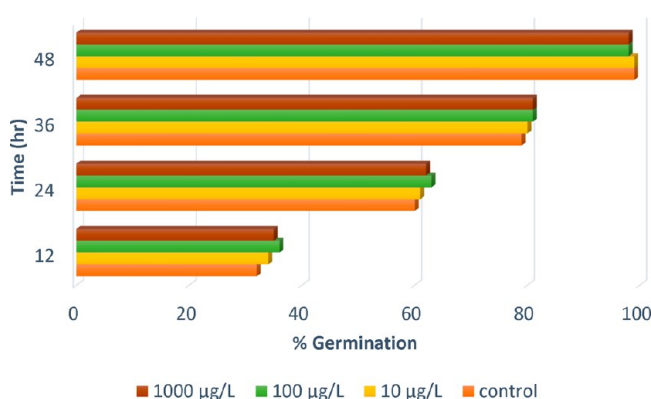
Figure 62. Effects of GO at different times on germination. Reproduced with permission from ref 272. Copyright@2015, Elsevier, Ltd., Environmental Toxicology and Pharmacology (redrew the image from the information available).

Figure 63. Comparison of root length in *Arabidopsis thaliana* seedling plants. Reproduced with permission from ref 272. Copyright@2015, Elsevier, Ltd., Environmental Toxicology and Pharmacology (redrew the image from the information available).

concentration, the *C. dubia* scientifically increases the ROS level (Table 16).[256]

12.4. *Drosophila melanogaster*. *Drosophila melanogaster* is a species of fly belong to family Drosophilidae. Different concentrations of GO caused nearly to 100% mortality on day 16. After exposure to GO, larval crawling was first decreased to 50 μg/mL and increased to 200 μg/mL. An amount of 300 μg/mL causes fatal damage to the neuromuscular coordination of larvae (Figure 44).[257]

12.5. *Artemia salina*. *Artemia salina* is a species of brine shrimp. LC_{50} and EC_{50} values after 48 h of exposure were found to be 489.30 ± 19.41 and 454.69 ± 25.24, respectively. Results also show saturated accumulation of GO with a concentration of 1 mg/L (Figure 45).[258]

12.6. W^{1118} Flies. Serotonin and dopamine levels of W^{1118} flies are approximately 30% wild-type levels, and octopamine levels are approximately 80% wild-type levels. The movement of flies decreased by half ($\sim$3 mm/s) compared to the untreated group ($\sim$6 mm/s) when treated with 10 μg/mL of GO. The weight of flies almost decreased by half ($\sim$0.74 mg). After treatment with 1, 5, and 10 μg/mL of GO, the lifespan of the flies decreased to 48, 50, and 40 days[259] (Figures 46 and 47).

12.7. A549 Cells. A549 cells are lung carcinoma cells that constitute a cell line. To find the toxicity of GO on A549 cells, they (cells) were exposed to different concentrations of GO: m-GO (430 ± 300 nm), l-GO (780−410 nm), and s-GO (160 ± 90 nm). s-GO has more cell viability loss than m-GO and l-GO (concentration-dependent). After 24 h of post-exposure, cell viability is 67% at 200 μg/m of Lof GO. It was observed that s-GO causes severe oxidative stress among all GO samples compared to others: s-GO caused 3.9 times, m-GO caused 2.1 times, while l-GO caused 2.6 times more ROS levels than the controlled group (Figure 48).[260]

12.8. Mouse Eye. Mouse is the most common species found widely all over the world. The eyes are an essential part of any animal to see the world. It was reported that after exposure of 50 μg/mL and 100 μg/mL of GO for one week, corneal opacity was developed (Figure 49). After 24 h of exposure, GO can significantly induce cell viability loss (Figure 50).[261]

12.9. Bacteria Biofilm. GO shows the concentration-dependent enhancement of cell growth in 12 h for all concentrations of bacteria biofilm (Figure 51). A concentration of 50 to 500 mg/L of GO enhances biofilm formation (Figure 52). It was observed that GO significantly enhances cell growth and biofilm formation up to 500 mg/L concentration.[262]
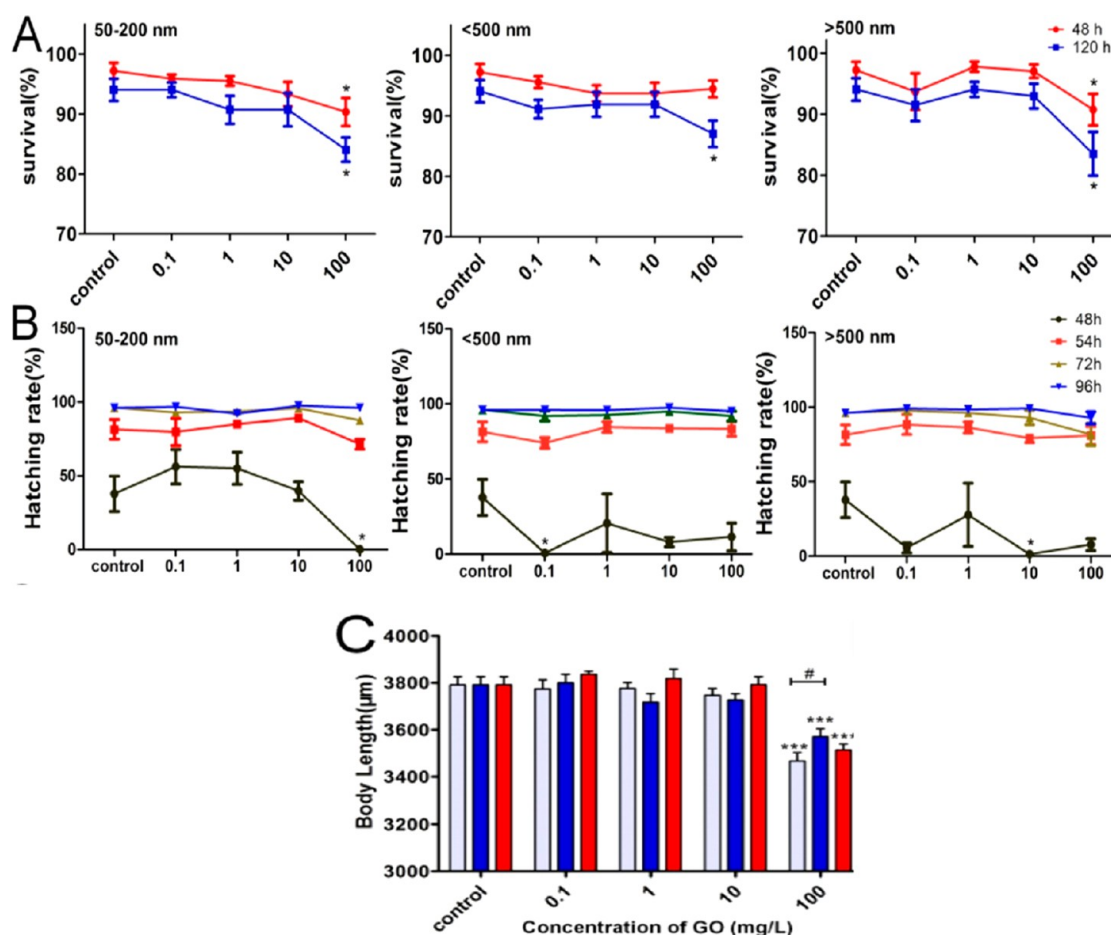
Figure 64. Dose-dependent effects of three different-sized GO (GO) particles (50−200 nm, <500 nm, and >500 nm) on zebrafish embryos and larvae after the 120 h exposure (4−124 h postfertilization). (a) Survival rate, (b) hatching rate, and (c) body length. Reproduced with permission from ref 273. Copyright@2020, Elsevier, Ltd., Ecotoxicology and Environmental Safety.
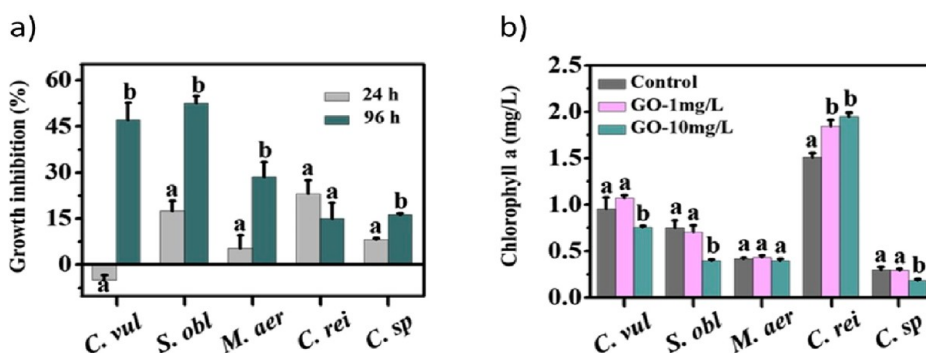
**Figure 65.** (a) Growth inhibition of five different algal cell types (*C. vulgaris*, *S. obliquus*, *C. reinhardtii*, *M. aeruginosa*, and *Cyclotella* sp.) exposed to 10 mg/L of GO at 24 and 96 h, respectively. (b) Content of chlorophyll a. Reproduced with permission from ref 274. Copyright@2020, Elsevier Ltd., Environmental Pollution.

12.10. *Pseudomonas putida*. *Pseudomonas putida* is a soil bacterium. It is an uncommon cause of skin and soft tissue infections. For the toxicity test of GO on *P. putida*, 10 g/L of aqueous GO solution was used. It was found that the presence of GO has a negative effect on the bacterial growth and viability of *P. putida*. The growth of *P. putida* was inhibited in 0.05 mg/mL of GO. Higher concentrations than 0.5 mg/mL and 1.0 mg/mL of GO have a negative impact on the viability of bacteria.[263]

12.11. *Chironomus riparius*. *Chironomus riparius* is a harlequin fly, a species of a non-biting midge. *C. riperius* fourth instar larvae were exposed to 0, 50, 500, and 3000 μg/L of sGO (500 nm), lGO (~10 μm), and mlGO (~9 μm) (monolayer) for 24 h and 96 h. After 24 h of exposure to the concentration of 3000 μg/L, GO accumulation was mainly found in the digestive tract (Figures 53, 54, and 55).[264]

In the experiment, it was observed that after 24 h of exposure to GO there was significant activation of SOD levels.
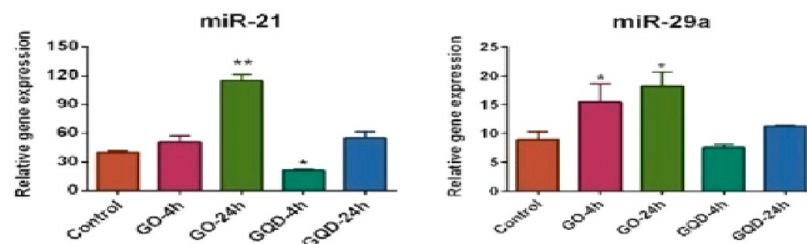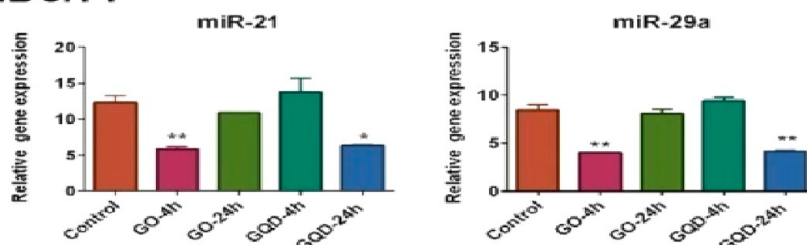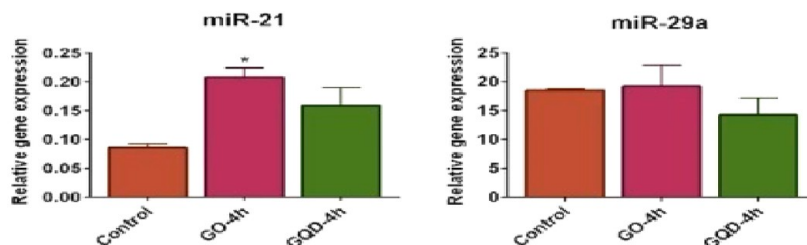
Figure 66. Relative expression of miR-21 and miR-29a in (a) MCF-7, (b) KMBC/71, and (c) HUVEC cells. These cells were exposed to GO-100 and GQDs-50 at a concentration of 15 μg mL^{-1} for 4 and 24 h. Reproduced with permission from ref 275. Copyright@2020, Elsevier, Ltd., Toxicology In Vitro.
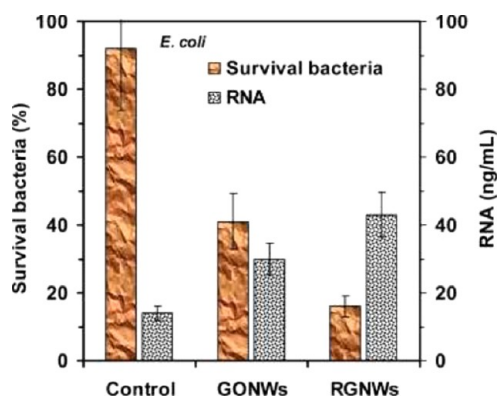
Figure 67. Cytotoxicity of GONWs and RGNWs to *E. coli* and concentrations of RNA in the PBS (phosphate buffer solution) of the *E. coli* bacteria exposed to the nanowalls. Reproduced with permission from ref 276. Copyright@2010, American Chemical Society, Ltd., American Chemical Society- Nano.
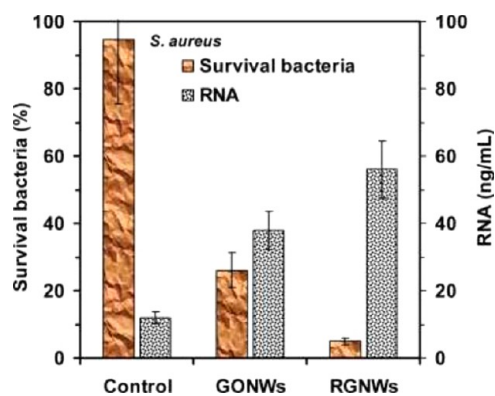
Figure 68. Cytotoxicity of GONWs and RGNWs to *S. aureus* and concentrations of RNA in the PBS (phosphate buffer solution) of the *S. aureus* bacteria exposed to the nanowalls. Reproduced with permission from ref 276. Copyright@2010, American Chemical Society, Ltd., American Chemical Society- Nano.

12.12. *Microcystis aeruginosa*. *Microcystis aeruginosa* is a type of cyanobacteria that lives in fresh water. It can cause harmful algal blooms that are important for the economy and the environment. After 96 h of exposure to GO, the EC$_{50}$ value was 49.32 mg/L. It was reported that the fluorescence intensity of GO was 15.0−58.5%, which is higher than the controlled group. It was concluded that after exposure to 96 h, chlorophyll was reduced by 7.4% at 0.1 mg/L of GO.[265]

12.13. Adult Zebrafish. Zebrafish is a freshwater fish belonging to the minnow family of the order Cypriniformes. Zebrafish was exposed to GO for ~14 days at concentrations of 0.1 and 1 ppm, a high ROS level is observed at a concentration of 1 ppm.[266]

12.14. *Lemna minor*. The common duckweed, also known as duckweed, is *Lemna minor*. It is a freshwater aquatic plant species. Three distinct synthetic approaches were used to test
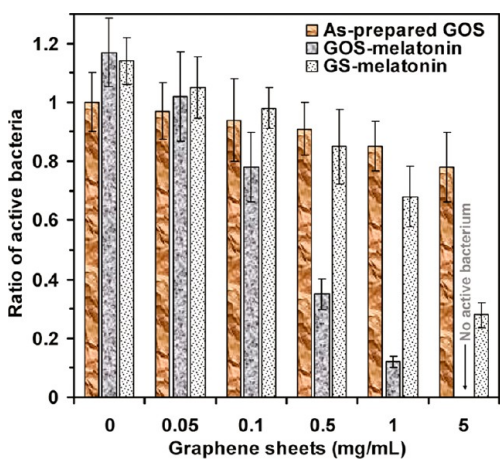
Figure 69. Ratio of the number of the active bacteria obtained from the as-prepared GOS−bacterial, the GOS−melatonin−bacterial, and and the GS−melatonin−bacterial suspensions. Reproduced with permission from ref 277. Copyright@2010, American Chemical Society, Ltd., The Journal of Physical Chemistry B.
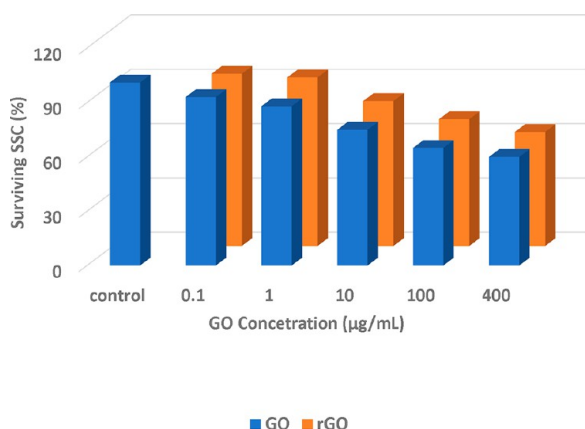
Figure 70. Survival of spermatogonial cells test treated with GO and rGO. Reproduced with permission from ref 278. Copyright@2016, Elsevier, Ltd., Colloids and Surfaces B: Biointerfaces (Redrawn the figure, based on the information available).
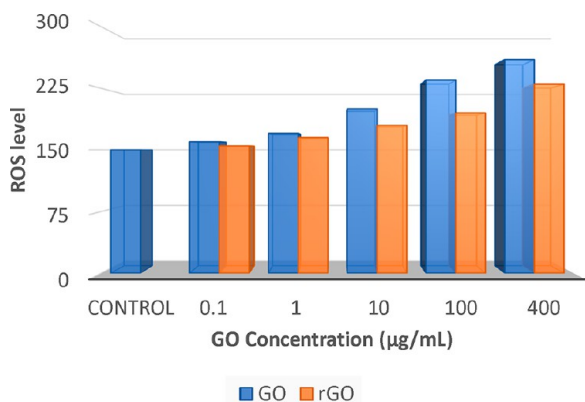
Figure 71. Plotting the measurement of free radicals.[278] Copyright@ 2016, Elsevier, Ltd., Colloids and Surfaces B: Biointerfaces (redrew the image from the information available).

the toxicity of *Lemna minor*: On day 3, the highest yield potential of photosystem ii (Fv/Fm) was approximately 0.8,
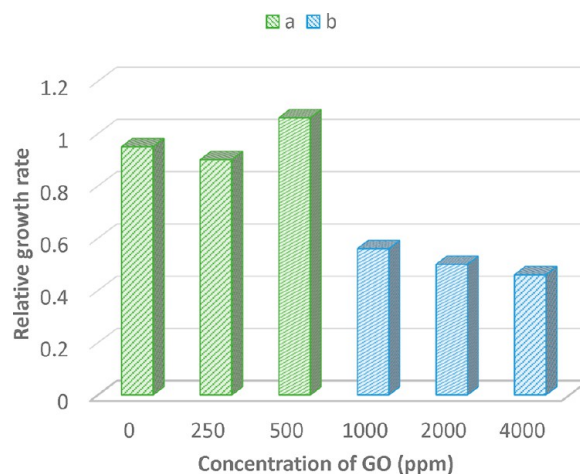
Figure 72. Yeast cells were coincubated with different concentrations of GO. Reproduced with permission from ref 279. Copyright@2016, Elsevier, Ltd., Ecotoxicology and Environmental Safety (redrew the image from the information available).
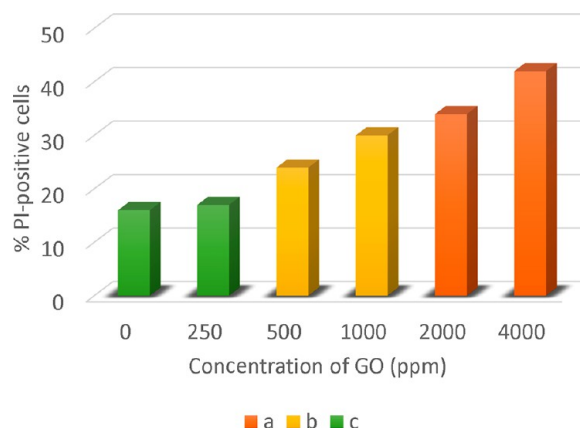
Figure 73. Treated cells stained with PI and observed by fluorescence microscopy. Reproduced with permission from ref 279. Copyright@ 2016, Elsevier, Ltd., Ecotoxicology and Environmental Safety (redrew the image from the information available).
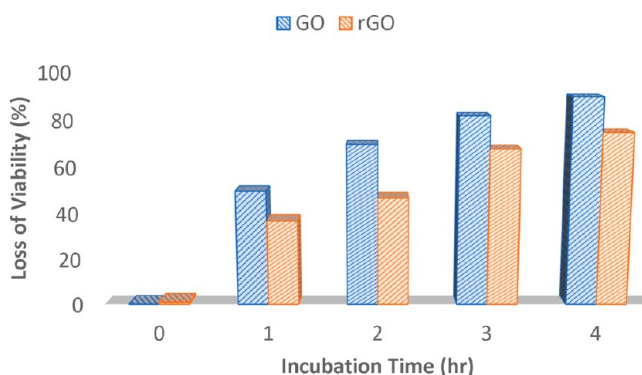
Figure 74. Time-dependent antibacterial activities of GO and rGO. An amount of 5 mL of GO or rGO (80 μg/mL) was incubated with *E. coli* (106 to 107 CFU/mL, 5 mL) for 4 h. The loss of visibility was measured at 0, 1, 2, 3, and 4 h, respectively. Reproduced with permission from ref 281. Copyright@2011, American Chemical Society, American Chemical Society- Nano (redrew the image from the information available).
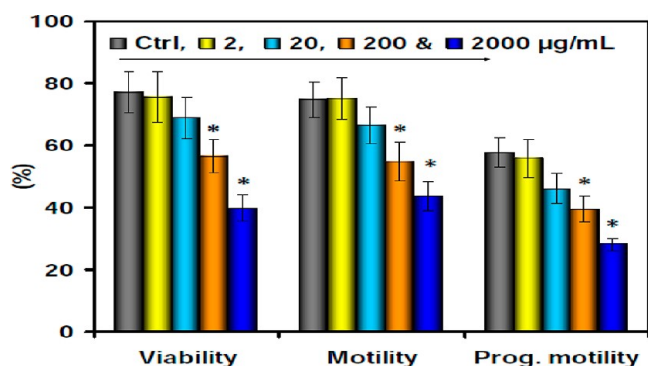
Figure 75. Viability, motility, and progressive motility. Reproduced with permission from ref 283. Copyright@2015, Elsevier Ltd., Carbon.
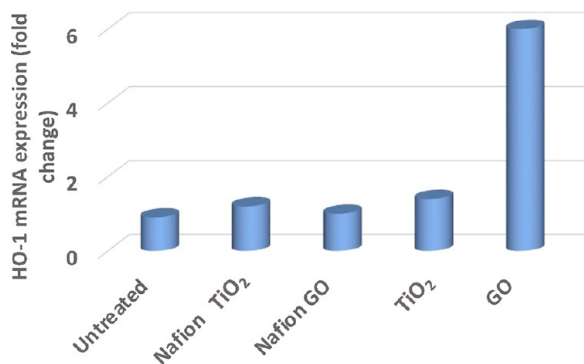
Figure 76. mRNA gene expression of HO-1 in zebrafish after exposure to free nanoparticles and nanocomposites. The HO-1 mRNA expression was increased only in free GO treatment. Reproduced with permission from ref 284. Copyright@2017, Frontiers in Physiology (redrew the image from the information available) (open access).
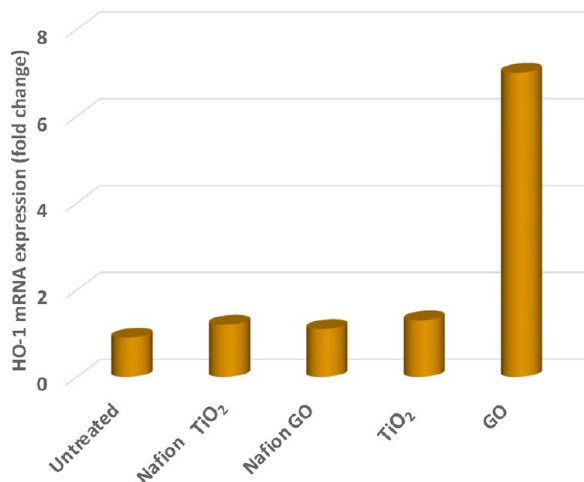
Figure 77. Gene expression of iNOS in zebrafish after exposure to free nanoparticles and nanocomposites. The iNOS mRNA expression was increased only in free GO treatment. Reproduced with permission from ref 284. Copyright@2017, Frontiers in Physiology (redrew the image from the information available) (open access).

but it dropped to 0.78 on days 5 and 7. The number of leaves were tripled from the original (Figure 56).[267]

12.15. Earthworm (*Eisenia fetida*). Two methods were used to determine the toxicity of GO on earthworm. One is a
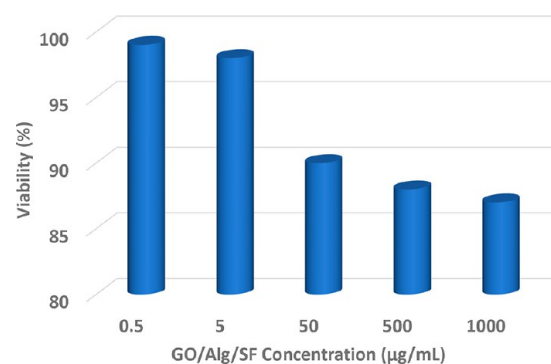
Figure 78. Cell viability histogram at different concentrations and picture of the MTT assay on the Hu02 cell line with different concentrations. Reproduced with permission from ref 286. Copyright@2020, Elsevier, Ltd., Carbohydrates Polymer (redrew the image from the information available).
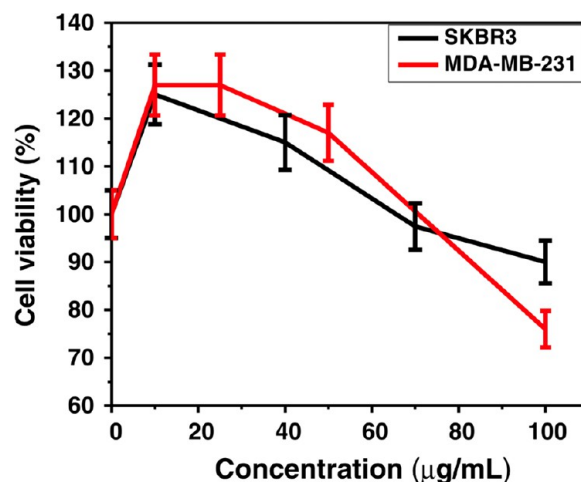
Figure 79. Cell viability of MDA-MB-231 and SKRB3 cell lines. Reproduced with permission from ref 288. Copyright@2015, Elsevier, Ltd., Materials Science and Engineering: C.

filter paper contact test, and another is a soil contact test. The author reported that after 24 and 48 h of exposure the EC_{50} values were 2.52 and 2.36 mg/mL, respectively. GO has a negative effect on earthworm growth, and earthworms had a significant weight loss of >30% at 10−30 mg/mL (Figure 57).[268]

12.16. Zebrafish Embryo (*Danio rerio*). The embryonic stage of zebrafish was investigated to find the toxic effects of GO. It was found that GO significantly affects the mortality rate at higher concentrations (0.4−1 mg/mL)[269] (Figures 58 and 59).

12.17. *Microcystis aeruginosa*. *Microcystis aeruginosa* is a species of freshwater cyanobacteria, and its EC_{50} value after exposure to GO for 96 h was found to be 11.1 μg/mL.[270]

12.18. Zebrafish Embryo. The toxicity of GO on zebrafish embryos has been reported. Solutions of GO having different concentrations of 1, 5, 10, 50, and 100 mg/L were prepared, and embryos were exposed to these solutions for 96 h (Figure 60).[271]

In the case of heart rate, it was reported that after exposure to GO (conc. of 100 mg/L) for 48 h the heart rate of zebrafish embryos was significantly decreased (Figure 61).[271]

12.19. *Arabidopsis thaliana*. *Arabidopsis thaliana* is a small flowering plant native to Eurasia and Africa. The toxic
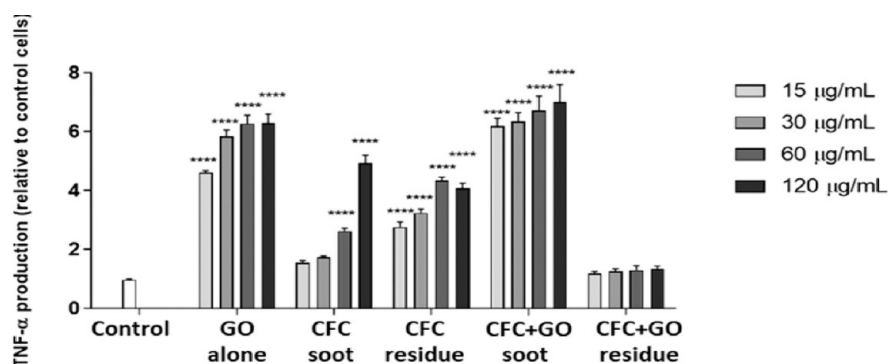
Figure 80. Pro-inflammatory response induced by the five samples as determined by the production of TNF-α. Reproduced with permission from ref 289. Copyright@2021, Elsevier, Ltd., Journal of Hazardous Material.
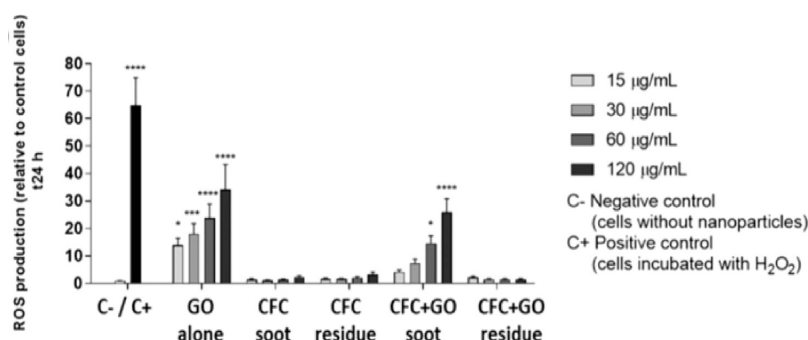
Figure 81. Oxidative stress induced by the five samples as determined by ROS production after 24 h. Reproduced with permission from ref 289. Copyright@2021, Elsevier, Ltd., Journal of Hazardous Material.
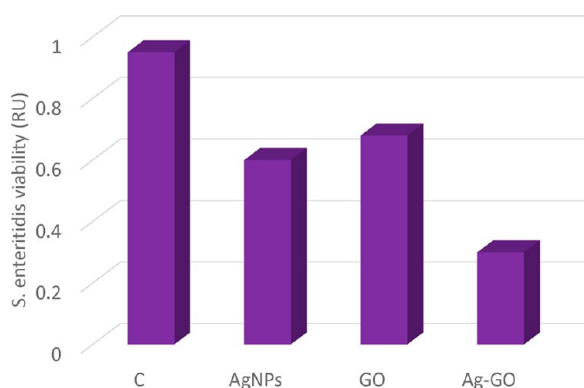
Figure 82. Enteritidis was incubated on silver nanoparticles and GO-coated nanoplatforms after incubation at 37 °C for 24 h. Reproduced with permission from ref 290. Copyright@2019, Springer, Ltd., Nanoscale Research Letters (redrew the image from the information available).

effect of GO on this species within the range of μg/L was investigated. No significant change in germination within the range (Figure 62).[272]

At a concentration of 1 μg/L, considerable accumulation of GO was found. It was reported that there was no significant change in seeding and root length from day 4 to day 8 (Figure 63).[272]

12.20. Zebrafish Embryo. The toxicity of different sized GO on zebrafish embryos was investigated. Three different sizes of GO, 50−200 nm (s-GO), <500 nm (m-GO), and >500 nm (l-GO), with an exposure time of 4−124 h, were investigated. Zebrafish embryos showed the sized-based side effects of GO. After exposure of 120 h, the survival rate was

significantly reduced. It was concluded that after 48 h hatching rates are inhibited in 100 mg/L of s-GO, 0.1 mg/L of m-GO, and 10 mg/L of l-GO. It was observed that body length was also inhibited at a high concentration of GO (100 mg/L) (Figure 64).[273]

12.21. Algae. The toxicity of GO on three classes of algae (cyanobacteria, green algae, and diatom) was examined. After 96 h of exposure to GO, algae growth was significantly inhibited with a 10 mg/L concentration. All species have resistance power to oppose the effect of any chemical, so different algae showed different side effects against GO, as shown in Figure 64. A significant difference in chlorophyll-a was observed with the concentration of 10 mg/L as compared to a control, as shown in Figure 65.[274]

12.22. miR-21 and miR-29a in Human Cell Lines. miR-21 and miR-29a are from the family of micro RNA. Micro RNA is a small single-stranded noncoding RNA. A noncytotoxic dose of 15 μg/mL of GO (100 nm) was selected to examine the toxicity of GO. A fluctuation of miR-21 in MCF-7, KMBC/71, and HUVEC cells was observed, while the expression of miR-29a was only changed in MCF-7 and KMBC/71. No significant change was observed in HUVEC cells of miR-29a (Figure 66).[275]

12.23. Bacteria. Gram-positive (*Staphylococcus aureus*) and gram-negative (*Escherichia coli*) models of bacteria were used to assess the toxicity of GO against bacteria. Cell damage was discovered when bacteria came into direct contact with the razor-sharp edges of the nanowalls. Gram-negative bacteria were less susceptible to the damage that nanowalls induced to their outer meninges than gram-positive bacteria. Nanowalls made of GO also have antibacterial properties. After 1 h, 26.5%
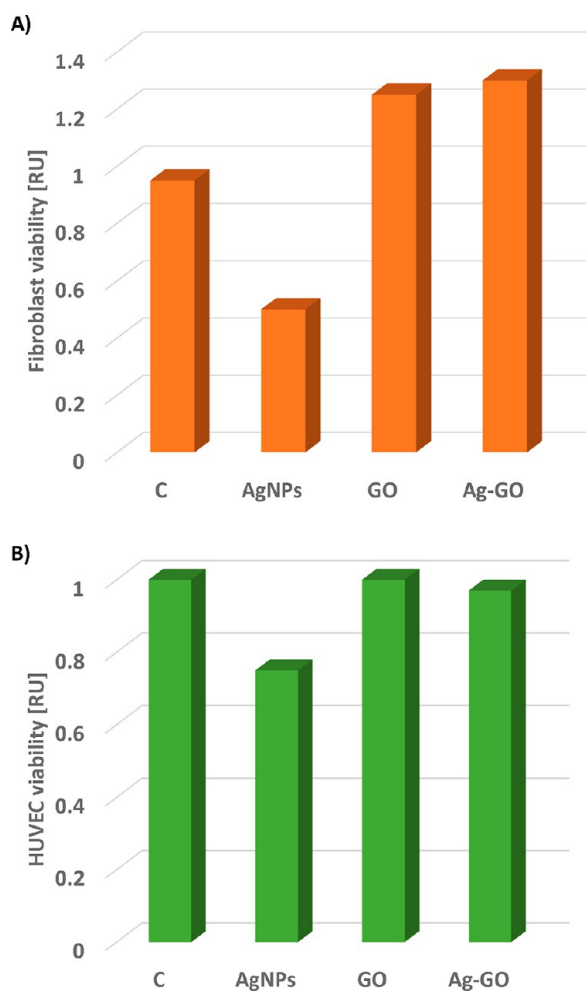
Figure 83. Fibroblast (a) and HUVEC (b) viability after 24 h of incubation on the nanoplatforms was determined using a Presto Blue assay. Reproduced with permission from ref 290. Copyright@2019, Springer, Ltd., Nanoscale Research Letters (redrew the image from the information available).
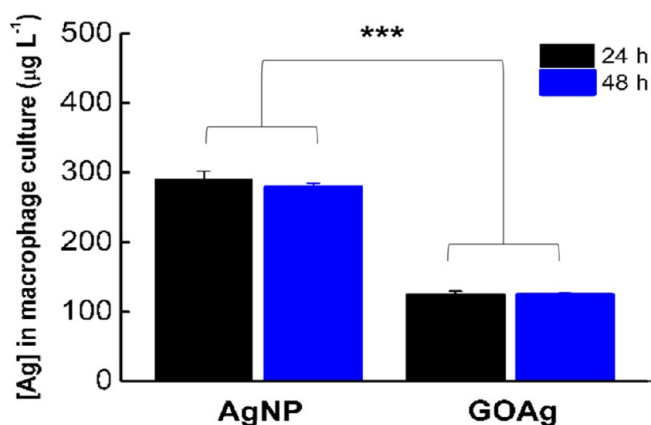
Figure 84. Concentration of silver inside the J774 tumoral macrophage. Cells cultivated in culture bottles were exposed to 1000 μg L^{-1} of pristine silver nanoparticles and GO−silver nanocomposites for 24 and 48 h. Reproduced with permission from ref 291. Copyright@ 2016, Springer, Ltd., Journal of Nano-biotechnology.

of *S. aureus* bacteria and 41.8% of *E. coli* bacteria could survive[276] (Figures 67 and 68).

12.24. *Escherichia coli*. Suspensions of GO of 0.05, 0.1, 0.5, 1, and 5 mg/mL concentrations were used to investigate the toxicity of GO toward *Escherichia coli*. The suspension of GOS−melatonin with a functional group containing oxygen might capture the bacteria. Bacterial activity in the bacterial suspension decreased as GOS concentration was increased. No active bacteria were found in the GOS−melatonin−bacterial suspension at a concentration of 5 mg/mL (Figure 69).[277]

12.25. Mice. GO was produced in concentrations of 1, 10, 100, and 400 g/mL, and exposure times of 24 h were used to determine the cyto-genotoxicity of GO on mouse spermatogonial stem cells. The number of spermatogonia colonies and viable cells dropped at concentrations of 100 and 400 g/mL, and there was considerable cell death (Figure 70). The ROS levels significantly increased at concentrations of 100 and 400 g/mL as well (Figure 71).[278]

12.26. *Pichia pastoris*. *P. pastoris* was exposed for 24 h to various GO concentrations (0−4000 ppm). Twenty-four hours of exposure to a higher concentration of 500 ppm greatly reduced the cell development (Figure 72). The IC$_{50}$ value for this study was found to be 1125 $\pm$ 40 ppm. Concentrations ≥1000 ppm of GO led to an increase of intercellular ROS level (Figure 73). A concentration greater than 1000 ppm caused membrane damage and oxidative stress together in *P. pastoris*.[279]

12.27. *Escherichia coli*. In this study, *E. coli* was exposed to GO concentrations for 0−48 h. The oxygen-containing functional groups of the GO were reported to have dropped by about 60%, indicating a relative chemical reduction of the sheets as a result of the interaction with the bacteria. After exposure, bacteria were shown to have reduced GO concentrations due to their metabolic activity, namely, their glycolysis process.[280]

12.28. *Escherichia coli*. In this study, GO was found to have antibacterial properties against *E. coli* at various concentrations (0−400 g/mL). GO has stronger antibacterial properties when compared to rGO, graphite, and gold oxide. They further stated that both the membrane and oxidative stress may be responsible for bacterial cytotoxicity. After being exposed to *E. coli* at 40 g/mL for 4 h, the viability gradually increased (Figure 74).[281]

12.29. Human Stem Cells. The building blocks of the body are stem cells. The authors evaluated the toxicity of rGONPs on human stem cells. rGONPs with average leteral dimensions (ALDs) of 114 nm showed strong potential in cell wall destruction at concentrations of 1 g/mL and could enter the hMSCs' nuclei and exhibit some genotoxicity due to DNA fragmentation and chromosomal aberrations at low concentrations of 0.1 and 1.0 mg/mL after 1 h. After 1 h, the cytotoxicity of rGO sheets with ALDs of 3.804 nm emerged at high concentrations of 100 g/mL.[282]

12.30. Mice. The findings of this study demonstrated that mice treated with a dose of 2000 g/mL had high levels of GO absorption in their testicles. Additionally, a 45% decrease in sperm viability and motility was discovered (Figure 75). After being exposed to GO, the mice's semen likewise produced ROS.[283]

13. COMPOSITE OF GRAPHENE OXIDE

13.1. Graphene oxide and Nafion Polymers on Zebrafish Embryos. In this study, the toxicity of nanocomposite membranes made using a Nafion polymer and GO has been investigated. The zebrafish is thought to be an
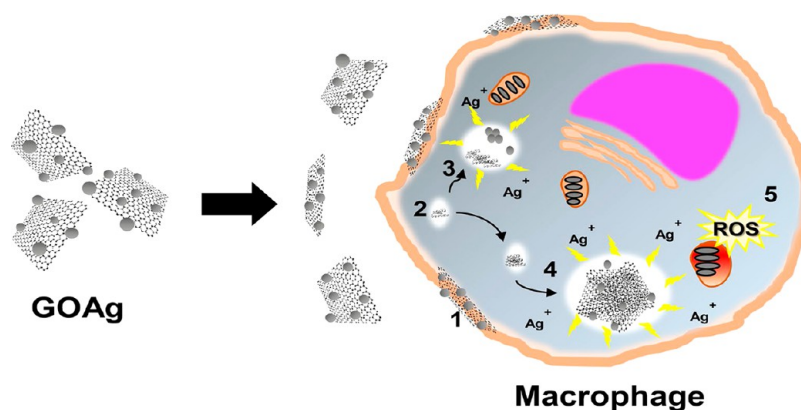
Figure 85. Macrophage cells' absorption and breakdown of the nanocomposite as well as the creation of oxidative stress. Reproduced with ref 291. Copyright@2016, Springer, Ltd., Journal of Nanobiotechnology.
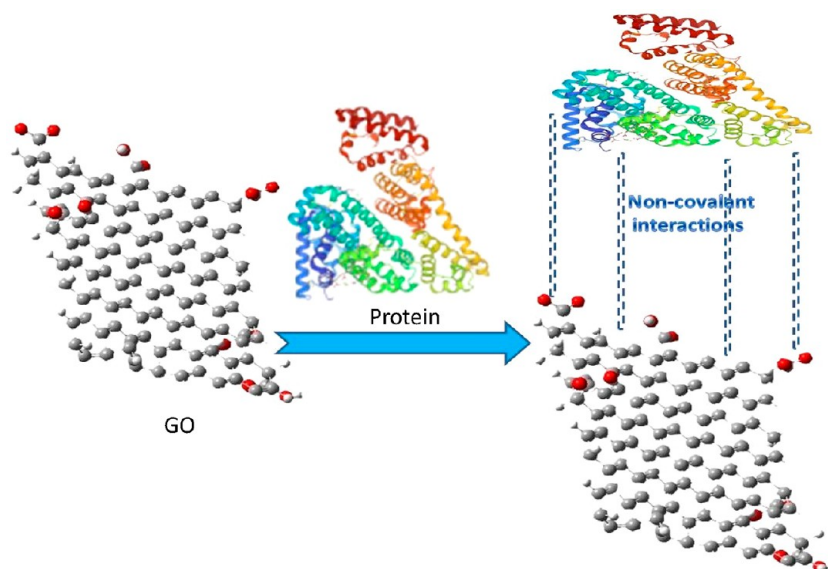
Figure 86. Schematic representation for the interaction of GO with a protein.

effective animal model for understanding developmental toxicity pathways. The author reported that the composite of GO and the nafion polymer did not show a significant effect on HO-1 and iNOS. They concluded that GO causes more toxicity to zebrafish embryos (Figures 76 and 77).[284]

13.2. GO−TiO₂ Composite on A549 Cells. In the present experiment, the cytotoxic effect of the GO−TiO$_2$ composite on A549 cells has been evaluated. The GO−TiO$_2$ composite showed a significant decrease in cell viability after an exposure of 4 h. It has been reported that a high concentration led to a low level of cell viability.[285]

13.3. GO/Alginate/Silk Fibroin Composite. Herein, modified GO with natural Alg and added SF were used to get a hybrid material, that is, GO/Alg/SF. The cell viability of this nanostructure was found to be 89.2%, and the hemolytic effect was found to be less than 6% at high concentrations (1000 μg/mL) (Figure 78).[286]

13.4. Magnetic Chitosan/GO (MCGO) Composite on A549 Cells. The toxicity of GO and its composite was evaluated on the A549 cells. Cells were exposed for 24 h in the concentration range of 50−250 μg, and the toxicity was investigated. It has been reported that viable cell percentages at 50 and 100 μg concentrations were 53.7% and 44.8%, respectively.[287]

13.6. Human Breast Cancer Cells. Human breast cancer cell lines (MDA-MB-231 and SKBR3 cell lines) were chosen to find the potential of curcumin/rGO. At a higher concentration of 100 μg/mL, ∼15−25%, the cell destruction has been observed (Figure 79).[288]

14. CARBON-FIBER-REINFORCED COMPOSITES (CFCS) AND GRAPHENE OXIDE COMPOSITE

The authors have reported that the CFC + GO residue did not show a pro-inflammatory response, while soot CFC + GO induced a significant difference to the control. There was no significant toxic effect on cytotoxicity due to CFC + GO. The authors have also reported that CFC + GO soot induced ROS production in a concentration-dependent manner (Figures 80 and 81).[289]

15. GRAPHENE OXIDE AND AG NANOPARTICLE COMPOSITES

Huge growth inhibition has been seen with GO−Ag composites after 24 h. After direct incubation of 24 h on fibroblasts and HUVECs (human umbilical vein endothelial
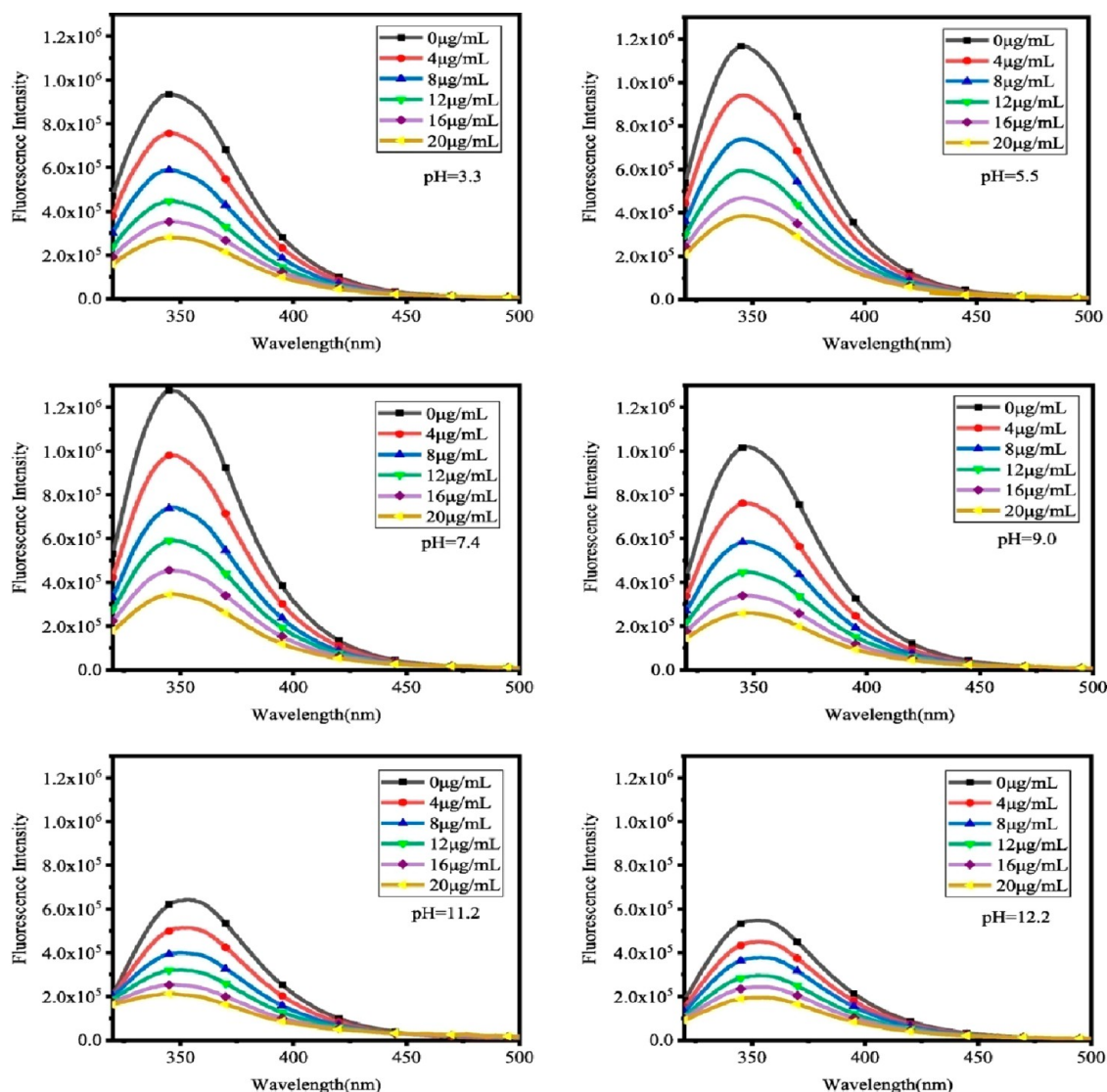
Figure 87. Fluorescence emission spectra of Lyz in the presence of various concentrations of GO at different pH. Concentrations of GO are (lg/mL): 0, 4, 8, 12, 16, and 20. Lyz = 0.143 mg/mL. k_{ex} = 286 nm. Reproduced with permission from ref 295. Copyright@2021, Elsevier, Ltd., Spectrochimica Acta Part A: Molecular and Biomolecular Spectroscopy.
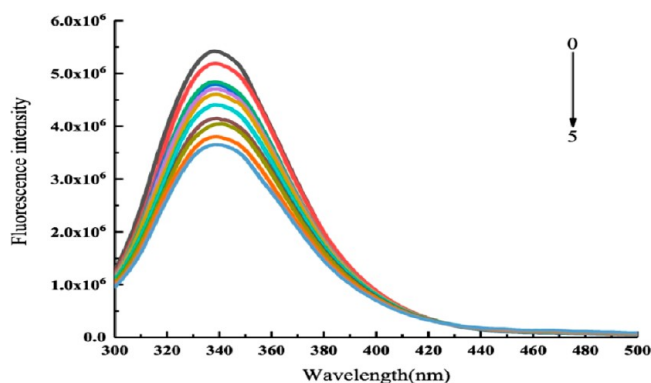
Figure 88. Fluorescence spectra of BSA in various concentrations of GO in aqueous solution (pH = 7.4) at 298 K. [BSA] = 3×10^{-6}mol/L. [GO] = 0.25, 0.5, 0.75, 1.0, 1.25, 1.5, 1.75, 2.0, 2.25, and 2.5×10^{-5} mol/L. Reproduced with permission from ref 296. Copyright@2019, Elsevier, Ltd., Spectrochimica Acta Part A: Molecular and Biomolecular Spectroscopy.
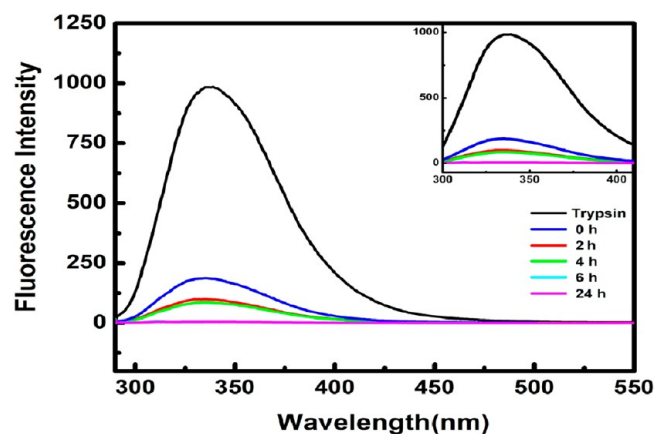
Figure 89. Fluorescence spectra of 1:1 Trp−GO at different time intervals. Reproduced with permission from ref 298. Copyright@ 2020, Elsevier, Ltd., International Journal of Biological Macromolecules.
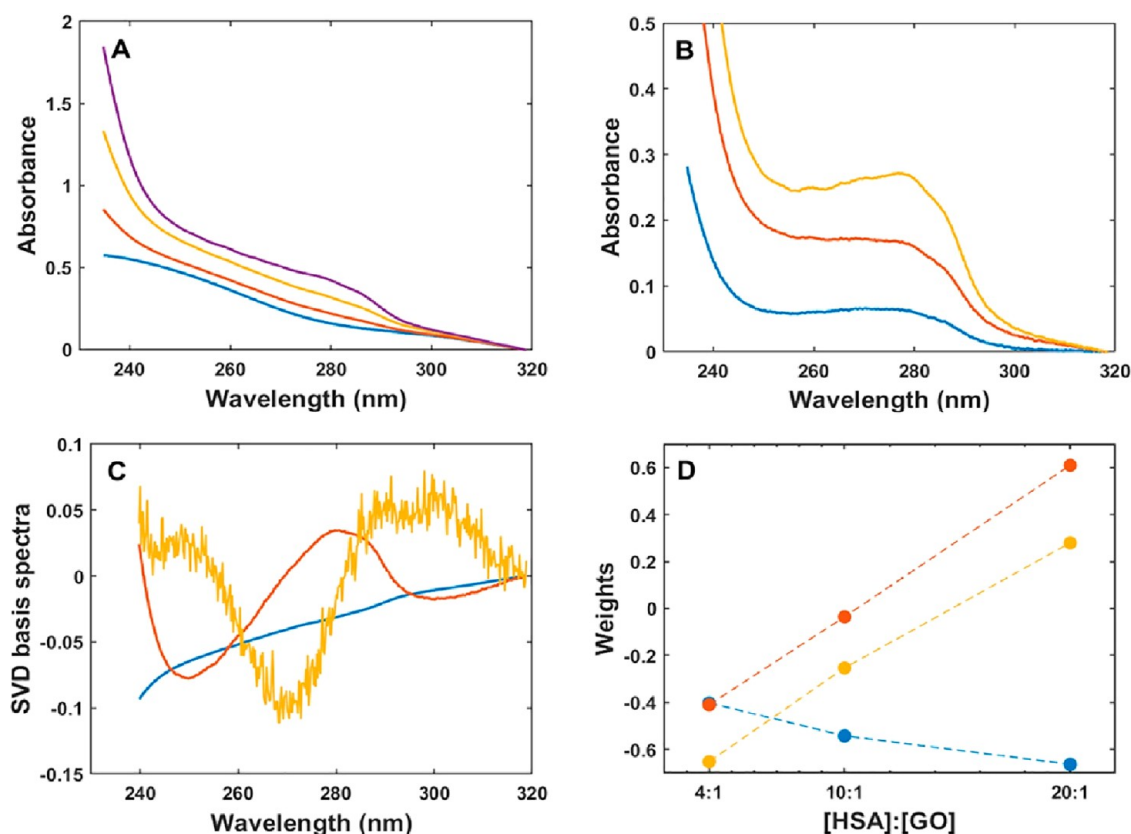
Figure 90. (A) Absorption spectra of pure GO (blue) and [HSA]:[GO] ratios of 4:1 (red), 10:1 (yellow), and 20:1 (purple). (B) Difference spectra of [HSA]:[GO] ratios of 4:1 (blue), 10:1 (red), and 20:1 (yellow). (C) Basis spectra obtained by SVD analysis: singular values of descending order: s1 - red, s2 - blue, and s3 - yellow, respectively. (D) Dependence of the weights (w1 - red, w2 - blue, w3 - yellow symbols) of the s1, s2, and s3 basis spectra, respectively, as a function of the [HSA]:[GO] ratio. Reproduced with permission by ref 299. Copyright@2021, Elsevier, Ltd., International Journal of Biological Macromolecules.

cells), cell viability was not significantly changed (Figures 82 and 83).[290]

16. GRAPHENE OXIDE + AG NANOCOMPOSITES

J774 is a cell line isolated from ascites of a patient with reticulum cell sarcoma. On exposing the composite to J774 for 24 and 48 h, IC50 values were found to be 2.9 and 3.8 μg/mL, respectively. Ag can be up taken by J774 tumoral macrophages after 24 and 48 h of exposure with a concentration of 1000 μg/L. After exposure to GO–Ag, 124 and 124.2 μg/L (12%) of Ag were internalized by J774 (Figure 84).[291]

GO–Ag NPs interact with the cell in multiple stages, which start from macrophage endocytosis along with vesicle maturation. After that the nanocomposite degrades, releasing the Ag ions into the cell/cytoplasm. Due to this release, mitochondria stop working properly, and their function imparted causes oxidative stress, as shown in Figure 85.

17. PROTEIN/DNA INTERACTION WITH GRAPHENE OXIDE

Protein–GO complex formation involves various interactions such as electrostatic, H-bonding, hydrophobic, and $\pi-\pi$ interactions and van der Waals forces.[292] Such interactions are surface-dependent; hence, the formation of a complex is dependent on the functional groups situated at the protein surface and GO, as shown in Figure 86.[293]

17.1. Graphene Oxide with Lysozyme. Fluorescence spectroscopy of GO interaction with lysozyme reflects changes in the structure of our protein. Due to conformational changes in lysozyme, there is some red shift.[294] The fluorescence intensity of our protein is observed to decrease when the pH is increased above 7.4, at which the intensity was the highest. Lower pH values did not show much change as shown in Figure 87. This shows that at higher pH lysozymes may undergo some conformational changes.[295]

17.2. Graphene Oxide with BSA. The fluorescence spectra (Figure 88) show some decrease in fluorescence with the increase in the GO concentration. This reduction in intensity is attributed to the strong interactions between GO and BSA.[296] These interactions altered the environment, and fluorescence intensities of fluorophores were lowered due to fluorescence quenching.[297]

17.3. Graphene Oxide with Trypsin. Fluorescence spectroscopy was done on the 1:1 construct of GO–trypsin. It can be seen in Figure 89 that there is a decrease in the intensity of the spectra which shows that GO quenches the protein. Also, there is a red shift on the interaction with protein, suggesting opening of the β-sheet structure of protein. Trypsin has a characteristic signal at 336 nm, but when it interacts with GO, the signal shifts to 342 nm, indicating that the sheet structure opens up and quenching occurs.[298]

17.4. Graphene Oxide–Human Serum Albumin (HSA). The UV spectra of GO–HSA overlap, which makes it difficult to differentiate the effect of their interaction. Singular value decomposition (SVD) of the spectra allowed us to separate the bands. On increasing the [GO]:[HSA] ratios,
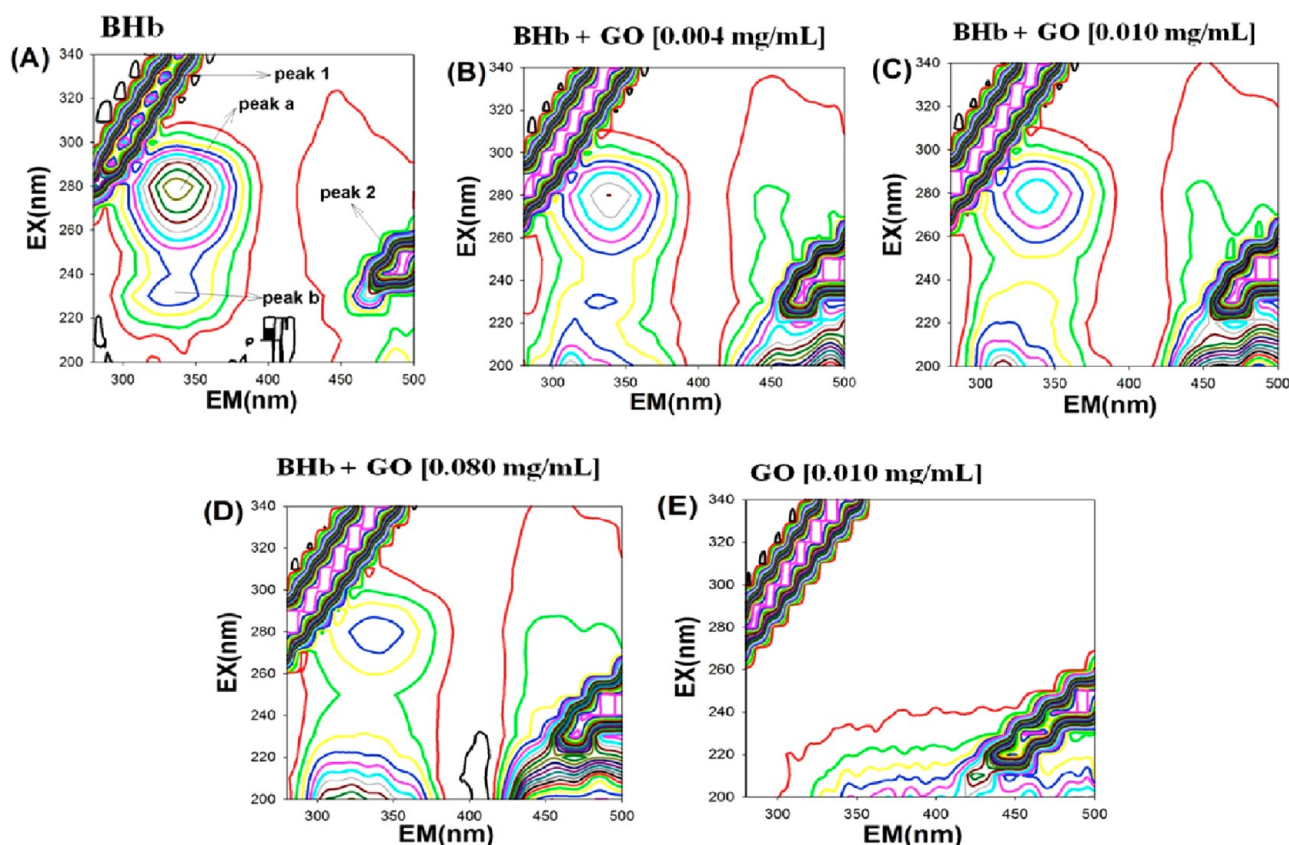
Figure 91. Three-dimensional fluorescence spectral contours of the (A) BHb, (B–D) BHb–GO system, and (E) GO. Conc. of BHb: (A) 5.0×10^{-6} mol/L, (B) 5.0×10^{-6} mol/L, (C) 5.0×10^{-6} mol/L, (D) 5.0×10^{-6} mol/L, and (E) 0.0×10^{-6} mol/L. Conc. of GO: (A) 0.00 mg/mL, (B) 0.004 mg/mL, (C) 0.010 mg/mL, (D) 0.080 mg/mL, and (E) 0.010 mg/mL. Reproduced with permission from ref 300. Copyright@2016, Elsevier, Ltd., Materials Chemistry and Physics.
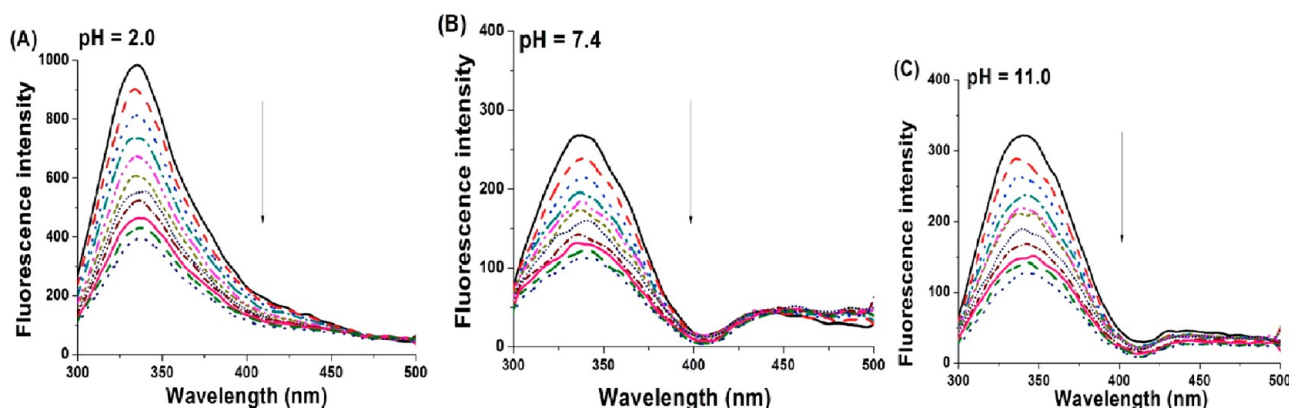
Figure 92. Fluorescence spectra of BHb (5.0×10^{-6} mol/L) in different concentrations of GO. $c(GO)/(\mu g/mL)$: 0, 2, 4, 6, 8, 10, 12, 14, 16, 18, and 20. $T = 298$ K, $\lambda_{ex} = 280$ nm. (A) pH = 2.0, (B) pH = 7.4, and (C) pH = 11.0. Reproduced with permission from ref 300. Copyright@2016, Elsevier, Ltd., Materials Chemistry and Physics.

there is a blue shift as the weight is increased, as shown by the shape of the curve (Figure 90).[299]

17.5. Graphene Oxide with Bovine Hemoglobin (BHb). Each α and β chain of BHb contains three tryptophan units. Three-dimensional fluorescence spectra showed quenching of BHb spectra when it interacts with GO. The quenching can also be identified through a decrease in the intensity of the fluorescence at different pH, which implies there are hydrophobic interactions possible.[300] Fluorescence emission spectra of BHb with different concentrations of GO at various pH levels are shown in Figures 91 and 92.

17.6. Corona-Coated Graphene Oxide. The author employed GO to observe the biological reaction to corona derived from various diseases. The author of this study determined the impact of corona-coated GO. With GO sheets, human plasma that had been exposed to various diseases was cultured. The results revealed that varied corona decorations on GO sheets affected the cellular toxicity, ROS generation, and lipid peroxidation in diverse ways.[301]

17.7. Human Epithelial Cells. The prevention of cell growth and activation of cell death were examined at a dosage of 100 μg/mL. The results also showed that a concentration
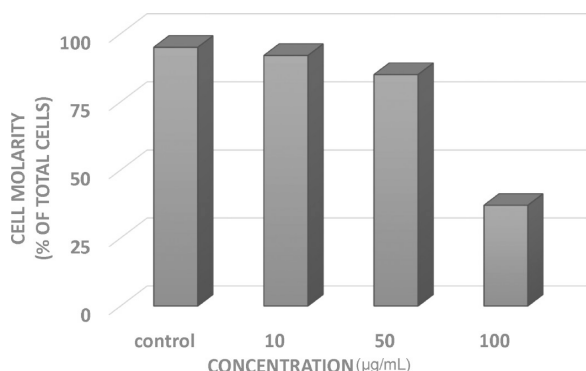
Figure 93. Viability of cells. Reproduced with permission from ref 302. Copyright@2014, Elsevier Ltd., Applied Surface Science (redrew the image from the information available).

≤50 μg/mL caused no significant toxicity to the cells. After 24 h post exposure at a concentration of 100 μg/mL, viability loss was observed (Figure 93).[302]

17.8. Human Mesenchymal Stem Cells. The toxicity of rGO nanoribbons (rGONRs) and rGO nanosheets (rGOSs) on human mesenchymal stem cells was investigated in this work. The author claimed that 10 g/mL of rGONRs produced cytotoxicity, including cell viability, after exposure for 1 h. The results demonstrated that 96 h after exposure the same cytotoxity was still present at a concentration of 100 g/mL. The findings also demonstrated that rGONRs, even at a concentration of 1.0 g/mL, produced DNA fragmentation following exposure for 1 h.[303]

17.9. Corona-Coated Spinal-Graphene Nanomaterial. In this study, the author assessed the therapeutic benefits of spinal-graphene nanoparticles coated with corona against cancer. The outcome demonstrated a correlation between the amount of protein corona absorbed on spinal graphene and local and global heating brought on by laser irradiation. The study's findings indicated that the effectiveness of graphene-based photothermal therapy in the treatment of cancer is correlated with the quantity of corona generated by laser irradiation. A reduction in the quantity of corona during laser irradiation had an impact on the therapeutic and harmful effects of NPs.[304]

18. OPTOELECTRONIC APPLICATIONS OF GO

GO can function as a fluorescence quencher by adsorbing dye molecules on its surface, followed by fluorescence resonance energy transfer (FRET), to quench the fluorescence signal.[305] GO absorbs laser light and transfers it to surface molecules. GO increases the Raman signal via a chemical process on its surface and possesses peroxidase-like enzymatic activity.[306] Electrochemical, optical (fluorescent, colorimetric, and Raman), and mass analysis biosensors have been developed using GO because of its useful inherent characteristics.[307] Choi et al. utilized intrinsic properties of GO and synthesized a GO sheet–Pt composite for dye-sensitized solar cells, and it was observed that GO sheets increased the surface area, number of active sites, and crystallinity of Pt.[307] In another example, GO nanosheets were synthesized via a simple method, and the results exhibited comparatively better characteristics, indicating that the synthesized GNSs are a credible potential option for optoelectronic devices such as solar cells, supercapacitors, electrochemical and bio sensors, and biomarkers and also appropriate for low-temperature fuel cells.[308] In a recent work

of Kant et al., the MgO–rGO nanocomposite was synthesize,d in which carbon networks with conductive properties were established and caused enhanced dielectric performance and better optical transmissions.[309] Biosensors using field effect transistor (FET) technology may detect BNP significantly faster than with traditional clinical trials. The usability of GO was found in another class of sensitive biosensors know as field effect transistors (FETs). A number of review articles have been published summarizing the advantages of using GO or GO derivatives for the preparation of biosensors.[310−312]

19. CONCLUSION

In this article, the authors present a variety of approaches for the synthesis and characterization of graphene oxide (GO) and its composites. At the moment, the Hummers method is utilized quite frequently for the synthesis of GO but with a few modifications. Due to the layered structure of GO, which also contains groups like carbonyls, hydroxyls, and epoxides that contain oxygen, the active surface area is quite large, as after exfoliation GO sheets are separated out. The results of several chemical reactions point to GO as a promising candidate for the role of catalyst. The regeneration of tissues and organs on GO scaffolds is an important field that needs additional research. This review also discusses certain other applications, such as photocatalytic activity and biological applications like drug delivery. Some of GO's applications are reported here. GO is not one of the best electrical conductors, but its conductivity can be altered by reducing the functional groups present on it to obtain rGO. rGO has quite a lot of applications in different fields as well. One feature that needs more attention is toxicity; it was discovered that the concentration of GO affects whether or not it is physiologically harmful, which restricts its use in the field of medicine. It has been found that there are a lot of animal species for which GO showed some cytotoxic nature. This is one of the aspects that needs more study. GO can be functionalized quite easily. Therefore, there is a need for more research to find ways to reduce its toxicity.

■ AUTHOR INFORMATION

Corresponding Authors

Indra Bahadur — *Department of Chemistry, Faculty of Natural and Agricultural Sciences, North-West University, Mmabatho, South Africa;* ● orcid.org/0000-0003-2906-473X; Email: bahadur.indra@gmail.com

Pallavi Jain — *Department of Chemistry, Faculty of Engineering and Technology, SRM Institute of Science and Technology, Uttar Pradesh, India;* Email: palli24@gmail.com

Prashant Singh — *Department of Chemistry, Atma Ram Sanatan Dharma College, University of Delhi, Delhi, India;* ● orcid.org/0000-0001-9648-2275; Email: psingh@arsd.du.ac.in

Authors

Sandeep Yadav — *Department of Chemistry, Atma Ram Sanatan Dharma College, University of Delhi, Delhi, India*

Anirudh Pratap Singh Raman — *Department of Chemistry, Atma Ram Sanatan Dharma College, University of Delhi, Delhi, India*

Harshvardhan Meena — *Department of Chemistry, Atma Ram Sanatan Dharma College, University of Delhi, Delhi, India; Department of Chemistry, Sri Venkateswara College*

and Department of Chemistry, University of Delhi, Delhi,
India

Abhay Giri Goswami − *Department of Chemistry, Atma Ram
Sanatan Dharma College, University of Delhi, Delhi, India*

Bhawna − *Department of Chemistry, Atma Ram Sanatan
Dharma College, University of Delhi, Delhi, India; Special
Centre for Nanoscience, Jawaharlal Nehru University, Delhi,
India*

Vinod Kumar − *Special Centre for Nanoscience, Jawaharlal
Nehru University, Delhi, India*

Gyanendra Kumar − *Department of Chemistry and Swami
Shraddhanand College, University of Delhi, Delhi, India;*
orcid.org/0000-0002-1975-5310

Mansi Sagar − *Department of Chemistry, University of Delhi,
Delhi, India*

Devendra Kumar Rana − *Department of Physics, Atma Ram
Sanatan Dharma College, University of Delhi, Delhi, India*

Complete contact information is available at:
https://pubs.acs.org/10.1021/acsomega.2c03171

Author Contributions

▲S.Y. and A.P.S.R. contributed equally.

Notes

The authors declare no competing financial interest.

■ ABBREVIATIONS

Ac-CD	Acrylate cyclodextrin
AGS	Human gastric adenocarcinoma cells
ALDs	Average leteral dimensions
ALP	Alkaline phosphatase
BBB	Blood−brain barrier
BHb	Bovine hemoglobin
BTE	Bone tissue engineering
CB	Conduction band
CSMA	Methacrylated chondroitin sulfate
CFC	Carbon fiber-reinforced composites
DAC	Dialdehyde cellulose
DDS	Drug delivery system
DFT	Density functional theory
DGEBA	Bisphenol A diglycidyl ether
DOX	Doxorubicin
EDX	Energy-dispersive X-ray analysis
FA	Fulvic acid
FESEM	Field emission scanning electron microscopy
FET	Field effect transistors
FRET	Fluorescence resonance energy transfer
FTIR	Fourier transform infrared spectroscopy
GFs	Growth factors
GO	Graphene oxide
GOF	Graphene oxide foam
GtO	Graphite oxide
GTPs	Green tea polyphenols
HET	Heterogeneous electron transfer
HMF	5-Hydroxymethylfurfural
hMSCs	Human mesenchymal stem cells
hNSCs	Human neural stem cells
HSA	Human serum albumin
HUVECs	Human umbilical vein endothelial cells
ICP-OES	Inductively coupled plasma optical emission spectrometry
LAP	Lysophosphatidic acid
LOHC	Liquid organic hydrogen carriers

MMT	Montmorillonite
MOF	Metal−organic framework
MSCs	Mesenchymal stem cell
NADPH	Adenine dinucleotide phosphate
NIPAM	*N*-Isopropylacrylamide
NTO	Natural transition orbital
PCL	Polycaprolactone
PD	Parkinson's disease
PDA	Polydopamine
PDADMAC	Polydiallyl methyl ammonium chloride nano-composite
PDLSCs	Periodontal ligament stem cells
PDMS	Polydimethylsiloxane
PECA	Magnetic poly(ethyl-2-cyanoacrylate)
PLC	Poly(ε-caprolactone)
PLGA	Polylactide-*co*-glycolide
PLLA	Poly-L-lactide
PVA	Polyvinyl alcohol
QDs	Quantum dots
rGO	Reduced graphene oxide
ROP	Ring-opening polymerization
ROS	Reactive oxygen species
SEM	Scanning electron microscopy
SGE	Spongy graphene electrodes
SNP	Single nucleotide polymorphism
SOD	Superoxide dismutase
SVD	Singular value decomposition
TCM	Traditional Chinese medicine
TEM	Transmission electron microscopy
TEMPO	2,2,6,6-Tetramethyl-piperidin-1-oxyl
TGA	Thermogravimetric analysis
TGO	Triamine-functionalized graphene oxide
XPS	X-ray photoelectron spectroscopy
XRD	X-ray diffraction
YAP	Hippo/yes-associated protein
VB	Valence band

■ REFERENCES

(1) Lee, C.; Wei, X.; Kysar, J. W.; Hone, J. Measurement of the Elastic Properties and Intrinsic Strength of Monolayer Graphene. *Science* **2008**, *321* (5887), 385−388.

(2) Eftekhari, A.; Jafarkhani, P. Curly Graphene with Specious Interlayers Displaying Superior Capacity for Hydrogen Storage. *J. Phys. Chem. C* **2013**, *117* (48), 25845−25851.

(3) Ullah, S.; Denis, P. A.; Menezes, M. G.; Sato, F. Tunable and Sizeable Band Gaps in Strained SiC3/HBN VdW Heterostructures: A Potential Replacement for Graphene in Future Nanoelectronics. *Comput. Mater. Sci.* **2021**, *188*, 110233.

(4) Yousuf, S.; Siddique, H. R.; Arjmand, F.; Tabassum, S. Functionalized Graphene Oxide Loaded GATPT as Rationally Designed Vehicle for Cancer-Targeted Drug Delivery. *J. Drug Deliv. Sci. Technol.* **2022**, *71*, 103281.

(5) Chen, Z.; Luo, Y.; Huang, C.; Shen, X. In Situ Assembly of ZnO/Graphene Oxide on Synthetic Molecular Receptors: Towards Selective Photoreduction of Cr(VI) via Interfacial Synergistic Catalysis. *Chem. Eng. J.* **2021**, *414*, 128914.

(6) Shen, Q.-Q.; Zhang, C.-Z.; Bai, Y.; Ni, M.-R. Synthesizing N-[4-Morpholinecarboximidamidoyl]Carboximidamidoylated Graphene Oxide for Fabricating High-Sensitive Humidity Sensors. *Diam. Relat. Mater.* **2022**, 109053.

(7) Budi, H. S.; Ansari, S. B.; Jasim, S.; Abdelbasset, W.; Bokov, D. Preparation of Antibacterial Gel/PCL Nanofibers Reinforced by Dicalcium Phosphate-Modified Graphene Oxide with Control Release of Clindamycin for Possible Application in Bone Tissue Engineering. *Inorg. Chem. Commun.* **2022**, *139*, 109336.

(8) Zhu, Y.; Kong, G.; Pan, Y.; Liu, L.; Yang, B.; et al. An Improved Hummers Method to Synthesize Graphene Oxide Using Much Less Concentrated Sulfuric Acid. *Chin. Chem. Lett.* **2022**, 33 (10), 4541−4544.

(9) Hamed, A. S.; Ali, E. M. Cu(II)-Metformin Immobilized on Graphene Oxide: An Efficient and Recyclable Catalyst for the Beckmann Rearrangement. *Res. Chem. Intermed.* **2020**, 46 (1), 701−714.

(10) Anouar, A.; Katir, N.; el Kadib, A.; Primo, A.; García, H. Palladium Supported on Porous Chitosan-Graphene Oxide Aerogels as Highly Effcient Catalysts for Hydrogen Generation from Formate. *Molecules* **2019**, 24 (18), 3290.

(11) Dhopte, K. B.; Raut, D. S.; Patwardhan, A. v.; Nemade, P. R. Graphene Oxide as Recyclable Catalyst for One-Pot Synthesis of α-Aminophosphonates. *Synth. Commun.* **2015**, 45 (6), 778−788.

(12) Thombal, R. S.; Jadhav, V. H. Sulfonated Graphene Oxide as Highly Efficient Catalyst for Glycosylation. *J. Carbohydr. Chem.* **2016**, 35 (1), 57−68.

(13) Mittal, A.; Kumari, S.; Parmanand; Yadav, D.; Sharma, S. K. A New Copper Complex on Graphene Oxide: A Heterogeneous Catalyst for N-Arylation and C-H Activation. *Appl. Organomet. Chem.* **2020**, 34 (2), 1−12.

(14) Rana, S.; Bhaskaruni, S. V. H. S.; Jonnalagadda, S. B. Tri-Amine Functionalized Graphene Oxide for Co-Operative Catalyst in the Henry Reaction. *Res. Chem. Intermed.* **2018**, 44 (3), 2157−2167.

(15) Eftekhar, M.; Raoufi, F. Synthesis, Characterization and First Application of Graphene Oxide Functionalized Cu(II) Complex for the Synthesis of 1,2,3-Triazole Derivatives. *Polycycl. Aromat. Compd.* **2021**, 1−13.

(16) Rajesh, R.; Ravichandran, Y. D. Development of New Graphene Oxide Incorporated Tricomponent Scaffolds with Polysaccharides and Hydroxyapatite and Study of Their Osteoconductivity on MG-63 Cell Line for Bone Tissue Engineering. *RSC Adv.* **2015**, 5 (51), 41135−41143.

(17) Wang, Q.; Chu, Y.; He, J.; Shao, W.; Zhou, Y.; Qi, K.; Wang, L.; Cui, S. A Graded Graphene Oxide-Hydroxyapatite/Silk Fibroin Biomimetic Scaffold for Bone Tissue Engineering. *Mater. Sci. Eng., C* **2017**, 80 (80), 232−242.

(18) Gonzalez-Mayorga, A.; Lopez-Dolado, E.; Gutierrez, M. C.; Collazos-Castro, J. E.; Ferrer, M. L.; del Monte, F.; Serrano, M. C. Favorable Biological Responses of Neural Cells and Tissue Interacting with Graphene Oxide Microfibers. *ACS Omega* **2017**, 2 (11), 8253−8263.

(19) Ghorbani, F.; Zamanian, A.; Aidun, A. Bioinspired Polydopamine Coating-Assisted Electrospun Polyurethane-Graphene Oxide Nanofibers for Bone Tissue Engineering Application. *J. Appl. Polym. Sci.* **2019**, 136 (24), 47656.

(20) Guo, R.; Li, J.; Chen, C.; Xiao, M.; Liao, M.; Hu, Y.; Liu, Y.; Li, D.; Zou, J.; Sun, D.; Torre, V.; Zhang, Q.; Chai, R.; Tang, M. Biomimetic 3D Bacterial Cellulose-Graphene Foam Hybrid Scaffold Regulates Neural Stem Cell Proliferation and Differentiation. *Colloids Surf. B* **2021**, 200, 111590.

(21) Cao, L.; Zhang, F.; Wang, Q.; Wu, X. Fabrication of Chitosan/Graphene Oxide Polymer Nanofiber and Its Biocompatibility for Cartilage Tissue Engineering. *Mater. Sci. Eng., C* **2017**, 79, 697−701.

(22) Thickett, S. C.; Hamilton, E.; Yogeswaran, G.; Zetterlund, P. B.; Farrugia, B. L.; Lord, M. S. Enhanced Osteogenic Differentiation of Human Fetal Cartilage Rudiment Cells on Graphene Oxide-PLGA Hybrid Microparticles. *J. Funct. Biomater.* **2019**, 10 (3), 33.

(23) Shamekhi, M. A.; Mirzadeh, H.; Mahdavi, H.; Rabiee, A.; Mohebbi-Kalhori, D.; Baghaban Eslaminejad, M. Graphene Oxide Containing Chitosan Scaffolds for Cartilage Tissue Engineering. *Int. J. Biol. Macromol.* **2019**, 127, 396−405.

(24) Chu, J.; Shi, P.; Yan, W.; Fu, J.; et al. PEGylated Graphene Oxide-Mediated Quercetin-Modified Collagen Hybrid Scaffold for Enhancement of MSCs Differentiation Potential and Diabetic Wound Healing. *Nanoscale* **2018**, 10 (20), 9547−9560.

(25) Nyambat, B.; Chen, C. H.; Wong, P. C.; Chiang, C. W.; Satapathy, M. K.; Chuang, E. Y. Genipin-Crosslinked Adipose Stem Cell Derived Extracellular Matrix-Nano Graphene Oxide Composite Sponge for Skin Tissue Engineering. *J. Mater. Chem. B.* **2018**, 6 (6), 979−990.

(26) Montazeri, A.; Saeedi, F.; Bahari, Y.; Ahmadi Daryakenari, A. Preclinical Assessment of Chitosan-Polyvinyl Alcohol-Graphene Oxide Nanocomposite Scaffolds as a Wound Dressing. *Polym. Polym. Compos.* **2021**, 29, S926−S936.

(27) Zhou, Q.; Yang, P.; Li, X.; Liu, H.; Ge, S. Bioactivity of Periodontal Ligament Stem Cells on Sodium Titanate Coated with Graphene Oxide. *Sci. Rep.* **2019**, 6 (2016), 171−185.

(28) Tahriri, M.; Del Monico, M.; Moghanian, A.; Tavakkoli Yaraki, M.; Torres, R.; Yadegari, A.; Tayebi, L. Materials Science & Engineering C Graphene and Its Derivatives : Opportunities and Challenges in Dentistry. *Mater. Sci. Eng., C* **2019**, 102, 171−185.

(29) Qi, X.; Jiang, F.; Zhou, M.; Zhang, W.; Jiang, X. Graphene Oxide as a Promising Material in Dentistry and Tissue Regeneration: A Review. *Smart Materials in Medicine.* **2021**, 2, 280−291.

(30) Yang, C.; You, X.; Cheng, J.; Zheng, H.; Chen, Y. A Novel Visible-Light-Driven In-Based MOF/Graphene Oxide Composite Photocatalyst with Enhanced Photocatalytic Activity toward the Degradation of Amoxicillin. *Appl. Catal.* **2017**, 200, 673−680.

(31) Niu, X.; Yan, W.; Zhao, H.; Yang, J. Synthesis of Nb Doped TiO_2 Nanotube/Reduced Graphene Oxide Heterostructure Photocatalyst with High Visible Light Photocatalytic Activity. *Appl. Surf. Sci.* **2018**, 440, 804−813.

(32) Yadav, H. M.; Kim, J. S. Solvothermal Synthesis of Anatase TiO_2-Graphene Oxide Nanocomposites and Their Photocatalytic Performance. *J. Alloys Compd.* **2016**, 688, 123−129.

(33) Cheng, T.-Y.; Chou, F.-P.; Huang, S.-C.; Chang, C.-Y.; Wu, T.-K. Electroluminescence and Photocatalytic Hydrogen Evolution of S,N Co-Doped Graphene Oxide Quantum Dots. *J. Mater. Chem. A* **2022**, 10 (7), 3650−3658.

(34) Keshipour, S.; Mohammad-Alizadeh, S.; Razeghi, M. H. Copper Phthalocyanine@graphene Oxide as a Cocatalyst of TiO_2 in Hydrogen Generation. *J. Phys. Chem. Solids* **2022**, 161, 110434.

(35) Gao, P.; Liu, J.; Lee, S.; Zhang, T.; Sun, D. D. High Quality Graphene Oxide-CdS-Pt Nanocomposites for Efficient Photocatalytic Hydrogen Evolution. *J. Mater. Chem.* **2012**, 22 (5), 2292−2298.

(36) Liu, S.; Jiang, T.; Fan, M.; Tan, G.; Cui, S.; Shen, X. Nanostructure Rod-like TiO_2-Reduced Graphene Oxide Composite Aerogels for Highly-Efficient Visible-Light Photocatalytic CO_2 Reduction. *J. Alloys Compd.* **2021**, 861, 158598.

(37) Xu, Y. F.; Yang, M. Z.; Chen, B. X.; Wang, X. D.; Chen, H. Y.; Kuang, D.; Su, C. Y. A $CsPbBr_3$ Perovskite Quantum Dot/Graphene Oxide Composite for Photocatalytic CO_2 Reduction. *J. Am. Chem. Soc.* **2017**, 139 (16), 5660−5663.

(38) Xu, D.; Cheng, B.; Wang, W.; Jiang, C.; Yu, J. Ag_2CrO_4/g-C_3N_4/Graphene Oxide Ternary Nanocomposite Z-Scheme Photocatalyst with Enhanced CO_2 Reduction Activity. *Appl. Catal.* **2018**, 231, 368−380.

(39) Li, M.; Yan, C.; Ramachandran, R.; Lan, Y.; Dai, H.; Shan, H.; Meng, X.; Cui, D.; Wang, F.; Xu, Z. Non-Peripheral Octamethyl-Substituted Cobalt Phthalocyanine Nanorods Supported on N-Doped Reduced Graphene Oxide Achieve Efficient Electrocatalytic CO_2 Reduction to CO. *Chem. Eng. J.* **2022**, 430, 133050.

(40) Buledi, J. A.; Mahar, N.; Mallah, A.; Solangi, A. R.; Palabiyik, I. M.; Qambrani, N.; Karimi, F.; Vasseghian, Y. Electrochemical Quantification of Mancozeb through Tungsten Oxide/Reduced Graphene Oxide Nanocomposite : A Potential Method for Environmental Remediation. *Food Chem. Toxicol.* **2022**, 161, 112843.

(41) Zhang, Q.; Wang, B. X.; Zhou, Y. L.; Hong, J.-m.; Yu, Y. B. Phys. Chem. Solids Electrocatalytic Degradation of Acetaminophen by Fluorine-Doped Graphene Oxide : Efficiency and Mechanism under Constant Current and Pulse Current Supply. *J. Phys. Chem. Solids* **2022**, 161, 110443.

(42) Uddin, M. E.; Kim, N. H.; Kuila, T.; Lee, S. H.; Hui, D.; Lee, J. H. Preparation of Reduced Graphene Oxide-$NiFe_2O_4$ Nanocomposites for the Electrocatalytic Oxidation of Hydrazine. *Compos. B. Eng.* **2015**, 79, 649−659.

(43) Yashaswini, Y. D.; Prabhu, A.; Anil, S.; Venkatesan, J. Preparation and Characterization of Dexamethasone Loaded Sodium Alginate-Graphene Oxide Microspheres for Bone Tissue Engineering. *J. Drug Deliv. Sci. Technol.* **2021**, *64*, 102624.

(44) Yang, K.; Lee, J.; Lee, J. S.; Kim, D.; Chang, G. E.; Seo, J.; Cheong, E.; Lee, T.; Cho, S. W. Graphene Oxide Hierarchical Patterns for the Derivation of Electrophysiologically Functional Neuron-like Cells from Human Neural Stem Cells. *ACS Appl. Mater. Interfaces.* **2016**, *8* (28), 17763−17774.

(45) Hoseini-Ghahfarokhi, M.; Mirkiani, S.; Mozaffari, N.; Abdolahi Sadatlu, M. A.; Ghasemi, A.; Abbaspour, S.; Akbarian, M.; Farjadian, F.; Karimi, M. Applications of Graphene and Graphene Oxide in Smart Drug/Gene Delivery: Is the World Still Flat? *Int. J. Nanomed.* **2020**, *15*, 9469.

(46) Pal, N.; Dubey, P.; Gopinath, P.; Pal, K. Combined Effect of Cellulose Nanocrystal and Reduced Graphene Oxide into Poly-Lactic Acid Matrix Nanocomposite as a Scaffold and Its Anti-Bacterial Activity. *Int. J. Biol. Macromol.* **2017**, *95*, 94−105.

(47) Benjamin, C. On the Atomic Weight of Graphite. *Philos. Trans. R. Soc.* **1859**, *149*, 249−259.

(48) Staudenmaier, L. Verfahren Zur Darstellung Der Graphitsäure. Berichte der deutschen chemischen. *Gesellschaft* **1898**, *31* (2), 1481−1487.

(49) Hummers, W. S.; Offeman, R. E. Preparation of Graphitic Oxide. *J. Am. Chem. Soc.* **1958**, *80* (6), 1339.

(50) Su, C. Y.; Xu, Y.; Zhang, W.; Zhao, J.; Tang, X.; Tsai, C. H.; Li, L. J. Electrical and Spectroscopic Characterizations of Ultra-Large Reduced Graphene Oxide Monolayers. *Chem. Mater.* **2009**, *21* (23), 5674−5680.

(51) Shen, J.; Hu, Y.; Shi, M.; Lu, X.; Qin, C.; Li, C.; Ye, M. Fast and Facile Preparation of Graphene Oxide and Reduced Graphene Oxide Nanoplatelets. *Chem. Mater.* **2009**, *21* (15), 3514−3520.

(52) Sun, L.; Fugetsu, B. Mass Production of Graphene Oxide from Expanded Graphite. *Mater. Lett.* **2013**, *109*, 207−210.

(53) Eigler, S.; Enzelberger-Heim, M.; Grimm, S.; Hofmann, P.; Kroener, W.; Geworski, A.; Dotzer, C.; Rockert, M.; Xiao, J.; Papp, C.; Lytken, O.; Steinruck, H.-P.; Muller, P.; Hirsch, A. Wet Chemical Synthesis of Graphene. *Adv. Mater.* **2013**, *25* (26), 3583−3587.

(54) Panwar, V.; Chattree, A.; Pal, K. A New Facile Route for Synthesizing of Graphene Oxide Using Mixture of Sulfuric-Nitric-Phosphoric Acids as Intercalating Agent. *Physica E Low Dimens. Syst. Nanostruct.* **2015**, *73*, 235−241.

(55) Chen, J.; Li, Y.; Huang, L.; Li, C.; Shi, G. High-Yield Preparation of Graphene Oxide from Small Graphite Flakes via an Improved Hummers Method with a Simple Purification Process. *Carbon* **2015**, *81* (1), 826−834.

(56) Dimiev, A. M.; Ceriotti, G.; Metzger, A.; Kim, N. D.; Tour, J. M. Chemical Mass Production of Graphene Nanoplatelets in ∼ 100% Yield. *ACS Nano* **2016**, *10* (1), 274−279.

(57) Rosillo-Lopez, M.; Salzmann, C. G. A Simple and Mild Chemical Oxidation Route to High-Purity Nano-Graphene Oxide. *Carbon* **2016**, *106*, 56−63.

(58) Yu, H.; Zhang, B.; Bulin, C.; Li, R.; Xing, R. High-Efficient Synthesis of Graphene Oxide Based on Improved Hummers Method. *Sci. Rep.* **2016**, *6* (1), 1−7.

(59) Pei, S.; Wei, Q.; Huang, K.; Cheng, H. M.; Ren, W. Green Synthesis of Graphene Oxide by Seconds Timescale Water Electrolytic Oxidation. *Nat. Commun* **2018**, *9*, 1−9.

(60) Akhavan, O. The Effect of Heat Treatment on Formation of Graphene Thin Films from Graphene Oxide Nanosheets. *Carbon* **2010**, *48* (2), 509−519.

(61) Zhu, Y.; Stoller, M. D.; Cai, W.; Velamakanni, A. Exfoliation of Graphite Oxide in Propylene Carbonate and Thermal Reduction of the Resulting Graphene Oxide Platelets. *ACS Nano* **2010**, *4* (2), 1227−1233.

(62) Akhavan, O.; Saadati, M.; Jannesari, M. Graphene Jet Nanomotors in Remote Controllable Self-Propulsion Swimmers in Pure Water. *Nano Lett.* **2016**, *16* (9), 5619−5630.

(63) Kigozi, M.; Koech, R. K.; Kingsley, O.; Ojeaga, I.; Tebandeke, E.; Kasozi, G. N.; Onwualu, A. P. Synthesis and Characterization of Graphene Oxide from Locally Mined Graphite Flakes and Its Supercapacitor Applications. *Results in Materials* **2020**, *7*, 100113.

(64) Muniyalakshmi, M.; Sethuraman, K.; Silambarasan, D. Synthesis and Characterization of Graphene Oxide Nanosheets. *Mater. Today: Proc.* **2020**, *21*, 408−410.

(65) Abdelhalim, A. O. E.; Sharoyko, V. v.; Meshcheriakov, A. A.; Martynova, S. D.; Ageev, S. V.; Iurev, G. O.; Semenov, K. N.; et al. Reduction and Functionalization of Graphene Oxide with L-Cysteine: Synthesis, Characterization and Biocompatibility. *Nanomedicine* **2020**, *29*, 102284.

(66) Ikram, R.; Jan, B. M.; Ahmad, W. An Overview of Industrial Scalable Production of Graphene Oxide and Analytical Approaches for Synthesis and Characterization. *J. Mater. Res. Technol.* **2020**, *9* (5), 11587−11610.

(67) Bousiakou, L. G.; Qindeel, R.; Al-Dossary, O. M.; Kalkani, H. Synthesis and Characterization of Graphene Oxide (GO) Sheets for Pathogen Inhibition: Escherichia Coli, Staphylococcus Aureus and Pseudomonas Aeruginosa. *J. King. Saud. Univ. Sci.* **2022**, *34* (4), 102002.

(68) Shaari, H. A. H.; Ramli, M. M; Mohtar, M. N.; Razali, N. H. F. Characterization and Conductivity of Graphene Oxide (GO) Dispersion in Different Solvents. In AIP Conf. Proc. *AIP Conf. Proc.* **2021**, *2332*, 60001.

(69) Alam, S. N.; Sharma, N.; Kumar, L.; Alam, S. N.; Sharma, N.; Kumar, L. Synthesis of Graphene Oxide (GO) by Modified Hummers Method and Its Thermal Reduction to Obtain Reduced Graphene Oxide (RGO)*. *Graphene* **2017**, *6*, 1−18.

(70) Alfawaz, Y. F.; Almutairi, B.; Kattan, H. F.; Zafar, M. S.; Farooq, I.; Naseem, M.; Vohra, F.; Abduljabbar, T. Dentin Bond Integrity of Hydroxyapatite Containing Resin Adhesive Enhanced with Graphene Oxide Nano-Particles—An SEM, EDX, Micro-Raman, and Microtensile Bond Strength Study. *Polymers* **2020**, *12*, 2978.

(71) Akhavan, O. Bacteriorhodopsin as a Superior Substitute for Hydrazine in Chemical Reduction of Single-Layer Graphene Oxide Sheets. *Carbon* **2015**, *81* (1), 158−166.

(72) Jain, A.; Ahmad, M. Z.; Linkès, A.; Martin-gil, V.; Castro-muñoz, R.; Izak, P.; Sofer, Z.; Hintz, W.; Fila, V. 6fda-dam:Daba Co-polyimide Mixed Matrix Membranes with Go and Zif-8 Mixtures for Effective Co2/Ch4 Separation. *Nanomaterials* **2021**, *11* (3), 668.

(73) Kumbhakar, P. P.; Pramanik, A.; Biswas, S.; Kole, A. K.; Sarkar, R.; Kumbhakar, P. P. In-Situ Synthesis of RGO-ZnO Nanocomposite for Demonstration of Sunlight Driven Enhanced Photocatalytic and Self-Cleaning of Organic Dyes and Tea Stains of Cotton Fabrics. *J. Hazard. Mater.* **2018**, *360*, 193−203.

(74) Iakunkov, A.; Talyzin, A. v. Swelling Properties of Graphite Oxides and Graphene Oxide Multilayered Materials. *Nanoscale* **2020**, *12*, 21060.

(75) Kumbhakar, P.; Chowde Gowda, C.; Mahapatra, P. L.; Mukherjee, M.; Malviya, K. D.; Chaker, M.; Chandra, A.; Lahiri, B.; Ajayan, P. M.; Jariwala, D.; Singh, A.; Tiwary, C. S. Emerging 2D Metal Oxides and Their Applications. *Mater. Today* **2021**, *45*, 142−168.

(76) Kumar, P.; Boukherroub, R.; Shankar, K. Sunlight-Driven Water-Splitting Using Two-Dimensional Carbon Based Semiconductors. *J. Mater. Chem. A* **2018**, *6* (27), 12876−12931.

(77) Das Jana, I.; Kumbhakar, P.; Banerjee, S. S.; Gowda, C. C.; Kedia, N.; Kuila, S. K.; Banerjee, S. S.; Das, N. C.; Das, A. K.; Manna, I.; Tiwary, C. S.; Mondal, A. Copper Nanoparticle-Graphene Composite-Based Transparent Surface Coating with Antiviral Activity against Influenza Virus. *ACS Appl. Nano Mater.* **2021**, *4* (1), 352−362.

(78) Kim, J.; Park, S. J.; Min, D. H. Emerging Approaches for Graphene Oxide Biosensor. *Anal. Chem.* **2017**, *89* (1), 232−248.

(79) Esfandiarpour, R.; Badalkhani-Khamseh, F.; Hadipour, N. L. Exploration of Phosphorene as Doxorubicin Nanocarrier: An Atomistic View from DFT Calculations and MD Simulations. *Colloids Surf. B* **2022**, *215*, 112513.

(80) Mian, S. A.; Khan, S. U.; Hussain, A.; Rauf, A.; Ahmed, E.; Jang, J. Molecular Modelling of Optical Biosensor Phosphorene-Thioguanine for Optimal Drug Delivery in Leukemia Treatment. *Cancers* **2022**, *14*, 545.

(81) Sultana, N.; Degg, A.; Upadhyaya, S.; Nilges, T.; Sen Sarma, N. sen. Synthesis, Modification, and Application of Black Phosphorus, Few-Layer Black Phosphorus (FLBP), and Phosphorene: A Detailed Review. *Materials Advances* **2022**, *3*, 5557−5574.

(82) Bhuvaneswari, R.; Nagarajan, V.; Chandiramouli, R. First-Principles Research on Adsorption Properties of o-Xylene and Styrene on 5−8 Phosphorene Sheets. *Chem. Phys. Lett.* **2021**, *765*, 138244.

(83) Rohaizad, N.; Mayorga-Martinez, C. C.; Fojtu, M.; Latiff, N. M.; Pumera, M. Two-Dimensional Materials in Biomedical, Biosensing and Sensing Applications. *Chem. Soc. Rev.* **2021**, *50* (1), 619−657.

(84) Yuksel, N.; Kose, A.; Fellah. A Density Functional Theory Study for Adsorption and Sensing of 5-Fluo Rouracil on Ni-Doped Boron Nitride Nanotube. *Mater. Sci. Semicond. Process.* **2022**, *137*, 106183.

(85) Kaviani, S.; Izadyar, M. First-Principles Study of the Binding Affinity of Monolayer BC 6 N Nanosheet : Implications for Drug Delivery. *Mater. Chem. Phys.* **2022**, *276*, 125375.

(86) Razavi, L.; Raissi, H.; Hashemzadeh, H.; Farzad, F. Molecular Insights into the Loading and Dynamics of Anticancer Drugs on Silicene and Folic Acid-Conjugated Silicene Nanosheets: DFT Calculation and MD Simulation. *J. Biomol. Struct. Dyn.* **2021**, *39* (11), 3892−3899.

(87) Wang, J.; Sui, L.; Huang, J.; Miao, L.; Nie, Y.; Wang, K.; Yang, Z.; Huang, Q.; Gong, X.; Nan, Y.; Ai, K. MoS2-Based Nanocomposites for Cancer Diagnosis and Therapy. *Bioact. Mater.* **2021**, *6* (11), 4209−4242.

(88) Lay, E.; Chng, K.; Pumera, M. Toxicity of Graphene Related Materials and Transition Metal Dichalcogenides. *RCS Adv.* **2015**, *5* (4), 3074−3080.

(89) Samy, O.; Zeng, S.; Birowosuto, M. D.; el Moutaouakil, A. A Review on MoS2 Properties, Synthesis, Sensing Applications and Challenges. *Crystals* **2021**, *11*, 355.

(90) Liang, W.; Luo, X. Theoretical Studies of MoS2 and Phosphorene Drug Delivery for Antituberculosis Drugs. *J. Phys. Chem. C* **2020**, *124* (15), 8279−8287.

(91) Pandya, A.; Sangani, K.; Jha, P. K. Band Gap Determination of Graphene, h-Boron Band Gap Determination of Graphene, h-Boron Nitride, Phosphorene, Silicene, stanene, and germanene nanoribbons. *J. Phys. D Appl. Phys.* **2020**, *53* (41), 415103.

(92) Kara, A.; Enriquez, H.; Seitsonen, A. P.; Lew Yan Voon, L.C.; Vizzini, S.; Aufray, B.; Oughaddou, H. A Review on Silicene - New Candidate for Electronics. *Surf. Sci. Rep.* **2012**, *67* (1), 1−18.

(93) Molaei, M. J. Materials beyond Graphene in Cancer Drug Delivery, Photothermal and Photodynamic Therapy, Recent Advances and Challenges Ahead : A Review. *J. Drug Deliv. Sci. Technol.* **2021**, *61*, 101830.

(94) Khatun, R.; Biswas, S.; Islam, S. S. M.; Biswas, I. H.; Riyajuddin, S.; Ghosh, K.; Islam, S. S. M. Modified Graphene Oxide Based Zinc Composite: An Efficient Catalyst for N-Formylation and Carbamate Formation Reactions Through CO2 Fixation. *ChemCatChem* **2019**, *11* (4), 1303−1312.

(95) Cahyana, A. H.; Liandi, A. R.; Yunarti, R. T.; Febriantini, D.; Ardiansah, B. Green Synthesis of Dihydropyrimidine Based on Cinnamaldehyde Compound under Solvent-Free Using Graphene Oxide as Catalyst. *AIP Conf. Proc.* **2019**, *2168*, 020069.

(96) Chattopadhyay, A. P.; Chattopadhyay, A. P. Highly Efficient and Recyclable Silver-Graphene Oxide Nano-Composite Catalyst in the Acylation of Amines under Solvent-Free Condition. *MOJ. bioorg. org. chem.* **2018**, *2* (4), 201−211.

(97) Bakht, M. A. Eco-Friendly Synthesis of Isatin-Thiazolidine Hybrid Using Graphene Oxide Catalyst in Deep Eutectic Solvent and Further Evaluated for Antibacterial, Anticancer and Cytotoxic Agents. *Sustain. Chem. Pharm.* **2020**, *16*, 100252.

(98) Zhang, W.; Wang, S.; Ji, J.; Li, Y.; Zhang, G.; Zhang, F.; Fan, X. Primary and Tertiary Amines Bifunctional Graphene Oxide for Cooperative Catalysis. *Nanoscale* **2013**, *5* (13), 6030−6033.

(99) Zarnegaryan, A.; Kargar, S. Graphene Oxide Nanosheet Supported Molybdenum Complex: An Efficient and Recoverable Catalyst for Epoxidation of Alkenes. *Appl. Surf. Sci. Advances* **2021**, *4*, 100073.

(100) Trzeciak, A. M.; Wojcik, P.; Lisiecki, R.; Gerasymchuk, Y.; Strek, W.; Legendziewicz, J. Palladium Nanoparticles Supported on Graphene Oxide as Catalysts for the Synthesis of Diarylketones. *Catalysts* **2019**, *9* (4), 319.

(101) Vu, T. H. T.; Nguyen, M. H.; Nguyen, M. D. Synthesis of Acidic Heterogeneous Catalysts with High Stability Based on Graphene Oxide/Activated Carbon Composites for the Esterification of Lactic Acid. *J. Chem.* **2019**, 7815697.

(102) Chen, Z.; Wen, Y.; Fu, Y.; Chen, H.; Ye, M.; Luo, G. Graphene Oxide: An Efficient Acid Catalyst for the Construction of Esters from Acids and Alcohols. *Synlett.* **2017**, *28* (08), 981−985.

(103) Zarnegaryan, A.; Elhamifar, D. An Efficient and Heterogeneous Pd-Containing Modified Graphene Oxide Catalyst for Preparation of Biaryl Compounds. *Heliyon* **2020**, *6* (4), No. e03741.

(104) Narayanan, D. P.; Gopalakrishnan, A.; Yaakob, Z.; Sugunan, S.; Narayanan, B. N. A Facile Synthesis of Clay - Graphene Oxide Nanocomposite Catalysts for Solvent Free Multicomponent Biginelli Reaction. *Arab. J. Chem.* **2020**, *13* (1), 318−334.

(105) Shuisheng Wu, S. W.; Donghui Lan, D. L.; Nianyuan Tan, N. T.; Ran Wang, R. W.; Chak Tong Au, C. Manganese Schiff Base Immobilized on Graphene Oxide Complex and Its Catalysis for Epoxidation of Styrene. *J. Chem. Soc. Pak.* **2021**, *43*, 57.

(106) Acocella, M. R.; Corcione, C. E.; Giuri, A.; Maggio, M.; Maffezzoli, A.; Guerra, G. Graphene Oxide as a Catalyst for Ring Opening Reactions in Amine Crosslinking of Epoxy Resins. *RSC Adv.* **2016**, *6* (28), 23858−23865.

(107) Zhang, K.; Suh, J. M.; Lee, T. H.; Cha, J. H.; Choi, J.-W.; Jang, H. W.; Varma, R. S.; Shokouhimehr, M. Copper Oxide-Graphene Oxide Nanocomposite: Efficient Catalyst for Hydrogenation of Nitroaromatics in Water. *Nano Converg.* **2019**, *6* (1), 1.

(108) Li, H.; Peng, X.; Nie, L.; Zhou, L.; Yang, M.; Li, F.; Hu, J.; Yao, Z.; Liu, L. Graphene Oxide-Catalyzed Trifluoromethylation of Alkynes with Quinoxalinones and Langlois' Reagent. *RSC Adv.* **2021**, *11* (61), 38667−38673.

(109) Sachdeva, H. Recent Advances in the Catalytic Applications of GO/RGO for Green Organic Synthesis. *Green Process. Synth.* **2020**, *9* (1), 515−537.

(110) Ganesan, N. S.; Suresh, P.; Saravana Ganesan, N.; Suresh, P. Synthesis of β-Amino Ketones Using Graphene Oxide: A Benign Carbonaceous Acid Catalyst for Mannich Reaction. *Res. Chem. Intermed.* **2021**, *47* (3), 3.

(111) Sarvi, I.; Zahedi, E.; Arvi, S. I.; Zahedi, E. Zinc Oxide/ Graphene Oxide as a Robust Active Catalyst for Direct Oxidative Synthesis of Nitriles from Alcohols in Water. *Catal. Lett.* **2022**, *152* (6), 1895−1903.

(112) Mirheidari, M.; Safaei-Ghomi, J. Design, Synthesis, and Catalytic Performance of Modified Graphene Oxide Based on a Cobalt Complex as a Heterogenous Catalyst for the Preparation of Aminonaphthoquinone Derivatives. *RSC Adv.* **2021**, *11* (28), 17108−17115.

(113) Kumar, A.; Rout, L.; Achary, L. S. K.; Mohanty, S. K.; Nayak, P. S.; Barik, B.; dash, P. Solvent Free Synthesis of Chalcones over Graphene Oxide-Supported MnO2 Catalysts Synthesized via Combustion Route. *Mater. Chem. Phys.* **2021**, *259*, 124019.

(114) Podolean, I.; Coman, S. M.; Bucur, C.; Teodorescu, C.; Kikionis, S.; Ioannou, E.; Roussis, V.; Primo, A.; Garcia, H.; Parvulescu, V. I. Catalytic Transformation of the Marine Polysaccharide Ulvan into Rare Sugars, Tartaric and Succinic Acids. *Catal. Today* **2022**, *383*, 345−357.

(115) Su, H.; Zhao, Q. Q.; Wang, Y.; Zhao, Q. Q.; Jang, C.; Niu, Y.; Lou, W.; Qi, Y. SnO Nanoparticles on Graphene Oxide as an Effective

Catalyst for Synthesis of Lubricating Ester Oils. *Catal. Commun.* **2022**, *162*, 106370.

(116) Dreyer, D. R.; Jia, H.-P.; Bielawski, C. W. Graphene Oxide: A Convenient Carbocatalyst for Facilitating Oxidation and Hydration Reactions. *Angew. Chem., Int. Ed.* **2010**, *122* (38), 6965−6968.

(117) Vijay Kumar, A.; Rama Rao, K. Recyclable Graphite Oxide Catalyzed Friedel-Crafts Addition of Indoles to *α,β*-Unsaturated Ketones. *Tetrahedron Lett.* **2011**, *52* (40), 5188−5191.

(118) Sedrpoushan, A.; Heidari, M.; Akhavan, O. Nanoscale Graphene Oxide Sheets as Highly Efficient Carbocatalysts in Green Oxidation of Benzylic Alcohols and Aromatic Aldehydes. *Chinese J. Catal.* **2017**, *38* (4), 745−757.

(119) Verma, S.; Mungse, H. P.; Kumar, N.; Choudhary, S.; Jain, S. L.; Sain, B.; Khatri, O. P. Graphene Oxide: An Efficient and Reusable Carbocatalyst for Aza-Michael Addition of Amines to Activated Alkenes. *ChemComm* **2011**, *47* (47), 12673−12675.

(120) Lv, G.; Wang, H.; Yang, Y.; Deng, T.; Chen, C.; Zhu, Y.; Hou, X. Graphene Oxide: A Convenient Metal-Free Carbocatalyst for Facilitating Aerobic Oxidation of 5-Hydroxymethylfurfural into 2, 5-Diformylfuran. *ACS Catal.* **2015**, *5* (9), 5636−5646.

(121) Yang, X.; Zhai, J.; Xu, T.; Xue, B.; Zhu, J.; Li, Y. Grafted Polyethylene Glycol-Graphene Oxide as a Novel Triphase Catalyst for Carbenes and Nucleophilic Substitution Reactions. *Catal. Lett.* **2019**, *149* (10), 2767−2775.

(122) Vacanti, J. P.; Langer, R. Tissue Engineering: The Design and Fabrication of Living Replacement Devices for Surgical Reconstruction and Transplantation. *The Lancet* **1999**, *354*, S32−S34.

(123) Lee, W. C.; Lim, C. H. Y. X.; Shi, H.; Tang, L. A. L.; Wang, Y.; Lim, C. T.; Loh, K. P. Origin of Enhanced Stem Cell Growth and Differentiation on Graphene and Graphene Oxide. *ACS Nano* **2011**, *5* (9), 7334−7341.

(124) Akhavan, O.; Ghaderi, E.; Shahsavar, M. Graphene Nanogrids for Selective and Fast Osteogenic Differentiation of Human Mesenchymal Stem Cells. *Carbon* **2013**, *59*, 200−211.

(125) Umar Aslam Khan, M.; Haider, S.; Haider, A.; Izwan Abd Razak, S.; Rafiq Abdul Kadir, M.; Shah, S. A.; Javed, A.; Shakir, I.; Al-Zahrani, A. A. Development of Porous, Antibacterial and Biocompatible GO/n-HAp/Bacterial Cellulose/*β*-Glucan Biocomposite Scaffold for Bone Tissue Engineering. *Arab. J. Chem.* **2021**, *14* (2), 102924.

(126) Tatavarty, R.; Ding, H.; Lu, G.; Taylor, R. J.; Bi, X. Synergistic Acceleration in the Osteogenesis of Human Mesenchymal Stem Cells by Graphene Oxide-Calcium Phosphate Nanocomposites. *ChemComm* **2014**, *50* (62), 8484−8487.

(127) Mohammadi, S.; Shafiei, S. S.; Asadi-Eydivand, M.; Ardeshir, M.; Solati-Hashjin, M. Graphene Oxide-Enriched Poly(*ε*-Caprolactone) Electrospun Nanocomposite Scaffold for Bone Tissue Engineering Applications. *J. Bioact. Compat. Polym.* **2017**, *32* (3), 325−342.

(128) Rajan Unnithan, A.; Ramachandra Kurup Sasikala, A.; Park, C. H.; Kim, C. S. A Unique Scaffold for Bone Tissue Engineering: An Osteogenic Combination of Graphene Oxide-Hyaluronic Acid-Chitosan with Simvastatin. *J. Ind. Eng. Chem.* **2017**, *46*, 182−191.

(129) Liu, Y.; Fang, N.; Liu, B.; Song, L.; Wen, B.; Yang, D. Aligned Porous Chitosan/Graphene Oxide Scaffold for Bone Tissue Engineering. *Mater. Lett.* **2018**, *233*, 78−81.

(130) Pazarçeviren, A. E.; Tahmasebifar, A.; Tezcaner, A.; Keskin, D.; Evis, Z. Investigation of Bismuth Doped Bioglass/Graphene Oxide Nanocomposites for Bone Tissue Engineering. *Ceram. Int.* **2018**, *44* (4), 3791−3799.

(131) Purohit, S. D.; Bhaskar, R.; Singh, H.; Yadav, I.; Gupta, M. K.; Mishra, N. C. Development of a Nanocomposite Scaffold of Gelatin-Alginate-Graphene Oxide for Bone Tissue Engineering. *Int. J. Biol. Macromol.* **2019**, *133*, 592−602.

(132) Liu, W.; Luo, H.; Wei, Q.; Liu, J.; Wu, J.; Zhang, Y.; Chen, L.; Ren, W.; Shao, L. Electrochemically Derived Nanographene Oxide Activates Endothelial Tip Cells and Promotes Angiogenesis by Binding Endogenous Lysophosphatidic Acid. *Bioact. Mater.* **2022**, *9*, 92−104.

(133) Qi, Z.; Chen, X.; Guo, W.; Fu, C.; Pan, S. Theanine-Modified Graphene Oxide Composite Films for Neural Stem Cells Proliferation and Differentiation. *J. Nanomater.* **2020**, 1.

(134) Qian, Y.; Song, J.; Zhao, X.; Chen, W.; Ouyang, Y.; Yuan, W.; Fan, C. 3D Fabrication with Integration Molding of a Graphene Oxide/Polycaprolactone Nanoscaffold for Neurite Regeneration and Angiogenesis. *Adv. Sci.* **2018**, *5* (4), 1700499.

(135) Bei, H. P.; Yang, Y.; Zhang, Q.; Tian, Y.; Luo, X.; Yang, M.; Zhao, X. Graphene-Based Nanocomposites for Neural Tissue Engineering. *Molecules* **2019**, *24* (4), 658.

(136) Akhavan, O.; Ghaderi, E. The Use of Graphene in the Self-Organized Differentiation of Human Neural Stem Cells into Neurons under Pulsed Laser Stimulation. *J. Mater. Chem. B* **2014**, *2* (34), 5602−5611.

(137) Heo, C.; Yoo, J.; Lee, S.; Jo, A.; Jung, S.; Yoo, H.; Lee, Y. H.; Suh, M. Biomaterials The Control of Neural Cell-to-Cell Interactions through Non-Contact Electrical Fi Eld Stimulation Using Graphene Electrodes. *Biomaterials* **2011**, *32* (1), 19−27.

(138) Akhavan, O.; Ghaderi, E. Flash Photo Stimulation of Human Neural Stem Cells on Graphene/TiO 2 Heterojunction for Di Ff Erentiation into Neurons. *Nanoscale* **2013**, *5*, 10316−10326.

(139) Akhavan, O.; Ghaderi, E.; Abouei, E.; Hatamie, S.; Ghasemi, E. Accelerated Differentiation of Neural Stem Cells into Neurons on Ginseng-Reduced Graphene Oxide Sheets. *Carbon* **2014**, No. 66, 395−406.

(140) Jafari, A.; Emami, A.; Ashtari, B. PC12 Cells Proliferation and Morphological Aspects: Inquiry into Raffinose-Grafted Graphene Oxide in Silk Fibroin-Based Scaffold. *Mater. Sci. Eng., C* **2021**, *121*, 111810.

(141) Feng, Z. Q.; Wang, T.; Zhao, B.; Li, J.; Jin, L. Soft Graphene Nanofibers Designed for the Acceleration of Nerve Growth and Development. *Adv. Mater.* **2015**, *27* (41), 6462−6468.

(142) Akhavan, O.; Ghaderi, E.; Shirazian, S. A.; Rahighi, R. Rolled Graphene Oxide Foams as Three-Dimensional Scaffolds for Growth of Neural Fibers Using Electrical Stimulation of Stem Cells. *Carbon* **2016**, *97*, 71−77.

(143) Liu, X.; Miller, A. L.; Park, S.; Waletzki, B. E.; Terzic, A.; Yaszemski, M. J.; Lu, L. Covalent Crosslinking of Graphene Oxide and Carbon Nanotube into Hydrogels Enhances Nerve Cell Responses. *J. Mater. Chem. B* **2016**, *4* (43), 6930−6941.

(144) Zhang, K.; Zheng, H.; Liang, S.; Gao, C. Aligned PLLA Nanofibrous Scaffolds Coated with Graphene Oxide for Promoting Neural Cell Growth. *Acta Biomater.* **2016**, *37*, 131−142.

(145) Farokhi, M.; Mottaghitalab, F.; Saeb, M. R.; Shojaei, S.; Zarrin, N. K.; Thomas, S.; Ramakrishna, S. Conductive Biomaterials as Substrates for Neural Stem Cells Differentiation towards Neuronal Lineage Cells. *Macromol. Biosci.* **2021**, *21* (1), 2000123.

(146) Zeinali, K.; Khorasani, M. T.; Rashidi, A.; Daliri Jouparid, M. Fabrication of Graphene Oxide Aerogel to Repair Neural Tissue. *J. of Clin. Res. Paramed. Sci.* **2021**, *10*, No. e119221.

(147) Magaz, A.; Li, X.; Gough, J. E.; Blaker, J. J. Graphene Oxide and Electroactive Reduced Graphene Oxide-Based Composite Fibrous Scaffolds for Engineering Excitable Nerve Tissue. *Mater. Sci. Eng., C* **2021**, *119*, 111632.

(148) Liao, J. F.; Qu, Y.; Chu, B.; Zhang, X.; Qian, Z. Biodegradable CSMA/PECA/Graphene Porous Hybrid Scaffold for Cartilage Tissue Engineering. *Sci. Rep.* **2015**, *5*, 1−16.

(149) Zhou, M.; Lozano, N.; Wychowaniec, J. K.; Hodgkinson, T.; Richardson, S. M.; Kostarelos, K.; Hoyland, J. A. Graphene Oxide: A Growth Factor Delivery Carrier to Enhance Chondrogenic Differentiation of Human Mesenchymal Stem Cells in 3D Hydrogels. *Acta Biomater.* **2019**, *96*, 271−280.

(150) Shen, H.; Lin, H.; Sun, A. X.; Song, S.; Wang, B.; Yang, Y.; Dai, J.; Tuan, R. S. Acceleration of Chondrogenic Differentiation of Human Mesenchymal Stem Cells by Sustained Growth Factor Release in 3D Graphene Oxide Incorporated Hydrogels. *Acta Biomater.* **2020**, *105*, 44−55.

(151) Gong, M.; Sun, J.; Liu, G.; Li, L.; Wu, S.; Xiang, Z. Graphene Oxide-Modified 3D Acellular Cartilage Extracellular Matrix Scaffold for Cartilage Regeneration. *Mater. Sci. Eng., C* **2021**, *119*, 111603.

(152) Maleki, M.; Zarezadeh, R.; Nouri, M.; Sadigh, A. R.; Pouremamali, F.; Asemi, Z.; Kafil, H. S.; Alemi, F.; Yousefi, B. Graphene Oxide: A Promising Material for Regenerative Medicine and Tissue Engineering. *Biomol* **2021**, *11* (1), 182−200.

(153) Mahmoudi, N.; Simchi, A. On the Biological Performance of Graphene Oxide-Modified Chitosan/Polyvinyl Pyrrolidone Nanocomposite Membranes: In Vitro and in Vivo Effects of Graphene Oxide. *Mater. Sci. Eng., C* **2017**, *70*, 121−131.

(154) Liao, K. H.; Lin, Y. S.; MacOsko, C. W.; Haynes, C. L. Cytotoxicity of Graphene Oxide and Graphene in Human Erythrocytes and Skin Fibroblasts. *ACS Appl. Mater. Interfaces.* **2011**, *3* (7), 2607−2615.

(155) Sadeghianmaryan, A.; Karimi, Y.; Naghieh, S.; Alizadeh Sardroud, H.; Gorji, M.; Chen, X. Electrospinning of Scaffolds from the Polycaprolactone/Polyurethane Composite with Graphene Oxide for Skin Tissue Engineering. *Appl. Biochem. Biotechnol.* **2020**, *191* (2), 567−578.

(156) Nizami, M. Z. I.; Takashiba, S.; Nishina, Y. Graphene Oxide: A New Direction in Dentistry. *Applied Mater. Today.* **2020**, *19*, 100576.

(157) Rodríguez-Lozano, F. J.; García-Bernal, D.; Aznar-Cervantes, S.; Ros-Roca, M. A.; Algueró, M. C.; Atucha, N. M.; Lozano-García, A. A.; Moraleda, J. M.; Cenis, J. L. Effects of Composite Films of Silk Fibroin and Graphene Oxide on the Proliferation, Cell Viability and Mesenchymal Phenotype of Periodontal Ligament Stem Cells. *J. Mater. Sci.: Mater. Med.* **2014**, *25* (12), 2731−2741.

(158) Zhang, W.; Chang, Q.; Xu, L.; Li, G.; Yang, G.; Ding, X.; Wang, X.; Cui, D.; Jiang, X. Graphene Oxide-Copper Nanocomposite-Coated Porous CaP Scaffold for Vascularized Bone Regeneration via Activation of Hif-1α. *Adv. Healthc. Mater.* **2016**, *5* (11), 1299−1309.

(159) Liu, S.; Sun, H.; Liu, S.; Wang, S. Graphene Facilitated Visible Light Photodegradation of Methylene Blue over Titanium Dioxide Photocatalysts. *Chem. Eng. J.* **2013**, *214*, 298−303.

(160) Víctor-Román, S.; García-Bordejé, E.; Hernández-Ferrer, J.; González-Domínguez, J. M.; Ansón-Casaos, A.; Silva, A. M. T.; Maser, W. K.; Benito, A. M. Controlling the Surface Chemistry of Graphene Oxide: Key towards Efficient ZnO-GO Photocatalysts. *Catal. Today* **2020**, *357*, 350−360.

(161) Mohanta, D.; Ahmaruzzaman, M. A Novel Au-SnO2-RGO Ternary Nanoheterojunction Catalyst for UV-LED Induced Photocatalytic Degradation of Clothianidin: Identification of Reactive Intermediates, Degradation Pathway and in-Depth Mechanistic Insight. *J Hazard Mater* **2020**, *397*, 122685.

(162) Akhavan, O.; Ghaderi, E. Photocatalytic Reduction of Graphene Oxide Nanosheets on TiO2 Thin Film for Photoinactivation of Bacteria in Solar Light Irradiation. *J. Phys. Chem. C* **2009**, *113* (47), 20214−20220.

(163) Akhavan, O.; Choobtashani, M.; Ghaderi, E. Protein Degradation and RNA Efflux of Viruses Photocatalyzed by Graphene-Tungsten Oxide Composite under Visible Light Irradiation. *J. Phys. Chem. C* **2012**, *116* (17), 9653−9659.

(164) Priyanka, R. N.; Joseph, S.; Abraham, T.; Plathanam, N. J.; Mathew, B. Rapid Sunlight-Driven Mineralisation of Dyes and Fungicide in Water by Novel Sulphur-Doped Graphene Oxide/Ag3VO4 Nanocomposite. *Environ. Sci. Pollut. Res.* **2020**, *27* (9), 9604−9618.

(165) Akhavan, O.; Ghaderi, E.; Rahimi, K. Adverse Effects of Graphene Incorporated in TiO 2 Photocatalyst on Minuscule Animals under Solar Light Irradiation. *J. Mater. Chem.* **2012**, *22* (43), 23260−23266.

(166) Van Tuan, P.; Tuong, H. B.; Tan, V. T.; Thu, L. H.; Khoang, N. D.; Khiem, T. N. SnO2/Reduced Graphene Oxide Nanocomposites for Highly Efficient Photocatalytic Degradation of Methylene Blue. *Opt Mater (Amst)* **2022**, *123*, 111916.

(167) Akhavan, O. Graphene Nanomesh by ZnO Nanorod Photocatalysts. *ACS Nano* **2010**, *4* (7), 4174−4180.

(168) Zhen, Q.; Gao, L.; Sun, C.; Gong, H.; Hu, P.; Song, S.; Li, R. Honeycomb-like TiO2@GO Nanocomposites for the Photodegradation of Oxytetracycline. *Mater. Lett.* **2018**, *228*, 318−321.

(169) Zhao, Y.; Li, L.; Zuo, Y.; He, G.; Chen, Q.; Meng, Q.; Chen, H. Reduced Graphene Oxide Supported ZnO/CdS Heterojunction Enhances Photocatalytic Removal Efficiency of Hexavalent Chromium from Aqueous Solution. *Chemosphere* **2022**, *286*, 131738.

(170) Tai, X. H.; Lai, C. W.; Yang, T. C. K.; Johan, M. R.; Lee, K. M.; Chen, C.-Y.; Juan, J. C. Highly Effective Removal of Volatile Organic Pollutants with P-n Heterojunction Photoreduced Graphene Oxide-TiO2 Photocatalyst. *J. Environ. Chem. Eng.* **2022**, *10* (2), 107304.

(171) Bhawna; Kumar, S.; Sharma, R.; Gupta, A.; Tyagi, A.; Singh, P.; Kumar, A.; Kumar, V. Recent Insights into SnO 2 -Based Engineered Nanoparticles for Sustainable H2 Generation and Remediation of Pesticides. *New J. Chem.* **2022**, *46* (9), 4014−4048.

(172) Chen, F.; Zhang, L.; Wang, X.; Zhang, R. Noble-Metal-Free NiO@Ni-ZnO/Reduced Graphene Oxide/CdS Heterostructure for Efficient Photocatalytic Hydrogen Generation. *Appl. Surf. Sci.* **2017**, *422*, 962−969.

(173) Wang, P.; Zhan, S.; Xia, Y.; Ma, S.; Zhou, Q.; Li, Y. The Fundamental Role and Mechanism of Reduced Graphene Oxide in RGO/Pt-TiO2 Nanocomposite for High-Performance Photocatalytic Water Splitting. *Appl. Catal.* **2017**, *207*, 335−346.

(174) Latorre-Sánchez, M.; Lavorato, C.; Puche, M.; Fornés, V.; Molinari, R.; Garcia, H. Visible-Light Photocatalytic Hydrogen Generation by Using Dye-Sensitized Graphene Oxide as a Photocatalyst. *Chem. Eur. J.* **2012**, *18* (52), 16774−16783.

(175) Yan, J. Q.; Sun, D. W.; Huang, J. H. Synergistic Poly(Lactic Acid) Photo reforming and H2 Generation over Ternary NixCo1-XP/ Reduced Graphene Oxide/g-C3N4 Composite. *Chemosphere* **2022**, *286* (3), 131905.

(176) Ha, E.; Liu, W.; Wang, L.; Man, H. W.; Hu, L.; Tsang, S. C. E.; Chan, C. T. L.; Kwok, W. M.; Lee, L. Y. S.; Wong, K. Y. Cu2ZnSnS4/MoS2-Reduced Graphene Oxide Heterostructure: Nanoscale Interfacial Contact and Enhanced Photocatalytic Hydrogen Generation. *Sci. Rep.* **2017**, *8* (2017), 962−969.

(177) Wang, X.; Li, Q.; Xu, H.; Gan, L.; Ji, X.; Liu, H.; Zhang, R. CuS-Modified ZnO Rod/Reduced Graphene Oxide/CdS Heterostructure for Efficient Visible-Light Photocatalytic Hydrogen Generation. *Int. J. Hydrog. Energy* **2020**, *45* (53), 28394−28403.

(178) Meng, F.; Cushing, S. K.; Li, J.; Hao, S.; Wu, N. Enhancement of Solar Hydrogen Generation by Synergistic Interaction of La2Ti2O7 Photocatalyst with Plasmonic Gold Nanoparticles and Reduced Graphene Oxide Nanosheets. *ACS Catal.* **2015**, *5* (3), 1949−1955.

(179) Wang, X.; Yuan, B.; Xie, Z.; Wang, D.; Zhang, R. ZnS-CdS/ Graphene Oxide Heterostructures Prepared by a Light Irradiation-Assisted Method for Effective Photocatalytic Hydrogen Generation. *J. Colloid Interface Sci.* **2015**, *446*, 150−154.

(180) Rivero, M. J.; Iglesias, O.; Ribao, P.; Ortiz, I. Kinetic Performance of TiO2/Pt/Reduced Graphene Oxide Composites in the Photocatalytic Hydrogen Production. *Int. J. Hydrog. Energy* **2019**, *44*, 101−109.

(181) Gao, X.; Wang, J.; Xue, Q.; Ma, Y. Y.; Gao, Y. AgBr/ Polyoxometalate/Graphene Oxide Ternary Composites for Visible Light-Driven Photocatalytic Hydrogen Production. *ACS Appl. Nano Mater.* **2021**, *4* (2), 2126−2135.

(182) Hafeez, H. Y.; Lakhera, S. K.; Bellamkonda, S.; Rao, G. R.; Shankar, M. v.; Bahnemann, D. W.; Neppolian, B. Construction of Ternary Hybrid Layered Reduced Graphene Oxide Supported G-C3N4-TiO2 Nanocomposite and Its Photocatalytic Hydrogen Production Activity. *Int. J. Hydrog. Energy* **2018**, *43* (8), 3892−3904.

(183) Kumar, D. P.; Hong, S.; Reddy, D. A.; Kim, T. K. Ultrathin MoS2 Layers Anchored Exfoliated Reduced Graphene Oxide Nanosheet Hybrid as a Highly Efficient Cocatalyst for CdS Nanorods

towards Enhanced Photocatalytic Hydrogen Production. *Appl. Catal.* **2017**, *212*, 7−14.

(184) An, X.; Li, K.; Tang, J. Cu2O/Reduced Graphene Oxide Composites for the Photocatalytic Conversion of CO2. *ChemSusChem* **2014**, *7* (4), 1086−1093.

(185) Nabil, S.; Hammad, A. S.; El-Bery, H. M.; Shalaby, E. A.; El-Shazly, A. H. The CO2 Photoconversion over Reduced Graphene Oxide Based on Ag/TiO2 Photocatalyst in an Advanced Meso-Scale Continuous-Flow Photochemical Reactor. *Environ. Sci. Pollut. Res.* **2021**, *28* (27), 36157−36173.

(186) Hiragond, C. B.; Lee, J.; Kim, H.; Jung, J. W.; Cho, C. H.; In, S. A Novel N-Doped Graphene Oxide Enfolded Reduced Titania for Highly Stable and Selective Gas-Phase Photocatalytic CO2 Reduction into CH4: An in-Depth Study on the Interfacial Charge Transfer Mechanism. *Chem. Eng. J.* **2021**, *416*, 127978.

(187) Zhang, J.; Shao, S.; Zhou, D.; Xu, Q.; Wang, T. ZnO Nanowire Arrays Decorated 3D N-Doped Reduced Graphene Oxide Nanotube Framework for Enhanced Photocatalytic CO2reduction Performance. *J. CO2 Util.* **2021**, *50*, 101584.

(188) Kumar, P.; Joshi, C.; Barras, A.; Sieber, B.; Addad, A.; Boussekey, L.; Szunerits, S.; Boukherroub, R.; Jain, S. L. Core-Shell Structured Reduced Graphene Oxide Wrapped Magnetically Separable RGO@CuZnO@Fe3O4 Microspheres as Superior Photocatalyst for CO2 Reduction under Visible Light. *Appl. Catal.* **2017**, *205*, 654−665.

(189) Wang, X.; Li, K.; He, J.; Yang, J.; Dong, F.; Mai, W.; Zhu, M. Defect in Reduced Graphene Oxide Tailored Selectivity of Photocatalytic CO2 Reduction on Cs4PbBr6 Pervoskite Hole-in-Microdisk Structure. *Nano Energy* **2020**, *78*, 105388.

(190) Zhu, Z.; Han, Y.; Chen, C.; Ding, Z.; Long, J.; Hou, Y. Reduced Graphene Oxide-Cadmium Sulfide Nanorods Decorated with Silver Nanoparticles for Efficient Photocatalytic Reduction Carbon Dioxide Under Visible Light. *ChemCatChem* **2018**, *10* (7), 1627−1634.

(191) Tan, L. L.; Ong, W. J.; Chai, S. P.; Mohamed, A. R. Reduced Graphene Oxide-TiO2 Nanocomposite as a Promising Visible-Light-Active Photocatalyst for the Conversion of Carbon Dioxide. *Nanoscale Res. Lett.* **2013**, *8* (1), 1−9.

(192) Chen, D.; Feng, H.; Li, J. Graphene Oxide: Preparation, Functionalization, and Electrochemical Applications. *Chem. Rev.* **2012**, *112* (11), 6027−6053.

(193) Liu, H.; Gao, J.; Xue, M.; Zhu, N.; Zhang, M.; Cao, T. Processing of Graphene for Electrochemical Application: Non-covalently Functionalize Graphene Sheets with Water-Soluble Electroactive Methylene Green. *Langmuir* **2009**, *25* (20), 12006−12010.

(194) Wang, Z.; Zhou, X.; Zhang, J.; Boey, F.; Zhang, H. Direct Electrochemical Reduction of Single-Layer Graphene Oxide and Subsequent Functionalization with Glucose Oxidase. *J. Phys. Chem. C* **2009**, *113* (32), 14071−14075.

(195) Wang, Y.; Wan, Y.; Zhang, D. Reduced Graphene Sheets Modified Glassy Carbon Electrode for Electrocatalytic Oxidation of Hydrazine in Alkaline Media. *Electrochem commun* **2010**, *12*, 187−190.

(196) Pumera, M. Graphene-Based Nanomaterials and Their Electrochemistry. *Chem. Soc. Rev.* **2010**, *39* (11), 4146−4157.

(197) Akhavan, O.; Ghaderi, E.; Rahighi, R. Toward Single-DNA Electrochemical Biosensing by Graphene Nanowalls. *ACS Nano* **2012**, *6* (4), 2904−2916.

(198) Akhavan, O.; Ghaderi, E.; Rahighi, R.; Abdolahad, M. Spongy Graphene Electrode in Electrochemical Detection of Leukemia at Single-Cell Levels. *Carbon* **2014**, *79*, 654−663.

(199) Akhavan, O.; Ghaderi, E.; Hashemi, E.; Rahighi, R. Ultra-Sensitive Detection of Leukemia by Graphene. *Nanoscale* **2014**, *6* (24), 14810−14819.

(200) Zhu, M.; Yan, Q.; Bai, X.; Cai, H.; Zhao, J.; Yan, Y.; Zhu, K.; Ye, K.; Yan, J.; Cao, D.; Wang, G. Construction of Reduced Graphene Oxide Coupled with CoSe2-MoSe2 Heterostructure for Enhanced

Electrocatalytic Hydrogen Production. *J. Colloid Interface Sci.* **2022**, *608*, 922−930.

(201) Li, J.; sen; Wang, Y.; Liu, C. H.; Li, S. L.; Wang, Y. G.; Dong, L. Z.; Dai, Z. H.; Li, Y. F.; Lan, Y. Q. Coupled Molybdenum Carbide and Reduced Graphene Oxide Electrocatalysts for Efficient Hydrogen Evolution. *Nat. Commun* **2016**, *7* (1), 1−8.

(202) Munde, A. v; Mulik, B. B.; Chavan, P. P.; Sathe, B. R. Electrochim. Acta Enhanced Electrocatalytic Activity towards Urea Oxidation on Ni Nanoparticle Decorated Graphene Oxide Nano-composite. *Electrochim. Acta* **2020**, *349*, 136386.

(203) Zhang, Z.; Ahmad, F.; Zhao, W.; Yan, W.; Zhang, W.; Huang, H.; Ma, C.; Zeng, J. Enhanced Electrocatalytic Reduction of CO2 via Chemical Coupling between Indium Oxide and Reduced Graphene Oxide. *Nano Lett.* **2019**, *19*, 4029−4034.

(204) Li, P.; Zeng, H. C. Sandwich-Like Nanocomposite of CoNiO x/Reduced Graphene Oxide for Enhanced Electrocatalytic Water Oxidation. *Adv. Funct. Mater.* **2017**, *27* (13), 1606325.

(205) Yin, D.; Liu, Y.; Song, P.; Chen, P.; Liu, X.; Cai, L.; Zhang, L. In Situ Growth of Copper/Reduced Graphene Oxide on Graphite Surfaces for the Electrocatalytic Reduction of Nitrate. *Electrochim. Acta* **2019**, *324*, 134846.

(206) Guan, X.; Avci-Adali, M.; Alarçin, E.; Cheng, H.; Kashaf, S. S.; Li, Y.; Chawla, A.; Jang, H. L.; Khademhosseini, A. Development of Hydrogels for Regenerative Engineering. *Biotechnol. J.* **2017**, *12* (5), 1600394.

(207) Kumar, G.; Chaudhary, K.; Mogha, N. K.; Kant, A.; Masram, D. T. Extended Release of Metronidazole Drug Using Chitosan/Graphene Oxide Bionanocomposite Beads as the Drug Carrier. *ACS Omega* **2021**, *6* (31), 20433−20444.

(208) Feng, L.; Liu, Z. Graphene in Biomedicine: Opportunities and Challenges. *Nanomedicine* **2011**, *6* (2), 317−324.

(209) Shen, H.; Zhang, L.; Liu, M.; Zhang, Z. Biomedical Applications of Graphene. *Theranostics* **2012**, *2* (3), 283.

(210) Ayazi, H.; Akhavan, O.; Raoufi, M.; Varshochian, R.; Motlagh, N. S. H.; Atyabi, F. Graphene Aerogel Nanoparticles for In-Situ Loading/PH Sensitive Releasing Anticancer Drugs. *Colloids Surf B Biointerfaces* **2021**, *186* (2020), 202−207.

(211) Sekhon, S. S.; Kaur, P.; Kim, Y. H.; Sekhon, S. S. 2D Graphene Oxide-Aptamer Conjugate Materials for Cancer Diagnosis. *2D Mater. Appl.* **2021**, *5* (1), 1−19.

(212) Fazaeli, Y.; Akhavan, O.; Rahighi, R.; Aboudzadeh, M. R.; Karimi, E.; Afarideh, H. In Vivo SPECT Imaging of Tumors by 198,199Au-Labeled Graphene Oxide Nanostructures. *Mater. Sci. Eng., C* **2014**, *45*, 196−204.

(213) Akhavan, O.; Ghaderi, E. Graphene Nanomesh Promises Extremely Efficient in Vivo Photothermal Therapy. *Small* **2013**, *9* (21), 3593−3601.

(214) Yang, Y.; Zhang, Y. M.; Chen, Y.; Zhao, D.; Chen, J. T.; Liu, Y. Construction of a Graphene Oxide Based Noncovalent Multiple Nanosupramolecular Assembly as a Scaffold for Drug Delivery. *Chemistry* **2012**, *18* (14), 4208−4215.

(215) Mukherjee, S.; Bytesnikova, Z.; Ashrafi, A.; Adam, V.; Richtera, L. Graphene Oxide as a Nanocarrier for Biochemical Molecules: Current Understanding and Trends. *Processes* **2020**, *8* (12), 1636.

(216) Rezaei, A.; Akhavan, O.; Hashemi, E.; Shamsara, M. Toward Chemical Perfection of Graphene-Based Gene Carrier via Ugi Multicomponent Assembly Process. *Biomacromolecules* **2016**, *17* (9), 2963−2971.

(217) Assali, A.; Akhavan, O.; Adeli, M.; Razzazan, S.; Dinarvand, R.; Zanganeh, S.; Soleimani, M.; Dinarvand, M.; Atyabi, F. Multifunctional Core-Shell Nanoplatforms (Gold@graphene Oxide) with Mediated NIR Thermal Therapy to Promote MiRNA Delivery. *Nanomedicine* **2018**, *14* (6), 1891−1903.

(218) Pan, Q.; Lv, Y.; Williams, G. R.; Tao, L.; Yang, H.; Li, H.; Zhu, L. Lactobionic Acid and Carboxymethyl Chitosan Functionalized Graphene Oxide Nanocomposites as Targeted Anticancer Drug Delivery Systems. *Carbohydr. Polym.* **2016**, *151*, 812−820.

(219) Du, J.; Cheng, H. M. The Fabrication, Properties, and Uses of Graphene/Polymer Composites. *Macromol. Chem. Phys.* **2012**, *213* (10−11), 1060−1077.

(220) Shariatinia, Z.; Zahraee, Z. Controlled Release of Metformin from Chitosan-Based Nanocomposite Films Containing Mesoporous MCM-41 Nanoparticles as Novel Drug Delivery Systems. *J. Colloid Interface Sci.* **2017**, *501*, 60−76.

(221) Wang, Y. C.; Li, Y.; Sun, T. M.; Xiong, M. H.; Wu, J.; Yang, Y. Y.; Wang, J. Core-Shell-Corona Micelle Stabilized by Reversible Cross-Linkage for Intracellular Drug Deliverya. *Macromol. Rapid Commun.* **2010**, *31* (13), 1201−1206.

(222) Namazi, H.; Bahrami, S.; Entezami, A. A. Synthesis and Controlled Release of Biocompatible Prodrugs of Beta-Cyclodextrin Linked with PEG Containing Ibuprofen or Indomethacin. *Iran Polym. J.* **2005**, *14−10* (64), 921−927.

(223) Namazi, H.; Adeli, M. Dendrimers of Citric Acid and Poly (Ethylene Glycol) as the New Drug-Delivery Agents. *Biomaterials* **2005**, *26* (10), 1175−1183.

(224) Hailemeskel, B. Z.; Addisu, K. D.; Prasannan, A.; Mekuria, S. L.; Kao, C.-Y.; Tsai, H.-C. Model Synthesis and Characterization of Diselenide Linked Poly(Ethylene Glycol) Nanogel as Multi-Responsive Drug Carrier. *Appl. Surf. Sci.* **2018**, *449*, 15−22.

(225) Karimzadeh, Z.; Javanbakht, S.; Namazi, H. Carboxymethyl-cellulose/MOF-5/Graphene Oxide Bio-Nanocomposite as Antibacterial Drug Nanocarrier Agent. *Bioimpacts* **2019**, *9* (1), 5−13.

(226) Wang, Z.; Colombi Ciacchi, L.; Wei, G. Recent Advances in the Synthesis of Graphene-Based Nanomaterials for Controlled Drug Delivery. *Appl. Sci.* **2017**, *7* (11), 1175.

(227) Ma, R.; Wang, Y. Y.; Qi, H.; Shi, C.; Wei, G.; Xiao, L.; Huang, Z.; Liu, S.; Yu, H.; Teng, C.; Liu, H.; Murugadoss, V.; Zhang, J.; Wang, Y. Y.; Guo, Z. Nanocomposite Sponges of Sodium Alginate/ Graphene Oxide/Polyvinyl Alcohol as Potential Wound Dressing: In Vitro and in Vivo Evaluation. *Compos. B. Eng.* **2019**, *167*, 396−405.

(228) Hao, B.; Li, W.; Zhang, S.; Zhu, Y.; Li, Y.; Ding, A.; Huang, X. Correction: A Facile PEG/Thiol-Functionalized Nanographene Oxide Carrier with an Appropriate Glutathione-Responsive Switch. *Polym. Chem.* **2020**, *11* (12), 2194−2204.

(229) Zhao, X.; Wei, Z.; Zhao, Z.; Miao, Y.; Qiu, Y.; Yang, W.; Jia, X.; Liu, Z.; Hou, H. Design and Development of Graphene Oxide Nanoparticle/Chitosan Hybrids Showing PH-Sensitive Surface Charge-Reversible Ability for Efficient Intracellular Doxorubicin Delivery. *ACS Appl. Mater. Interfaces.* **2018**, *10* (7), 6608−6617.

(230) Kabiri, R.; Namazi, H. Surface Grafting of Reduced Graphene Oxide Using Nanocrystalline Cellulose via Click Reaction. *J. Nanoparticle Res.* **2014**, *16* (7), 1−13.

(231) Matiyani, M.; Rana, A.; Pal, M.; Rana, S.; Melkani, A. B.; Sahoo, N. G. Polymer Grafted Magnetic Graphene Oxide as a Potential Nanocarrier for PH-Responsive Delivery of Sparingly Soluble Quercetin against Breast Cancer Cells. *RSC Adv.* **2022**, *12* (5), 2574−2588.

(232) Ghamkhari, A.; Abbaspour-Ravasjani, S.; Talebi, M.; Hamishehkar, H.; Hamblin, M. R. Development of a Graphene Oxide-Poly Lactide Nanocomposite as a Smart Drug Delivery System. *Int. J. Biol. Macromol.* **2021**, *169*, 521−531.

(233) Xiong, S.; Luo, J.; Wang, Q. Q.; Li, Z.; Li, J.; Liu, Q.; Gao, L.; Fang, S.; Li, Y.; Pan, H.; Wang, H.; Zhang, Y.; Wang, Q. Q.; Chen, X.; Chen, T. Targeted Graphene Oxide for Drug Delivery as a Therapeutic Nanoplatform against Parkinson's Disease. *Biomater Sci* **2021**, *9* (5), 1705−1715.

(234) Jun, S. W.; Manivasagan, P.; Kwon, J.; Nguyen, V. T.; Mondal, S.; Ly, C. D.; Lee, J.; Kang, Y. H.; Kim, C. S.; Oh, J. Folic Acid-Conjugated Chitosan-Functionalized Graphene Oxide for Highly Efficient Photoacoustic Imaging-Guided Tumor-Targeted Photo-thermal Therapy. *Int J Biol Macromol* **2020**, *155*, 961−971.

(235) Pooresmaeil, M.; Namazi, H. Fabrication of a Smart and Biocompatible Brush Copolymer Decorated on Magnetic Graphene Oxide Hybrid Nanostructure for Drug Delivery Application. *Eur. Polym. J.* **2021**, *142*, 110126.

(236) Omor Faruk Patwary, M.; Mahbubur Rahman, M.; Khalid Bin Islam, M.; Ackas Ali, M.; Halim, M. A.; Ahmed, F.; Patwary, M. O. F. Probing the Non-Bonding Interaction of Small Molecules with Graphene Oxide Using DFT Based Vibrational Circular Dichroism. *Comput. Theor. Chem.* **2022**, *1207*, 113503.

(237) Cao, X.; Zhao, J.; Wang, Z.; Xing, B. New Insight into the Photo-Transformation Mechanisms of Graphene Oxide under UV-A, UV-B and UV-C Lights. *J. Hazard. Mater.* **2021**, *403*, 123683.

(238) Wang, D.; Zhang, J.; Cao, R.; Zhang, Y.; Li, J. The Detection and Characterization Techniques for the Interaction between Graphene Oxide and Natural Colloids: A Review. *Sci. Total Environ.* **2022**, *808*, 151906.

(239) Sharifi, M.; Marjani, A.; Mahdavian, L.; Shamlouei, H. R. Computational Study on Production Mechanism of Nano-Graphene Oxide/Poly Diallyl Dimethyl Ammonium Chloride (NGO/PDAD-MAC) Nanocomposite. *Polycycl. Aromat. Compd.* **2022**, 1−14.

(240) Meng, Z.; Yang, X.; Li, H. DFT-Based Theoretical Simulation on Electronic Transition for Graphene Oxides in Solvent Media. *J. Mol. Liq.* **2022**, *348*, 118049.

(241) Malhotra, M.; Puglia, M.; Kalluri, A.; Chowdhury, D.; Kumar, C. v. Adsorption of Metal Ions on Graphene Sheet for Applications in Environmental Sensing and Wastewater Treatment. *Sensors and Actuators Reports* **2022**, *4*, 100077.

(242) Zojaji, M.; Hydarinasab, A.; Hasan Hashemabadi, S.; Mehranpour, M. Rheological Study of the Effects of Size/Shape of Graphene Oxide and SiO 2 Nanoparticles on Shear Thickening Behaviour of Polyethylene Glycol 400-Based Fluid: Molecular Dynamics Simulation. *Mol. Simul.* **2022**, *48* (2), 120−130.

(243) Hashem, A. H.; Hasanin, M.; Kamel, S.; Dacrory, S. A New Approach for Antimicrobial and Antiviral Activities of Biocompatible Nanocomposite Based on Cellulose, Amino Acid and Graphene Oxide. *Colloids Surf. B* **2022**, *209*, 112172.

(244) Orekhov, N. D.; Bondareva, J. v.; Potapov, D. O.; Dyakonov, P. v.; Dubinin, O. N.; Tarkhov, M. A.; Diudbin, G. D.; Maslakov, K. I.; Logunov, M. A.; Kvashnin, D. G.; Evlashin, S. A. Mechanism of Graphene Oxide Laser Reduction at Ambient Conditions: Exper-imental and ReaxFF Study. *Carbon* **2022**, *191*, 546−554.

(245) Zhang, Q.; Yang, Y. L.; Zhou, Y.; lian; Hong, J. Paracetamol Degradation via Electrocatalysis with B and N Co-Doped Reduced Graphene Oxide: Insight into the Mechanism on Catalyst Surface and in Solution. *Chemosphere* **2022**, *287*, 132070.

(246) da Silva Bruckmann, F.; Mafra Ledur, C.; Zanella da Silva, I.; Luiz Dotto, G.; Rodrigo Bohn Rhoden, C. A DFT Theoretical and Experimental Study about Tetracycline Adsorption onto Magnetic Graphene Oxide. *J. Mol. Liq.* **2022**, *353*, 118837.

(247) Vithalani, R. S.; Modi, C. K.; Sharma, V.; Jha, P. K.; Srivastava, H. DFT Assisted Study on Activation of Surface Acidic -COOH Debris in Graphene Oxide Supported Catalyst for Benzyl Alcohol Oxidation. *J. Mol. Struct.* **2022**, *1249*, 131620.

(248) Chen, J.; Wu, H.; Sheng, G.; Li, H.; Li, M.; Guo, X.; Dong, H. Graphene Oxide-Mediated the Reduction of U(VI), Re(VII), Se(VI) and Se(IV) by Fe(II) in Aqueous Solutions Investigated via Combined Batch, DFT Calculation and Spectroscopic Approaches. *Chem. Eng. J.* **2022**, *433*, 133844.

(249) Foadin, C. S. T.; Tchangnwa Nya, F.; Malloum, A.; Conradie, J. Data of Electronic, Reactivity, Optoelectronic, Linear and Non-Linear Optical Parameters of Doping Graphene Oxide Nanosheet with Aluminum Atom. *Data Br.* **2022**, *41*, 107840.

(250) Zhu, B.; Wang, K.; Sun, W.; Fu, Z.; Ahmad, H.; Fan, M.; Gao, H. Revealing the Adsorption Energy and Interface Characteristic of Cellulose-Graphene Oxide Composites by First-Principles Calcula-tions. *Compos. Sci. Technol.* **2022**, *218*, 109209.

(251) Hao, X.; Yang, S.; E, T.; Li, Y. High Efficiency and Selective Removal of Cu(II) via Regulating the Pore Size of Graphene Oxide/ Montmorillonite Composite Aerogel. *J. Hazard. Mater.* **2022**, *424*, 127680.

(252) Yan, F.; Guo, Y.; Wang, Z.; Zhao, L.; Zhang, X. Efficient Separation of CO2/CH4 by Ionic Liquids Confined in Graphene

Oxide: A Molecular Dynamics Simulation. *Sep. Purif. Technol.* **2022**, *289*, 120736.

(253) Zhu, R.; Zhu, Y.; Chen, F.; Patterson, R.; Zhou, Y.; Wan, T.; Hu, L.; Wu, T.; Joshi, R.; Li, M.; Cazorla, C.; Lu, Y.; Han, Z.; Chu, D. Boosting Moisture Induced Electricity Generation from Graphene Oxide through Engineering Oxygen-Based Functional Groups. *Nano Energy* **2022**, *94*, 106942.

(254) Lv, X.; Yang, Y.; Tao, Y.; Jiang, Y.; Chen, B.; Zhu, X.; Cai, Z.; Li, B. A Mechanism Study on Toxicity of Graphene Oxide to Daphnia Magna: Direct Link between Bioaccumulation and Oxidative Stress. *Environ. Pollut.* **2018**, *234*, 953−959.

(255) Zhao, S.; Wang, Y.; Duo, L. Biochemical Toxicity, Lysosomal Membrane Stability and DNA Damage Induced by Graphene Oxide in Earthworms. *Environ. Pollut.* **2021**, *269*, 116225.

(256) Souza, J. P.; Venturini, F. P.; Santos, F.; Zucolotto, V. Chronic Toxicity in Ceriodaphnia Dubia Induced by Graphene Oxide. *Chemosphere* **2018**, *190*, 218−224.

(257) Sood, K.; Kaur, J.; Singh, H.; Kumar Arya, S.; Khatri, M. Comparative Toxicity Evaluation of Graphene Oxide (GO) and Zinc Oxide (ZnO) Nanoparticles on Drosophila Melanogaster. *Toxicol. Rep.* **2019**, *6*, 768−781.

(258) Lu, J.; Zhu, X.; Tian, S.; Lv, X.; Chen, Z.; Jiang, Y.; Liao, X.; Cai, Z.; Chen, B. Graphene Oxide in the Marine Environment: Toxicity to Artemia Salina with and without the Presence of Phe and Cd2+. *Chemosphere* **2018**, *211*, 390−396.

(259) Guo, Q.; Yang, Y.; Zhao, L.; Chen, J.; Duan, G.; Yang, Z.; Zhou, R. Graphene Oxide Toxicity in W1118 Flies. *Sci. Total Environ.* **2022**, *805*, 150302.

(260) Chang, Y.; Yang, S. T.; Liu, J. H.; Dong, E.; Wang, Y.; Cao, A.; Liu, Y.; Wang, H. In Vitro Toxicity Evaluation of Graphene Oxide on A549 Cells. *Toxicol. Lett.* **2011**, *200* (3), 201−210.

(261) An, W.; Zhang, Y.; Zhang, X.; Li, K.; Kang, Y.; Akhtar, S.; Sha, X.; Gao, L. Ocular Toxicity of Reduced Graphene Oxide or Graphene Oxide Exposure in Mouse Eyes. *Exp. Eye Res.* **2018**, *174*, 59−69.

(262) Guo, Z.; Xie, C.; Zhang, P.; Zhang, J.; Wang, G.; He, X.; Ma, Y.; Zhao, B.; Zhang, Z. Toxicity and Transformation of Graphene Oxide and Reduced Graphene Oxide in Bacteria Biofilm. *Sci. Total Environ.* **2017**, *580*, 1300−1308.

(263) Combarros, R. G.; Collado, S.; Díaz, M. Toxicity of Graphene Oxide on Growth and Metabolism of Pseudomonas Putida. *J. Hazard. Mater.* **2016**, *310*, 246−252.

(264) Martin-Folgar, R.; Esteban-Arranz, A.; Negri, V.; Morales, M. Toxicological Effects of Three Different Types of Highly Pure Graphene Oxide in the Midge Chironomus Riparius. *Sci. Total Environ.* **2022**, *815*, 152465.

(265) Yan, Z.; Yang, X.; Lynch, I.; Cui, F. Comparative Evaluation of the Mechanisms of Toxicity of Graphene Oxide and Graphene Oxide Quantum Dots to Blue-Green Algae Microcystis Aeruginosa in the Aquatic Environment. *J. Hazard. Mater.* **2022**, *425*, 127898.

(266) Audira, G.; Lee, J. S.; Siregar, P.; Malhotra, N.; Rolden, M. J. M.; Huang, J. C.; Chen, K. H. C.; Hsu, H. S.; Hsu, Y.; Ger, T. R.; Hsiao, C. der. Comparison of the Chronic Toxicities of Graphene and Graphene Oxide toward Adult Zebrafish by Using Biochemical and Phenomic Approaches. *Environ. Pollut.* **2021**, *278*, 116907.

(267) Malina, T.; Lamaczová, A.; Maršálková, E.; Zbořil, R.; Maršálek, B. Graphene Oxide Interaction with Lemna Minor: Root Barrier Strong Enough to Prevent Nanoblade-Morphology-Induced Toxicity. *Chemosphere* **2022**, *291*, 132739.

(268) Duo, L.; Wang, Y.; Zhao, S. Ecotoxicol. Environ. Saf. Individual and Histopathological Responses of the Earthworm (Eisenia Fetida) to Graphene Oxide Exposure. *Ecotoxicol. Environ. Saf.* **2022**, *229*, 113076.

(269) Bangeppagari, M.; Park, S. H.; Kundapur, R. R.; Lee, S. J. Graphene Oxide Induces Cardiovascular Defects in Developing Zebrafish (Danio Rerio) Embryo Model: In-Vivo Toxicity Assessment. *Sci. Total Environ.* **2019**, *673*, 810−820.

(270) Cruces, E.; Barrios, A. C.; Cahue, Y. P.; Januszewski, B.; Gilbertson, L. M.; Perreault, F. Similar Toxicity Mechanisms between Graphene Oxide and Oxidized Multi-Walled Carbon Nanotubes in Microcystis Aeruginosa. *Chemosphere* **2021**, *265*, 129137.

(271) Liu, X. T.; Mu, X. Y.; Wu, X. L.; Meng, L. X.; Guan, W. B.; Ma, Y. Q.; Sun, H.; Wang, C. J.; Li, X. F. Toxicity of Multi-Walled Carbon Nanotubes, Graphene Oxide, and Reduced Graphene Oxide to Zebrafish Embryos. *Biomed. Environ. Sci.* **2014**, *27* (9), 676−683.

(272) Zhao, S.; Wang, Q.; Zhao, Y.; Rui, Q.; Wang, D. Toxicity and Translocation of Graphene Oxide in Arabidopsis Thaliana. *Environ. Toxicol. Pharmacol.* **2015**, *39* (1), 145−156.

(273) Chen, Z.; Yu, C.; Khan, I. A.; Tang, Y.; Liu, S.; Yang, M. Toxic Effects of Different-Sized Graphene Oxide Particles on Zebrafish Embryonic Development. *Ecotoxicol. Environ. Saf.* **2020**, *197*, 110608.

(274) Yin, J.; Fan, W.; Du, J.; Feng, W.; Dong, Z.; Liu, Y.; Zhou, T. The Toxicity of Graphene Oxide Affected by Algal Physiological Characteristics: A Comparative Study in Cyanobacterial, Green Algae, Diatom. *Environ. Pollut.* **2020**, *260*, 113847.

(275) Hashemi, M. S.; Gharbi, S.; Jafarinejad-Farsangi, S.; Ansari-Asl, Z.; Dezfuli, A. S. Secondary Toxic Effect of Graphene Oxide and Graphene Quantum Dots Alters the Expression of MiR-21 and MiR-29a in Human Cell Lines. *Toxicol. In Vitro* **2020**, *65*, 104796.

(276) Akhavan, O.; Ghaderi, E. Toxicity of Graphene and Graphene Oxide Nanowalls Against Bacteria. *ACS Nano.* **2010**, *4* (10), 5731−5736.

(277) Akhavan, O.; Ghaderi, E.; Esfandiar, A. Wrapping Bacteria by Graphene Nanosheets for Isolation from Environment, Reactivation by Sonication, and Inactivation by Near-Infrared Irradiation. *J. Phys. Chem. B* **2011**, *115* (19), 6279−6288.

(278) Hashemi, E.; Akhavan, O.; Shamsara, M.; Daliri, M.; Dashtizad, M.; Farmany, A. Colloids and Surfaces B : Biointerfaces Synthesis and Cyto-Genotoxicity Evaluation of Graphene on Mice Spermatogonial Stem Cells. *Colloids Surf. B* **2016**, *146*, 770−776.

(279) Zhang, M.; Yu, Q.; Liang, C.; Liu, Z.; Zhang, B.; Li, M. Ecotoxicol. Environ. Saf. Graphene Oxide Induces Plasma Membrane Damage, Reactive Oxygen Species Accumulation and Fatty Acid pro Fi Les Change in Pichia Pastoris. *Ecotoxicol. Environ. Saf.* **2016**, *132*, 372−378.

(280) Akhavan, O.; et al. Escherichia Coli Bacteria Reduce Graphene Oxide to Bactericidal Graphene in a Self-Limiting Manner. *Carbon* **2012**, *50* (5), 1853−1860.

(281) Liu, S.; Zeng, T. H.; Hofmann, M.; Burcombe, E.; Wei, J.; Jiang, R.; Kong, J.; Chen, Y. Antibacterial Activity of Graphite, Graphite Oxide, Graphene Oxide, and Reduced Graphene Oxide : Membrane and Oxidative Stress. *ACS Nano* **2011**, *5*, 6971−6980.

(282) Akhavan, O.; Ghaderi, E.; Akhavan, A. Biomaterials Size-Dependent Genotoxicity of Graphene Nanoplatelets in Human Stem Cells. *Biomaterials* **2012**, *33* (32), 8017−8025.

(283) Akhavan, O.; Ghaderi, E.; Hashemi, E.; Akbari, E. Dose-Dependent Effects of Nanoscale Graphene Oxide on Reproduction Capability of Mammals. *Carbon* **2015**, *95*, 309−317.

(284) Pecoraro, R.; D'Angelo, D.; Filice, S.; Scalese, S.; Capparucci, F.; Marino, F.; Iaria, C.; Guerriero, G.; Tibullo, D.; Scalisi, E. M.; Salvaggio, A.; Nicotera, I.; Brundo, M. v. Toxicity Evaluation of Graphene Oxide and Titania Loaded Nafion Membranes in Zebrafish. *Front. Physiol.* **2018**, *8*, 1−7.

(285) Jin, C.; Wang, F.; Tang, Y.; Zhang, X.; Wang, J.; Yang, Y. Distribution of Graphene Oxide and TiO2-Graphene Oxide Composite in A549 Cells. *Biol. Trace Elem. Res.* **2014**, *159* (1−3), 393−398.

(286) Eivazzadeh-Keihan, R.; Radinekiyan, F.; Madanchi, H.; Aliabadi, H. A. M.; Maleki, A. Graphene Oxide/Alginate/Silk Fibroin Composite as a Novel Bionanostructure with Improved Blood Compatibility, Less Toxicity and Enhanced Mechanical Properties. *Carbohydr. Polym.* **2020**, *248*, 116802.

(287) Samuel, M. S.; Shah, S. S.; Bhattacharya, J.; Subramaniam, K.; Pradeep Singh, N. D. Adsorption of Pb(II) from Aqueous Solution Using a Magnetic Chitosan/Graphene Oxide Composite and Its Toxicity Studies. *Int. J. Biol. Macromol.* **2018**, *115*, 1142−1150.

(288) Hatamie, S.; Akhavan, O.; Sadrnezhaad, S. K.; Ahadian, M. M.; Shirolkar, M. M.; Wang, H. Q. Curcumin-Reduced Graphene

Oxide Sheets and Their Effects on Human Breast Cancer Cells. *Mater. Sci. Eng., C* **2015**, *55*, 482−489.

(289) Chapple, R.; Chivas-Joly, C.; Kose, O.; Erskine, E. L.; Ferry, L.; Lopez-Cuesta, J. M.; Kandola, B. K.; Forest, V. Graphene Oxide Incorporating Carbon Fibre-Reinforced Composites Submitted to Simultaneous Impact and Fire: Physicochemical Characterisation and Toxicology of the by-Products. *J. Hazard. Mater.* **2022**, *424*, 127544.

(290) Wierzbicki, M.; Jaworski, S.; Sawosz, E.; Jung, A.; Gielerak, G.; Jaremek, H.; Łojkowski, W.; Wozniak, B.; Stobiński, L.; Małolepszy, A.; et al. Chwalibog. Graphene Oxide in a Composite with Silver Nanoparticles Reduces the Fibroblast and Endothelial Cell Cytotoxicity of an Antibacterial Nanoplatform. *Nanoscale Res. Lett.* **2019**, *14*, 1−11.

(291) Sulheim, E.; Baghirov, H.; von Haartman, E.; Bøe, A.; Aslund, A. K. O.; Mørch, Y.; Davies, C. d. L. Comparative in Vitro Toxicity of a Graphene Oxide-Silver Nanocomposite and the Pristine Counterparts toward Macrophages. *J. Nanobiotechnology* **2016**, *14*, 1−17.

(292) Hernández-Cancel, G.; Suazo-Dávila, D.; Ojeda-Cruzado, A. J.; García-Torres, D.; Cabrera, C. R.; Griebenow, K. Graphene Oxide as a Protein Matrix: Influence on Protein Biophysical Properties. *J. Nanobiotechnology* **2015**, *13* (1), 1−12.

(293) Chaudhary, K.; Kumar, K.; Venkatesu, P.; Masram, D. T. Protein Immobilization on Graphene Oxide or Reduced Graphene Oxide Surface and Their Applications: Influence over Activity, Structural and Thermal Stability of Protein. *Adv. Colloid Interface Sci.* **2021**, *289*, 102367.

(294) Amara, C. B.; Degraeve, P.; Oulahal, N.; Gharsallaoui, A. PH-Dependent Complexation of Lysozyme with Low Methoxyl (LM) Pectin. *Food Chem.* **2017**, *236*, 127−133.

(295) Li, B.; Hao, C.; Liu, H.; Yang, H.; Zhong, K.; Zhang, M.; Sun, R. Interaction of Graphene Oxide with Lysozyme:Insights from Conformational Structure and Surface Charge Investigations. *Spectrochim. Acta A Mol. Biomol. Spectrosc.* **2022**, *264*, 120207.

(296) Nan, Z.; Hao, C.; Ye, X.; Feng, Y.; Sun, R. Interaction of Graphene Oxide with Bovine Serum Albumin: A Fluorescence Quenching Study. *Spectrochim. Acta A Mol. Biomol. Spectrosc.* **2019**, *210*, 348−354.

(297) Liu, P.; Zhang, C.; Liu, X.; Cui, P. Preparation of Carbon Quantum Dots with a High Quantum Yield and the Application in Labeling Bovine Serum Albumin. *Appl. Surf. Sci.* **2016**, *368*, 122−128.

(298) Kumari, S.; Sharma, P.; Ghosh, D.; Shandilya, M.; Rawat, P.; Hassan, M. I.; Moulick, R. G.; Bhattacharya, J.; Srivastava, C.; Majumder, S. Time-Dependent Study of Graphene Oxide-Trypsin Adsorption Interface and Visualization of Nano-Protein Corona. *Int. J. Biol. Macromol.* **2020**, *163*, 2259−2269.

(299) Taneva, S. G.; Krumova, S.; Bogár, F.; Kincses, A.; Stoichev, S.; Todinova, S.; Danailova, A.; Horváth, J.; Násztor, Z.; Kelemen, L.; Dér, A. Insights into Graphene Oxide Interaction with Human Serum Albumin in Isolated State and in Blood Plasma. *Int. J. Biol. Macromol.* **2021**, *175*, 19−29.

(300) Wang, Y.; Zhu, Z.; Zhang, H.; Chen, J.; Tang, B.; Cao, J. Investigation on the Conformational Structure of Hemoglobin on Graphene Oxide. *Mater. Chem. Phys.* **2014**, *10* (1016), 272−279.

(301) Hajipour, M. J.; Raheb, J.; Akhavan, O.; Arjmand, S.; Mashinchian, O.; Rahman, M.; Abdolahad, M.; Serpooshan, V.; Laurent, S.; Mahmoudi, M. Personalized Disease-Specific Protein Corona Influences the Therapeutic Impact of Graphene Oxide. *Nanoscale* **2015**, *7* (19), 8978−8994.

(302) Mbeh, D. A.; Akhavan, O.; Javanbakht, T.; Mahmoudi, M.; Yahia, L. Cytotoxicity of Protein Corona-Graphene Oxide Nanoribbons on Human Epithelial Cells. *Appl. Surf. Sci.* **2014**, *320*, 596−601.

(303) Akhavan, O.; Ghaderi, E.; Emamy, H.; Akhavan, F. Genotoxicity of Graphene Nanoribbons in Human Mesenchymal Stem Cells. *Carbon* **2013**, *54*, 419−431.

(304) Hajipour, M. J.; Akhavan, O.; Meidanchi, A.; Laurent, S.; Mahmoudi, M. Hyperthermia-Induced Protein Corona Improves the Therapeutic Effects of Zinc Ferrite Spinel-Graphene Sheets against Cancer. *RSC Adv.* **2014**, *4* (107), 62557−62565.

(305) Kim, J.; Cote, L. J.; Kim, F.; Huang, J. Visualizing Graphene Based Sheets by Fluorescence Quenching Microscopy. *J. Am. Chem. Soc.* **2010**, *132* (1), 260−267.

(306) Song, Y.; Qu, K.; Zhao, C.; Ren, J.; Qu, X. Graphene Oxide: Intrinsic Peroxidase Catalytic Activity and Its Application to Glucose Detection. *Adv. Mater.* **2010**, *22* (19), 2206−2210.

(307) Choi, J. S.; Park, H.; bin; Yoon, O. J.; Kim, H. J. Investigation on the Role of Graphene Oxide Sheet-Platinum Composite Counter Electrode in Dye-Sensitized Solar Cell. *Thin Solid Films* **2022**, *745*, 139098.

(308) Aslam, S.; Mustafa, F.; Ahmad, M. A. Facile Synthesis of Graphene Oxide with Significant Enhanced Properties for Optoelectronic and Energy Devices. *Ceram. Int.* **2018**, *44* (6), 6823−6828.

(309) Kant, R.; Sharma, T.; Bhardwaj, S.; Kumar, K. Structural, Electrical and Optical Properties of MgO-Reduced Graphene Oxide Nanocomposite for Optoelectronic Applications. *Curr. Appl. Phys.* **2022**, *36*, 76−82.

(310) Shahriari, S.; Sastry, M.; Panjikar, S.; Singh Raman, R. Graphene and Graphene Oxide as a Support for Biomolecules in the Development of Biosensors. *Nanotechnol. Sci. Appl.* **2021**, *14*, 197−220.

(311) Gosai, A.; Khondakar, K. R.; Ma, X.; Ali, M. A. Application of Functionalized Graphene Oxide Based Biosensors for Health Monitoring: Simple Graphene Derivatives to 3D Printed Platforms. *Biosensors* **2021**, *11* (10), 384.

(312) Sengupta, J.; Hussain, C. M. Graphene-Based Field-Effect Transistor Biosensors for the Rapid Detection and Analysis of Viruses: A Perspective in View of COVID-19. *Carbon Trends* **2021**, *2*, 100011.